INTEGRATING CHEMICAL HAZARD ASSESSMENT INTO THE DESIGN OF INHERENTLY SAFER PROCESSES

A Dissertation

by

YUAN LU

Submitted to the Office of Graduate Studies of
Texas A&M University
in partial fulfillment of the requirements for the degree of

DOCTOR OF PHILOSOPHY

December 2011

Major Subject: Chemical Engineering

Integrating Chemical Hazard Assessment into the Design of Inherently Safer Processes

INTEGRATING CHEMICAL HAZARD ASSESSMENT INTO THE DESIGN OF INHERENTLY SAFER PROCESSES

A Dissertation

by

YUAN LU

Submitted to the Office of Graduate Studies of
Texas A&M University
in partial fulfillment of the requirements for the degree of

DOCTOR OF PHILOSOPHY

Approved by:

Chair of Committee,	M. Sam Mannan
Committee Members,	Rayford Anthony
	Zhengdong Cheng
	Debjyoti Banerjee
Head of Department,	Charles Glover

December 2011

Major Subject: Chemical Engineering

ABSTRACT

Integrating Chemical Hazard Assessment into the Design of Inherently Safer Processes.

(December 2011)

Yuan Lu, B.S., East China University of Science and Technology;

M.S., East China University of Science and Technology;

M.S., Texas A&M University

Chair of Advisory Committee: Dr. M. Sam Mannan

Reactive hazard associated with chemicals is a major safety issue in process industries. This kind of hazard has caused the occurrence of many accidents, leading to fatalities, injuries, property damage and environment pollution. Reactive hazards can be eliminated or minimized by applying Inherently Safer Design (ISD) principles such as "substitute" or "moderate" strategies. However, ISD would not be a feasible option for industry without an efficient methodology for chemical hazard assessment, which provides the technical basis for applying ISD during process design.

In this research, a systematic chemical hazard assessment methodology was developed for assisting the implementation of ISD in the design of inherently safer process. This methodology incorporates the selection of safer chemicals and determination of safer process conditions, which correspond to "substitute" and "moderate" strategies in ISD.

The application of this methodology in conjunction with ISD technique can effectively save the time and investment spent on the process design.

As part of selecting safer chemicals, prediction models were developed for predicting hazardous properties of reactive chemicals. Also, a hazard index was adopted to rate chemicals according to reactive hazards. By combining the prediction models with the hazard index, this research can provide important information on how to select safer chemicals for the processes, which makes the process chemistry inherently safer.

As part of determining safer process conditions, the incompatibility of Methyl Ethyl Ketone Peroxide (MEKPO) with iron oxide was investigated. It was found that iron oxide at low levels has no impact on the reactive hazards of MEKPO as well as the operational safety. However, when iron oxide is beyond 0.3 wt%, it starts to change the kinetics of MEKPO runaway reaction and even the reaction mechanism. As a result, with the presence of a certain level of iron oxide (> 0.3 wt%), iron oxide can intensify the reactive hazards of MEKPO and impose higher risk to process operations. The investigation results can help to determine appropriate materials for fabricating process equipment and safer process conditions.

DEDICATION

To my father: Jianan Lu

my mother: Yuluan Geng

and

my wife: Xiang Li

ACKNOWLEDGEMENTS

I would like to sincerely thank my advisor, Dr. M. Sam Mannan for his guidance, understanding and encouragement during my past five year at Texas A&M University. It was an honor for me to join his research group and work with him to make safety the second nature. He encouraged me not only to figure out fundamentals of problems but also always keep the big picture in mind: how can I apply my research to make industry a safer place to work. He exposed me to various opportunities to make me grow as a researcher as well as a professional ready to join industry. I cannot reach where I am without his consistent support, help and guidance. I am indebted to him more than he knows.

My sincere thanks and appreciation goes to my committee members, Dr. Rayford Gaines Anthony, Dr. Debjyoti Banerjee and Dr. Zhengdong Cheng for their time, effort and advice.

I gratefully acknowledge Dr. Dedy Ng, my former team leader and research scientist with Mary Kay O'Connor Process Safety Center (MKOPSC), for his contribution and friendship. The extensive discussions with him broadened my idea in research and triggered my intellectual maturity. Also, his editorial advice was essential for my journal publications as well as this dissertation.

I owe my most sincere gratitude to Dr. Victor Carreto Vazquez, my current team leader. I have benefited by advice and training from him who also always generously grants me his precious time and effort.

Also, many thanks go to all the member of MKOPSC for their help to make this research project reach this final stage.

Last but not least, I am deeply grateful to my parents and my wife for their love, understanding and support through the years.

NOMENCLATURE

APTAC	Automatic Pressure Tracking Adiabatic Calorimeter
DSC	Differential Scanning Calorimeter
MEKPO	Methyl Ethyl Ketone Peroxide
QSPR	Quantitative Structure-Property Relationship
MLR	Multiple linear regression
PLS	Partial least square
ISD	Inherently safer design
DFT	Density Functional Theory
RHI	Reaction hazard index
TRI	Thermal risk index
THI	Thermal hazard index
HWS	Heat-wait-search
HRS	Heat-ramp-search
ASTM	American Society for Testing and Materials
TST	Transition State Theory
CHETAH	Chemical Engineering Thermodynamics and Hazard Evaluation
CART	Calculated Adiabatic Reaction Temperature
NFPA	National Fire Protection Association
EP	Explosion Potential
TMR	Time to maximum rate

SADT	Self Accelerating Decomposition Temperature
CSB	U.S. Chemical Safety Board

TABLE OF CONTENTS

Page

CHAPTER Page

LIST OF FIGURES

Page

LIST OF TABLES

Page

CHAPTER I

INTRODUCTION

Reactive chemicals are widely used in the chemical industry to manufacture a variety of products due to their capacities to undergo chemical reactions. However, while this kind of capability, also called reactivity, is critical important for the chemical industry, it can also lead to significant risk if reactive hazards associated are not properly understood and controlled. The U.S. chemical safety and hazard investigation board (CSB) reported 167 serious incidents occurred in the United States involving uncontrolled chemical reactivity from 1980 to 2001 [1]. The distribution of these incidents over time is shown in Figure 1.1. These incidents caused 108 fatalities and lots of injuries. Also, these incidents led to a variety of consequences, such as fires, explosions, toxic gas release and spills of hazardous liquids (Figure 1.2), which resulted in hundreds of millions of dollars of properties damage and irreversible impact to the environment.

Facing the great hazards imposed by reactive chemicals to process industries, there is an urgent need to effectively manage these hazards and eliminate them if possible. The hazards associated with reactive chemicals are defined by multiple factors. First, reactive hazards heavily depend on the nature of the chemicals used in processes. Chemicals with higher reactivity normally impose greater hazards to the processes. Also, reactive

---

This dissertation follows the style of *Industrial & Engineering Chemistry Research*.

hazards are affected by various process conditions, such as quantities of chemicals handled, concentrations of chemicals, operating temperature and pressure, and the presence of incompatible substances. Therefore, all these factors contributing to reactive hazards should be taken under consideration when developing the global plan to effectively reduce or manage the reactive hazards in process industries.

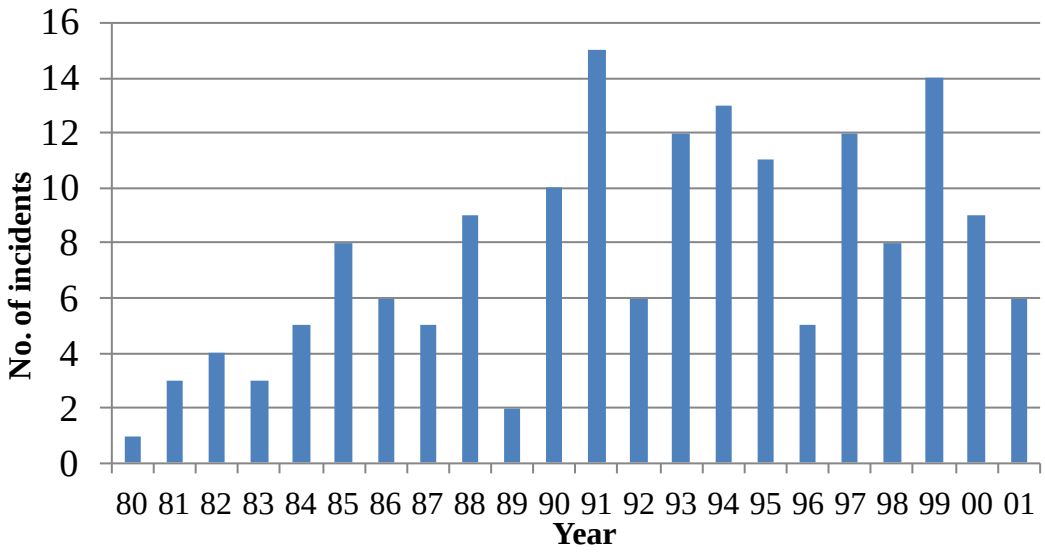

Figure 1.1 Total incidents by year, 1980-2001[data source: CSB report [1]]

An effective approach to handle reactive hazards associated with industrial processes is to apply Inherently Safer Design (ISD) concept in the process design stage. ISD is a fundamentally differently way of thinking about process design. It mainly focuses on the elimination or reduction of a hazard rather than on management and control [2-6]. There are four widely accepted principles for ISD: minimize, substitute, moderate and simplify [2, 7]. These principles are further explained as follows:

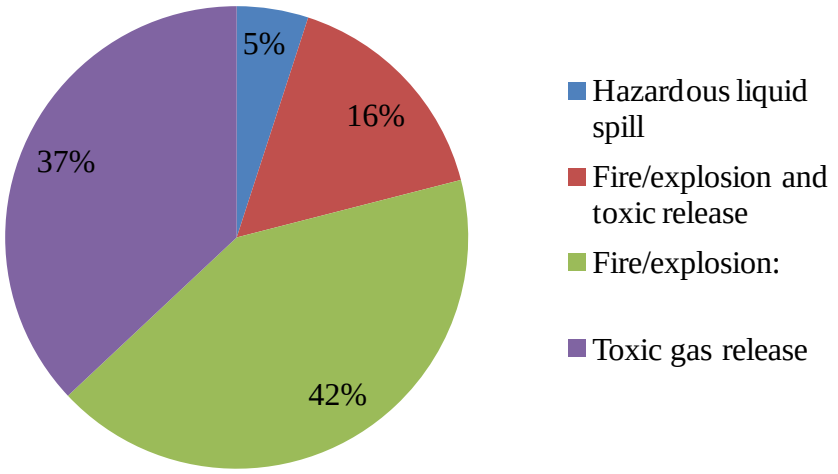

Figure 1.2 Consequences of incidents [data source: CSB report [1]]

Substitute: Replace a hazardous material with a less hazardous substance, e.g., alternative chemistry using less hazardous materials.

Minimize: Use smaller quantities of hazardous substances, e.g., replace bath reactors with efficient continuous reactors, therefore reduce inventory of raw materials and in-process intermediates.

Moderate: Use less hazardous process conditions, a less hazardous form of a material, or facilities which minimize the impact of a release of hazardous material or energy.

Simplify: Design facilities which eliminate unnecessary complexity and make operating errors less likely, and which are forgiving of errors that are made.

ISD is a revolutionary approach to improve the safety performance of process industries by making processes intrinsic safe. It is also a good option in business, which can result in lower capital cost in new plant design, and produce lower operating cost [2]. However,

the application of ISD in the process design stage requires a comprehensive understanding and evaluation of the reactive hazards associated with chemicals. For example, when applying the principle "substitute", it is important to evaluate the reactive hazards of chemicals so the safer candidate can be selected. Also, when applying the principle "moderate" in process design through adopting less hazardous process condition, it is important to understand the effects of process conditions on the reactive hazards associated with chemicals in the process. Therefore, in order to make ISD a feasible approach to design inherently safer process, a chemical hazard methodology is needed to understand and evaluate the reactive hazards associated with chemicals employed in processes, based on which the right decisions can be made on the process design.

An experimental approach is the common practice in chemical hazard assessment, where calorimeters are the popular tools. Calorimeter such as Differential Scanning Calorimeter (DSC) and Reactive System Screening Tool (RSST) can screen chemicals based on reactive hazards [8, 9]. More detailed studies on reactive hazards can be conducted using apparatuses such as adiabatic calorimeters or isothermal calorimeters. Besides calorimeter tests, other types of experimental methods have also been developed for hazard assessment with specific purposes. Self accelerating decomposition temperature (SADT) test was designed to provide the guidance on the safe transport of organic peroxides [10]. The consequence of an explosion scenario caused by reactive chemicals can be studied through a pressure vessel test and lead pipe deformation test [11].

However, these experimental methods require high investment on test apparatus and long test procedures, which become an obstacle for the application of ISD principles in the process design stage.

This research aims at developing an efficient and relative economic methodology in estimating reactive hazards, which can assist the implementation of ISD in the course of process design. This methodology is composed of two major parts: selection of a safer candidate out of a chemical family (*e.g.*, organic peroxides or nitro compounds), and determination of safer process conditions. In the chemical selection part, the prediction models were derived for prediction of hazardous properties and the classification system was developed to classify chemicals according to reactive hazards. In the process conditions determination part, a systematic investigation was performed to quantify the impact of the process contaminant on reactive hazards. Also, some key safety parameters were estimated and analyzed for the purpose of determining safer operating conditions. These two parts of the methodology corresponds to two important ISD principles, "substitute" and "moderate", and therefore serve as the important tools for the important decision-making during the design of inherently safer processes by providing a solid technical basis. The framework of this methodology and its relationship with ISD technique are depicted in Figure 1.3.

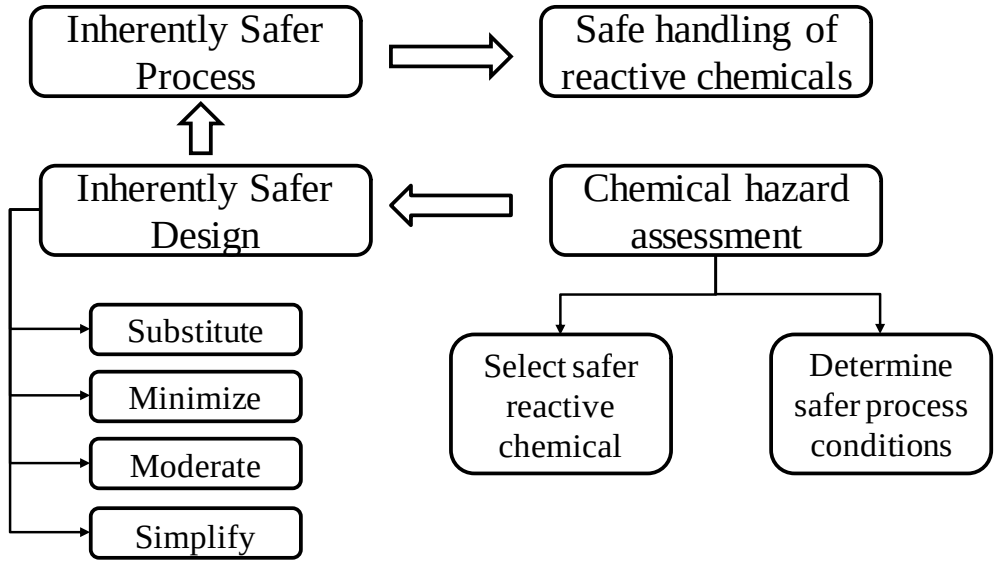

Figure 1.3 Proposed chemical hazard assessment methodology

The hazard evaluation methodology proposed in this research provides a feasible approach to implement ISD to address the issue of reactive hazards in process industries. By utilizing techniques such as molecular and kinetic modeling, the number of experimental tests required for the evaluation of reactive hazards can be minimized. Therefore, it is very helpful for industry especially small companies, where large number of tests is not a feasible option.

In this research, the family of organic peroxides was chosen as an example to develop the methodology of chemical hazard assessment because of their wide usage and great hazard associated with organic peroxides. In the chemical industry, organic peroxides have been widely used in various processes with different purposes. According to the data published by CSB, between 1980 to 2001, 7% of all serious incidents, having

chemical reactivity involved, happened to US process industries are related to organic peroxides [1]. The methodology developed based on organic peroxides can be easily applied for other chemical families.

In this dissertation, the term "safer" is frequently used, indicating the comparison between ISD and regular strategies in the control of process hazards.

Chapter II presents the research methodology employed in this dissertation and all important techniques involved. Chapter III introduces how to select safer chemical according to reactive hazards, using organic peroxides as the chemical family. The content of this chapter includes the development of the prediction models for reactive hazards and the classification system. Chapter IV discusses the determination of safer process condition, including calorimetry test, kinetic analysis and estimation of key safety parameters. Chapter V summarizes this dissertation by stating the conclusions of this research and recommendations for future work.

CHAPTER II

METHODOLOGY AND EXPERIMENTAL SETUP

2.1 Research approach

The research approach of this dissertation is presented in Figure 2.1. This approach is composed of a theoretical part and an experimental part, corresponding to two major objectives - select safer chemicals and determine safer process conditions. In this approach, various techniques such as Quantitative Structure-Property Relationship (QSPR), molecular modeling and kinetic modeling were employed in order to achieve relative high efficiency and low cost in estimating chemical hazards. The details of these methodologies/techniques are introduced in this chapter.

2.2 Quantitative structure property relationship

Quantitative structure property relationship (QSPR) was designed to investigate the relationships between chemical structure and desired properties at the quantum chemistry level. These relationships derived through QSPR can be used to make predictions on the desired properties. QSPR methodology has been successfully applied in the drug design field and has become an important tool in medicinal chemistry [12-15]. In recent years, QSPR methodology has been involved in predicting physical and chemical properties for various types of substances and it has been demonstrated to be an effective approach in this field.

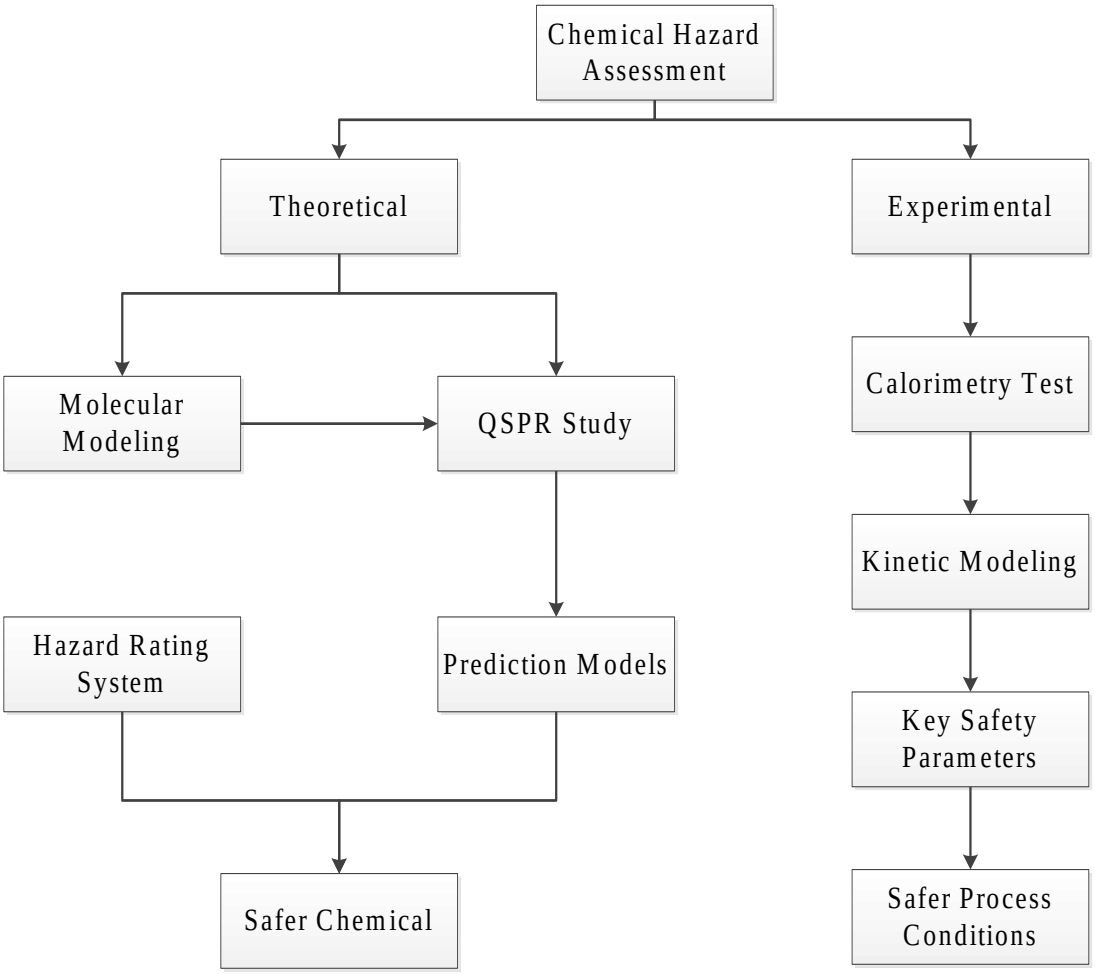

Figure 2.1 Research approach for developing the chemical hazard assessment methodology

The QSPR study starts from the collection of a training set, selection and calculation of descriptors characterizing chemical structures. Then mathematic model regression is performed to derive the correlation between the training set and descriptors. Validation test is also required in the QSPR study to verify the quality of the correlation model. The details of these elements in QSPR study are presented as follows.

2.2.1 Training set collection

Training set in this research includes the data of onset temperature and heat of reaction. The data in the training set were collected from calorimetry test performed on 16 organic peroxides. The details of the calorimetry test are presented in Section 2.5.1.

As seen in Table 3.2, chemicals in the training set covers the most important categories of organic peroxides, such as dialkyl peroxide, peroxyester and hydroperoxide. The ranges of the onset temperature (87 – 170 ^{o}C) and heat of reaction (65 – 664 kJ/mol) data in the training set also cover most of the commercial grade organic peroxides.

2.2.2 Selection of descriptors

In order to achieve good accuracy in predicting hazardous properties, different types of descriptors were employed to characterize the properties of the organic peroxides, including global descriptors, local descriptors, Density Functional Theory (DFT) descriptors and descriptors specifically designed for organic peroxide. All the descriptors applied in QSPR study are listed in Table 2.1 and the description of these descriptors is presented in the following paragraphs.

Table 2.1 List of descriptors used in QSPR study

No.	Type	Descriptor
1	Global descriptor	OB
2		MW
3		DM
4	Local descriptor	Q_O
5		E_a
6		d_{OO}
7		$\angle_{ROOR'}$
8		$\angle_{ROO}$
9	DFT descriptor	ε_{HOMO}
10		ε_{LUMO}
11		η
12		μ
13		ω
14	Peroxide descriptor	C
15		N_P

a. global descriptor

Global descriptors are used to characterize the whole molecule by describing the global properties of the entire structure. In this paper, molecular weight (*MW*) was employed as a global descriptor. Oxygen balance (*OB*), which indicates the degree to which an explosive can be oxidized, was also selected as an important global descriptor [16]. The *OB* can be calculated by using Equation 2-1.

$$OB = \frac{\left[-1600 * (2X + Y/2 - Z)\right]}{MW} \qquad 2\text{-}1$$

where *X*, Y, Z indicate the number of carbon atoms, hydrogen atoms and oxygen atoms respectively.

Dipole moment (*DM*) is another physical property chosen as a global descriptor in this research. It is defined as the amount of force that would be required to flip the molecule in an externally applied electric field.

b. local descriptor

Local descriptors focus on a local area (*e.g.* functional group) within the molecular structure by characterizing its local properties. In this research, relevant properties describing electronic structure, geometry and energy of the peroxide functional group were employed as local descriptors. For organic peroxides, the dissociation of the oxygen-oxygen bond in the peroxide functional group is the first and also rate-determining step of the decomposition reaction [17]. The dissociation energy (E_a) of the oxygen-oxygen bond is the energy barrier for initiating the decomposition reaction, indicating how easily organic peroxides can decompose. Therefore, this parameter was selected as a descriptor for QSPR study. In this dissertation, in order to reduce the simulation work, it was simplify calculated as the energy difference between the products and the reactants (Equation 2-2) [18]. For organic peroxides with multiple

peroxide functional groups, this descriptor was defined as the dissociation energy of the weakest oxygen-oxygen bond.

$$RO-OR' \rightarrow RO^{\bullet} + {}^{\bullet}OR'$$
$$E_a = E(RO^{\bullet}) + E({}^{\bullet}OR') - E(ROOR') \qquad \text{2-2}$$

Some other important properties of the peroxide functional group were also employed as local descriptors, such as oxygen-oxygen bond length (d_{OO}), torsion angle (($\angle_{ROOR'}$), bond angle ($\angle_{ROO}$) and atomic charge of oxygen (Q_O). According to previous research, some of these descriptors can influence the stability of organic peroxide, such as atomic charge of oxygen and torsion angle [19-21]. In this research, the bond angle was calculated as the average of bond angles in the same peroxide functional group. Similarly, the atomic charge of oxygen is also calculated as the average value of two oxygen atoms in the peroxide functional group.

c. Density Functional Theory descriptors

Global descriptors estimated through density functional theory method can be used as the index to characterize the molecular reactivity and have been successful applied in the QSPR study of explosives [22-24]. In this research, some Density Functional Theory (DFT) descriptors were employed in the QSPR study of organic peroxides in order to achieve good accuracy in prediction of reactive hazards.

DFT descriptors selected by this research include energy of lowest unoccupied molecular orbital (ε_{LUMO}) and energy of the highest occupied molecular orbital (ε_{HOMO}). Other DFT descriptors used in this research can be derived from these two descriptors, such as electrophilicity index (ω) [25], chemical potential (μ) [26], and hardness (η) [27]. These descriptors can be calculated using the following equations:

$$\mu = \frac{\left(\varepsilon_{HOMO} + \varepsilon_{LUMO}\right)}{2} \quad \text{2-3}$$

$$\eta = \varepsilon_{LUMO} - \varepsilon_{HOMO} \quad \text{2-4}$$

$$\omega = \frac{\mu^2}{2\eta} \quad \text{2-5}$$

d. Peroxide descriptors

The number of peroxide functional groups (N_P) is a descriptor specifically designed for organic peroxides. According to the experimental observation in this research, it was found that organic peroxides with multiple peroxide functional groups tend to have lower thermal stability and higher heat of reaction. Therefore, in this research, N_P was applied in the QSPR study as a descriptor for the prediction of both onset temperature and heat of reaction.

Concentration of organic peroxides, a non-intrinsic parameter, was employed as the descriptor in the QSPR study because of its contribution to onset temperature. In this study, reactive hazards data in the training set were collected from DSC tests, where the

concentration of organic peroxides varied from 34 to 98 wt%. Through previous research and investigation conducted by MKOPSC, concentration was found to be a factor contributing to the onset temperature of organic peroxide [28, 29]. Therefore, this parameter was also selected as a descriptor in this research.

2.2.3 Regression method

Two mathematic regression methods, partial least square (PLS) method and multiple linear regression (MLR) method, were used in this research to develop the prediction models for reactive hazards. The accuracy of these two methods was then compared to determine the model with the better prediction power. The mathematic regression as well as the validation test were performed using Materials Studio software package [30].

a. Multiple linear regression method

MLR is a relatively simple method and has been widely used in the model regression. This method derives the relationship between explanatory variables and the response variable through linear model fitting. The MLR method implemented in this research incorporates a stepping algorithm, which selects a subset of explanatory variables based on the contribution of these variables to the response variable. Therefore, the final model only includes those explanatory variables significant for the response variable. The general form of the regression model derived using MLR method is shown by Equation 2-6.

$$Y = A_0 + A_1 x_1 + A_2 x_2 + \cdots + A_n X_n \quad \text{2-6}$$

where x_i are the descriptors characterizing molecular properties and Y is the desired hazardous property, A_i are the corresponding regression constants for descriptors.

b. Partial least square method

PLS method uses principal component-like quantities derived from the explanatory variables, also known as latent variables, to perform model regression. These latent variables are orthogonal and are analyzed in conjunction with the response variable to develop the prediction model [31]. The general underlying model of PLS analysis can be depicted by the Equation 2-7 and 2-8.

$$X = TP^T + E \quad \text{2-7}$$

$$Y = TQ^T + F \quad \text{2-8}$$

where X is an $n \times m$ matrix of explanatory variables, Y is an $n \times p$ matrix of response variables, T is a $n \times l$ matrix of latent variable, P and Q are $m \times l$ and $p \times l$ loading matrices, and matrices E and F are the error terms.

Different from MLR method, PLS method does not include the step wise selection of the significant explanatory variables. As the result, all explanatory variables are included in the final regression model developed using PLS method. In order to address this issue, a methodology (Figure 2.2) was proposed here to exclude those insignificant explanatory variables from the final regression model [32, 33]. In this methodology, after each PLS analysis, a sensitivity analysis is performed to determine the significance of explanatory

variables. Based on the sensitivity analysis results, the most insignificant explanatory variable needs to be excluded from the further study. Then, PLS analysis is performed again to develop another regression model. This iteration continues until the R_{CV}^2 of the regression model cannot be improved further (The definition of R_{CV}^2 is introduced in Section 2.2.4).

By eliminating the inter-correlation between explanatory variables, PLS method is a particularly useful tool for data sets with a high level of redundancy due to collinearity or multicollinearity [34]. Since the number of latent variable are normally much less than explanatory variables, PLS method has the capability to handle the case where the number of explanatory variables is comparable to or greater than the number of data in the training set.

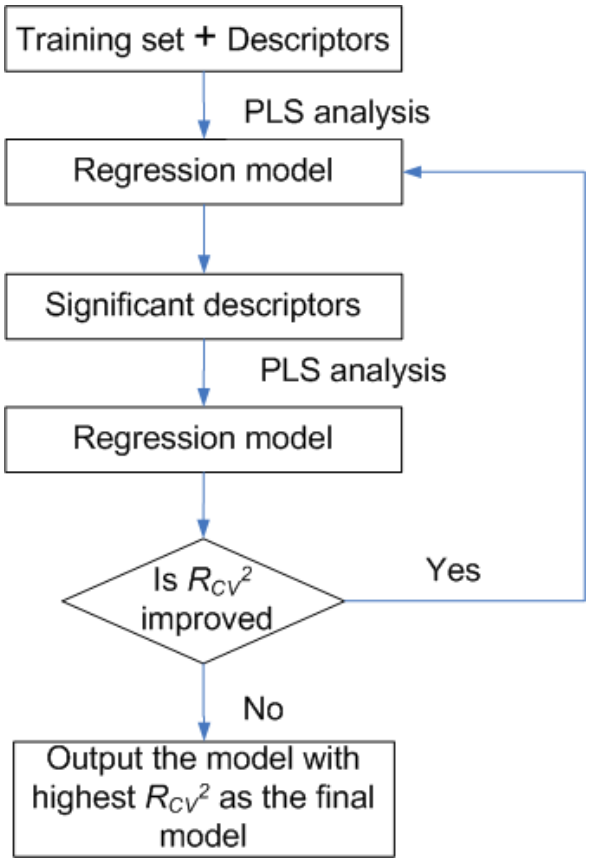

Figure 2.2 PLS analysis procedure

2.2.4 Validation test

In this research, the accuracy of the prediction models was judged by two criteria: coefficient of determination (R^2) and cross validation test (R_{CV}^2).

Coefficient of determination is a parameter used to measure how well a model fits experimental data. It is interpreted as the proportion of response variation "explained" by the regressors in the model. Coefficient can be calculated using the following equations.

$$SS_{tot} = \sum_i (y_i - \bar{y})^2 \quad 2\text{-}9$$

$$SS_{err} = \sum_i (y_i - f_i)^2 \quad 2\text{-}10$$

$$\bar{y} = \frac{1}{n}\sum_1^n y_i \quad 2\text{-}11$$

$$R^2 = 1 - \frac{SS_{err}}{SS_{tot}} \quad 2\text{-}12$$

where y_i is the *ith* experimental data, f_i is the *ith* predicted data and $\bar{y}$ is the mean value of experimental data.

Cross validation is an important statistical tool used in this research to estimate the predictive power of the models. This test can verify whether the regression model represents the desired relationship or just a mathematic fitting. The prediction power of the model is measured by R_{CV}^2, which can be calculated using the following equations.

$$R_{CV}^{\ 2} = 1 - \frac{PRESS}{TSS} \quad 2\text{-}13$$

$$PRESS = \sum_{i=1}^{n} (y_i - y_i')^2 \quad 2\text{-}14$$

$$TSS = \sum_{i=1}^{n} (y_i - \bar{y})^2 \quad 2\text{-}15$$

where y_i is the *ith* experimental data, y_i' is the predicted value for y_i, $\bar{y}$ is the mean value of experimental data.

In the cross validation test, some data (y_i) are removed from the training set before performing model regression. Once the model has been built using the data left in the training set, the data which have been removed can be used as the test set to evaluate the performance of the model on making predictions. This procedure repeats until all the data in the training set have been used as the test set. Here PRESS is prediction sum of squares and TSS is total sum of squares.

2.3 Computational quantum chemistry simulation

Computational quantum chemistry simulation was employed in this research to characterize molecular structure of organic peroxides and estimate values of descriptors. This method is based on the quantum molecular theory, whose core idea is that the motion and distribution of electrons can be described in term of probability distributions or molecular orbitals. This method offers a mathematic description of behavior of electrons, with Schrodinger's equation as the theoretical basis.

A variety of theoretical levels are available for computational quantum chemistry simulation, such as the semi-empirical method, the Hartree-Fock method, the Density Functional Theory method and the Complete Basis Set method. Out of these theoretical levels, Density functional Theory (DFT) method was employed for the molecular simulation in this research. DFT method was developed based on the density functional theory, which assumes the ground state energy of an electron system is a function of the electron charge density. Therefore, this method calculates the molecular energy using electron density instead of wave functions. In the DFT method, the electronic energy is partitioned into several parts and computed separately by functions: electron-nuclear

interaction, kinetic energy, the coulomb repulsion and exchange-correlation term (account for the remainder for the electron-electron interaction). Because of the way to calculate electron correlation, this method can achieve pretty good accuracy with relatively low cost [18]. B3LYP is a common theory level of the DFT method and was utilized in this research [35, 36].

In this research, quantum chemistry simulation was performed using Gaussian-03 program package in the gaseous phase at 298 K and 1 atm pressure [37, 38]. The 6-31G(d) basis set [39, 40], including polarization function for angular flexibility [41], was used for geometry optimization and frequency calculation. Geometry optimization calculation was performed for each chemical to find the optimized molecular structures with the lowest energy. The optimized structure was then verified by frequency calculation results. Each optimized structure was characterized as a local minimum with no imaginary frequency.

2.4 Classification systems for reactive chemicals

In the attempt to classify reactive chemicals based on their reactive hazards, several hazard indices were employed by this research. The classification results of these hazard indices were compared to select the most appropriate one for the family of organic peroxides. The hazard indices involved in this research are introduced as follows.

2.4.1 Reaction hazard index

Reaction hazard index (RHI) is an empiric index developed by D.R [42]. Stull. It utilizes thermodynamic data to evaluate the hazards presented by flammable or explosive. RHI is defined as:

$$RHI = \frac{10T_m}{T_m + 30E_a} \qquad 2\text{-}16$$

where T_m is maximum adiabatic temperature reached by the reaction, E_a is the activation energy of the reaction.

T_m can be calculated using the following equation.

$$T_m = T_0 + \frac{\Delta H_r}{C_P} \qquad 2\text{-}17$$

where T_0 is the onset temperature of the decomposition reaction, ΔH_r is the heat of reaction and C_P is the heat capacity of the reaction system.

E_a can be estimated by solving Equation 2.18

$$\frac{dT}{dt} = -\frac{\Delta H_r k_B T}{C_P h} \exp(-\frac{E_a}{RT}) \qquad 2\text{-}18$$

where k_B is the Boltzmann's factor, h is Planck's constant, T is the temperature of the reaction system and R is the gas constant. When calculating E_a, T is defined as T_0, and dT/dt is defined as 0.1 ° C/min, a common criterion for detecting an exothermic reaction.

2.4.2 Thermal risk index

Thermal risk index (TRI) is a rating system for reactive chemicals developed by Wang *et al.* [43]. It integrates the concept of risk, which is a function of probability and consequence, into the rating system. This rating system classifies chemicals based on two parameters: heat of reaction and time to maximum rate. These two parameters indicate consequence and probability respectively. The definition of TRI is shown as follows:

$$TRI = \left(\frac{\Delta H_r}{\Delta H_r'}\right) * \left(\frac{TMR_{ad}'}{TMR_{ad}}\right) \qquad 2\text{-}19$$

where TMR_{ad} is time to maximum rate at adiabatic condition, ΔH_r is heat of reaction. $\Delta H_r'$ and TMR_{ad}' are parameters of the reference chemical.

For the reaction with relative high activation energy, TMR_{ad} can be calculated using Equation 2-20 [43].

$$TMR_{ad} = \frac{C_P R T^2}{q E_a} \qquad 2\text{-}20$$

where q is the heat release rate at temperature T, E_a is the activation energy, and C_P is the heat capacity of the reaction system.

2.4.3 Thermal hazard index

Thermal hazard index (THI) is designed to rate reactive chemicals when multiple safety parameters need to be considered [44]. In THI, the relative significance of each safety parameters considered in rating system is quantified by the hazardous index W. The general form to calculate W is shown by Equation 2-21.

$$W_i = 100 \cdot \frac{x_i - x_{i,\min}}{x_{i,\max} - x_{i,\min}} \qquad 2\text{-}21$$

where W_i is the hazardous index of parameter i, x_i is the value of parameter i, $x_{i,min}$ and $x_{i,max}$ are the minimum and maximum value of parameter i respectively.

The rating score of THI is calculated based on hazardous indices and their weight factors (y_i) (Equation 2-22).

$$THI = \sum_{i=1}^{n} y_i \cdot W_i \qquad 2\text{-}22$$

where y_i is the weight factor of hazardous index W_i.

In this research, onset temperature and heat of reaction are considered to be equally important to reactive hazards. Therefore, y_i is defined as 1 for these two hazardous indices.

2.5 Experimental setup

2.5.1 Differential Scanning Calorimeter

Differential Scanning Calorimeter (DSC) is an important screening test apparatus, which measures a number of characteristic properties of the sample materials. It has been used to study subjects such as crystallization, glass transition, oxidation and other chemical reactions. In the process safety area, it has been widely used as a screening tool for hazardous materials. It can determine whether a material undergoes an endothermic or exothermic reaction [45].

The schematic of DSC is shown in Figure 2.3. DSC is equipped with two independent heaters used to heat a sample and a reference respectively. During the test run, a sample and a reference are placed in two identical sample pans and subjected to a continuously increasing temperature. Meanwhile, heat is added to the reference to maintain it at the same temperature as the sample. This added heat compensates for the heat loss or gained as a consequence of an overall endothermic or exothermic reaction.

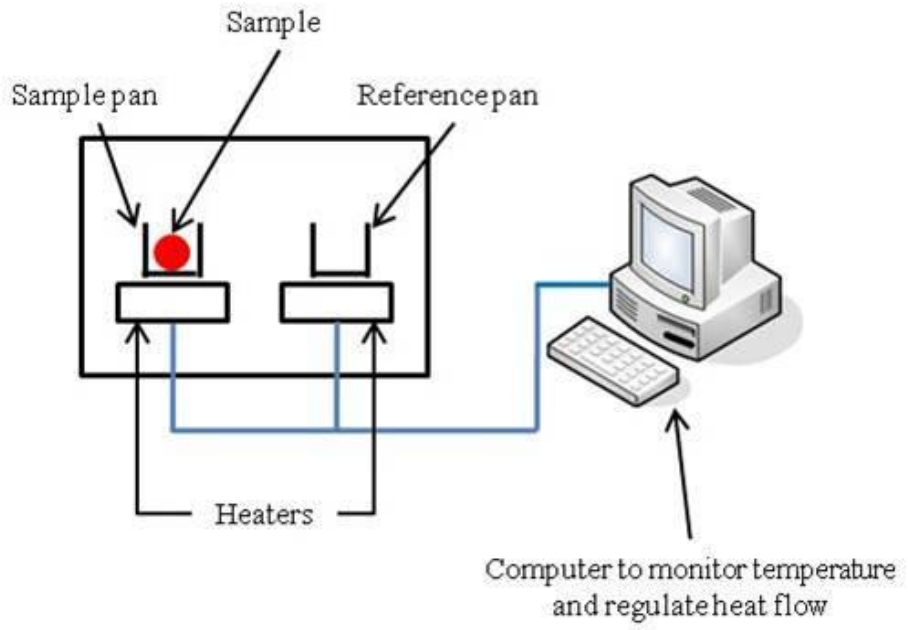

Figure 2.3 Schematic of DSC

A Pyris 1 DSC from PerkinElmer was used in this research to collect the data of reactive hazards for organic peroxides. Stainless steel sample pans with O-rings were used to contain sample material because of the high internal pressure during runaway reaction. When running tests, nitrogen was used to purge the DSC vessel. During each experiment, the sample was heated from 30 to 60 ^{o}C at the heating rate of 10 ^{o}C min^{-1}, and then the heating rate was switched to 4 ^{o}C min^{-1} from 60 to 250 ^{o}C. Onset temperature and heat of reaction were determined by Pyris software based on the output data of DSC tests. Each sample was tested three times to establish reproducibility.

2.5.2 Automatic Pressure Tracking Adiabatic Calorimeter

a. Apparatus description

Automatic Pressure Tracking Adiabatic Calorimeter (APTAC) is an important apparatus used in this research to perform a calorimetry study. It is an adiabatic closed-cell reaction calorimeter developed by Arthur D. Little. Because near-adiabatic conditions are normally achieved by processes in commercial scale, APTAC is very useful in simulating runaway reactions in real industrial processes. In this research, APTAC is used to study the impact of process conditions on the reactive hazards of organic peroxides.

In APTAC, the sample material is placed in a small spherical test cell with a volume of around 130 ml, which can be made of glass, stainless steel or titanium. This test cell is surrounded by four main heaters: bottom, top, side, and tube heaters. These heaters can compensate for the heat loss from the test call and therefore maintain the adiabatic environment. The heaters and the reaction vessel are insulated and placed in a 500-ml pressure vessel which can be pressurized up to 2,000 psig. Within the pressure vessel space, seven type-N thermocouples continuously measure the temperature of four heaters, nitrogen gas, sample material and the wall of the test cell. This temperature measurement system enables continuous monitoring and control of adiabatic conditions. During the test, nitrogen gas is injected into the pressure vessel at a rate sufficient to keep a low differential pressure (normally less than 10 psi) across the wall of the test cell. Because of this pressure compensation function, APTAC can be operated under

high pressure and high pressure rate without the rupture of the test cell. The schematic of APTAC is shown in Figure 2.4.

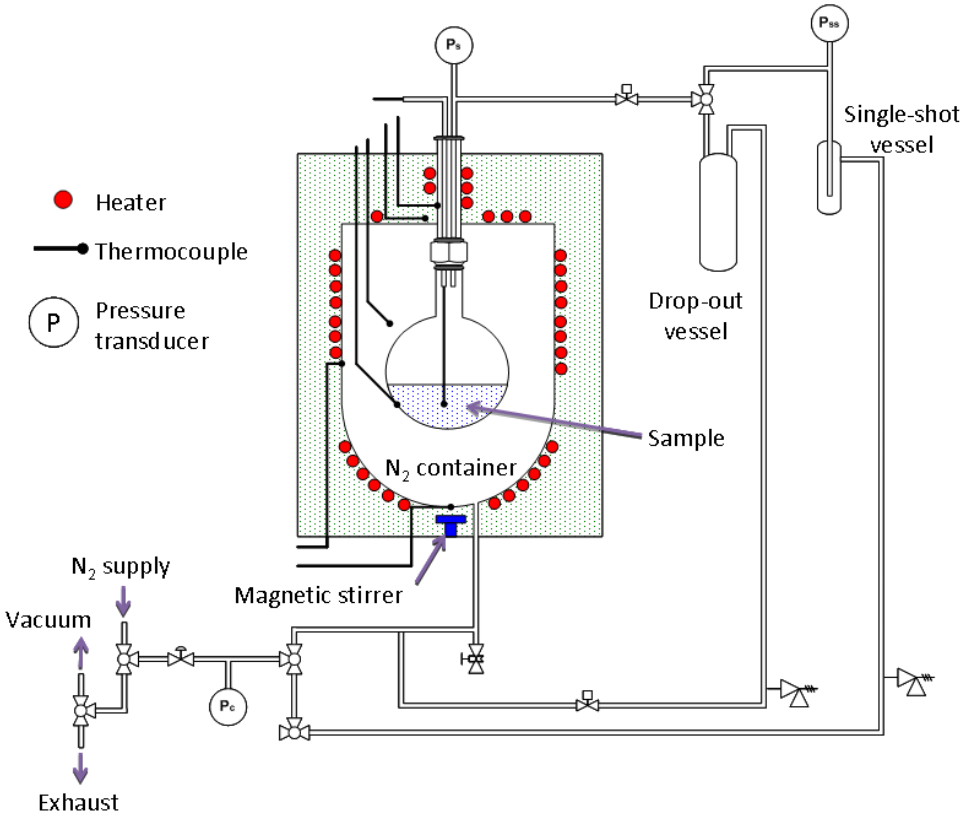

Figure 2.4 Schematic of APTAC [with the permission from Elsevier] [46]

b. Operation mode

APTAC allows operation under different modes such as heat-wait-search (HWS), heat-ramp-search (HRS) and isothermal. These operation modes are introduced in detail as follows.

Under HWS mode, the sample material is heated in small steps following a predefined procedure. At each step, when the sample temperature reaches and stabilizes at the target temperature, the exotherm search is performed. If the self-heating rate of the sample material exceeds the pre-defined criteria, the heating mode shifts to an adiabatic mode. After reaching the maximum temperature of the reaction, the HWS mode switches back for further exotherm search until limits of time or temperature are exceeded where sample is cooled down to the pre-defined value. The typical temperature and pressure behaviors under HWS mode are presented in Figure 2.5.

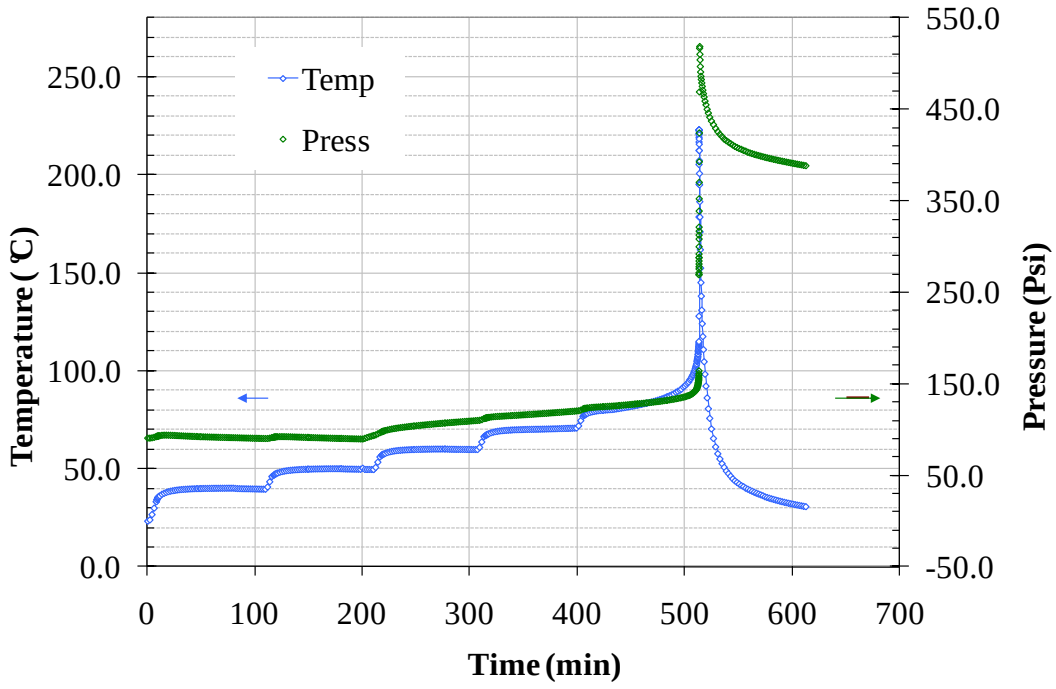

Figure 2.5 Temperature-pressure profiles under HWS mode

Under heat ramp mode, the sample material is heated at a constant heating rate until the end temperature is achieved. In isothermal mode, the sample material is heated to the pre-determined temperature and maintained there until the time limit is reached.

In this research, calorimetry tests were performed under HWS mode to study the impact of process contaminant on reactive hazards associated with organic peroxides.

c. Quality of experimental data

In order to maintain high quality of APTAC measurement, a series of calibration tests were performed in this research to ensure the reproducibility and accuracy of calorimetry test.

It is very important to keep the test cell leak tight during the test run. A small leak from the test cell can lead to loss of ingredients and significant heat loss as a result of evaporative cooling and cause very large effects on the test results. At the start of each test, a leak detection test was performed to exam the sealability of the test cell. During this test, the test cell is pressurized to 200 psi and monitored for a 20 min period. The apparatus is considered to be leak tight if the pressure change is between -0.01 to 0.01 psi/min. This leak detection is also required each time a tube or a thermocouple is replaced.

The relative calibration was performed to ensure that the sample, test cell wall, and nitrogen thermocouples provide the same temperature reading to data logging system

when reaching the same temperature. Any small deviation between these temperature readings can lead to substantial error. Experience has shown that at modest pressure within the containment vessel, 1^{o}C temperature difference between nitrogen and sample thermocouple will lead to a drift rate of about 0.1^{o}C/min [47]. This relative calibration test can minimize the potential for either positive or negative drift when the machine is running under exotherm search mode.

The relative calibration test was performed using an empty and clean test cell and operated following the calibration wizard integrated in APTAC control interface. In this research, the initial pressure in the test cell was set as 500 psi for relative calibration test. The calibration test started from 50^{o}C and ended at 410^{o}C at the heating rate of 4^{o}C/min. After completing the calibration, the thermocouple offsets at 50^{o}C intervals between 50 and 400^{o}C were automatically stored. The offsets data were subsequently used by the control program to adjust the sample thermocouple when running a standard experiment.

Absolute calibration for thermocouple was performed to ensure the accuracy of temperature reading. In this research, absolute calibration was performed through ice point check at 0^{o}C, which adjusts the thermocouple zero point by placing the nitrogen, wall and sample thermocouple in the ice/water mixture.

The pressure transducers were calibrated by measuring the water vapor pressure curve. This calibration test was performed by heating 50 g pure water in a clean, evacuated test

cell and then cooled down to the ambient conditions. The experimental pressure curve was then compared against experimental stem tables in the reference [48].

d. Experimental setup

In this research, in order to avoid any possible contamination, a glass cell was used in this research as the test cell.

35 wt% MEKPO (diluted in 2,2,4-trimethyl-1,3-pentanediol diisobutyrate) purchased from the Sigma-Aldrich and 99.999 wt% iron oxide purchased from Acros Organics were used in this research. The particle size of iron oxide is 100 mesh.

2.6 Calorimetry data analysis

2.6.1 Kinetic modeling

Based on the experimental data obtained from calorimetry test, kinetic modeling was performed to study the kinetics of runaway reactions, estimate important kinetic parameters and develop kinetic models which can simulate the runaway reaction process under various conditions. Two kinetic models were used in this research: nth order reaction model and autocatalytic reaction model.

a. nth order reaction

Assuming the closed reaction system, constant volume, ideal thermal isolation and negligible pressure effect, for nth order reaction with single reactant, the reaction rate can be expressed as follows:

$$\frac{dC}{dt} = r = -kC^n \qquad 2\text{-}23$$

where, k is the reaction rate constant, n is the order of reaction, C is the reactant contraction at time t.

For an exothermic reaction in an adiabatic environment, it is believed that the conversion rate is proportional to the temperature increase. Therefore, the following equation can be obtained.

$$C = \frac{T_{\max} - T}{T_{\max} - T_0} C_0 \qquad 2\text{-}24$$

where, C_0 is the initial concentration of the reactant and T_0 is the initial temperature of the reaction system.

Here the maximum adiabatic temperature increase, ΔT_{ad}, is defined by Equation 2-25.

$$\Delta T_{ad} = T_{\max} - T_0 \qquad 2\text{-}25$$

Heat of reaction can be calculated as a function of ΔT_{ad}:

By differentiating Equation 2-24 with respect to t and then combining it with Equation 2-23, the following equation is obtained.

$$\frac{dT}{dt} = k\left(\frac{T_{\max} - T}{\Delta T_{ad}}\right)^n \Delta T_{ad} C_0^{\,n-1} \qquad 2\text{-}26$$

This equation can be rearranged as:

$$k^* = kC_0^{\,n-1}\frac{dT}{dt}\frac{(\Delta T_{ad})^{n-1}}{(T_{\max} - T)^n} \qquad 2\text{-}27$$

where, k^* is a pseudo 0^{th} order rate constant. This equation allows us to calculate k^* based on the data of dT/dt, T_{max}, T and ΔT_{ad}, which can be obtained from calorimetry tests.

It is known that the reaction rate constant follows Arrhenius equation:

$$k = A\exp\left(\frac{-E_A}{RT}\right) \qquad 2\text{-}28$$

where A is the frequency factor, E_a is the activation energy, and R is the gas constant. The following equation can be derived by substituting Equation 2-28 into Equation 2-27.

$$\log(k^*) = \log\left(AC_0^{\,n-1}\right) - \frac{E_a}{RT} \qquad 2\text{-}29$$

According to this equation, plotting $logk^*$ versus $1/T$ can yield a straight line. The slope of the straight line represents E_a/R and its intercept represents $log(AC_0^{n-1})$. Based on the slope and intercept, E_a and A can be calculated.

b. autocatalytic reaction

Autocatalytic reactions are those in which at least one product also serves as a reactant. This type of reaction can be simply depicted as follows. In this reaction, B is the product but also acts as the reactant.

$$A + B \leftrightarrow 2B$$

According to the experimental observation, the generalized autocatalytic reaction model was employed for the simple single-stage reaction. The reaction model is shown as follows [49].

$$\frac{d\alpha}{dt} = k(1-\alpha)^{n_1}(\alpha^{n_2} + z) \qquad 2\text{-}30$$

where, α is conversion rate, n_1 and n_2 are reaction orders, z is a constant.

Because the reaction rate is a function of both reactant and product, the reaction rate of autocatalytic reaction increases with the increase of conversion rate.

2.6.2 Model fitting

Identification of a kinetic reaction model is an important approach in the investigation of reactive hazards for reactive chemicals. The kinetic reaction model can be used for the simulation of runaway reactions under various conditions and the estimation of key safety parameters in process operation.

Non-linear optimization method is a general approach in selecting the kinetic model and evaluating kinetic parameters and was employed in this research. This method ensures the best fit to the experimental data by minimizing the measure of residuals between experimental and simulated responses. The majority of nonlinear optimization algorithms are based on the Least Square Method (LSM), which uses the sum of squares of residuals as the measure. In this research, the following objective function is employed to perform the model fitting.

$$SS(\overline{P}) = \frac{1}{2}\sum_{(i)}\left(\frac{Y\exp(t_i) - Ysim(\overline{P}, t_i)}{\varepsilon_i}\right)^2 \rightarrow \min = SS(\overline{P_r}) \qquad 2\text{-}31$$

where, $Y_{exp}(t_i)$ is the experimental observation at time t_i, $Y_{sim}(\overline{P}, t_i)$ is the simulated response at t_i, ε_i is the experimental error for the *ith* observation, SS($\overline{P}$) is the weighted sum of the squares of the residuals.

In this research, all the modeling fitting and simulation of runaway reactions was performed using MATLAB.

2.6.3 Thermal inertia

In the APTAC test, even though the adiabatic environment is maintained for the reaction system, part of the heat generated by the reaction is used to heat up the test cell. Energy balance of the system is established to describe the heat loss in calorimeter test (Equation 2-32).

$$m_s C_s \Delta T_{ad,adj} = (m_s C_s + m_c C_c)\Delta T_{ad,meas} \quad 2\text{-}32$$

where, m_s is sample mass, C_s is heat capacity of the sample, C_c is heat capacity of test cell, $\Delta T_{ad,meas}$ is measured adiabatic temperature rise of the overall system and $\Delta T_{ad,adj}$: adjusted adiabatic temperature rise.

Thermal inertia is a term used to describe the property related to thermal conductivity and volumetric capacity of the test cell, which cause the heat loss in a calorimetry test. The thermal inertia factor, ϕ, is defined as:

$$\phi = \frac{(m_s C_s) + (m_c C_c)}{(m_s C_s)} \quad 2\text{-}33$$

This factor can be used to perform the conversion between the adiabatic temperature rise measured and the adjusted adiabatic temperature rise (Equation 2-34). Under perfect adiabatic condition, ϕ equals to one, indicating no heat absorption by the test cell. The more ϕ approaches 1, the closer the reaction system is to the adiabatic condition.

$$\Delta T_{ad,adj} = \phi \Delta T_{ad,meas} \quad 2\text{-}34$$

The following equation can be derived by rearranging Equation 2-34. This equation can convert the temperature between systems with different ϕ. By assigning 1 to ϕ_2, the temperature measured by APTAC can be converted to temperature in the adiabatic condition.

$$T_2 = T_{O,2} + \left(\frac{\phi_1}{\phi_2}\right)\left(T_1 - T_{O,1}\right) \qquad 2\text{-}35$$

Self heating rate can also be converted to the data in adiabatic condition by applying thermal inertia factor. Since Equation 2-34 is valid for any time interval, the following equation can be derived:

$$\left(\frac{dT}{dt}\right)_{ad} = \phi\left(\frac{dT}{dt}\right)_{meas} \qquad 2\text{-}36$$

where $(dT/dt)_{ad}$ is the self-heating rate in adiabatic condition and $(dT/dt)_{meas}$ is the measured self-heating rate in calorimetry test.

2.6.4 Non-condensable gas generation

In many cases, the gas generated during the runaway reaction significantly contributes to the pressure hazards. The non-condensable gas generation rate can be calculated based on the calorimetry test results.

Normally, when calculating non-condensable gas generation based on the measured pressure data, the vapor pressure in the reaction system needs to be taken under

consideration. The vapor pressure for the reaction system can be calculated with the Antoine equation [50]. However, for a runaway reaction, the contribution of vapor pressure to overall pressure of the reaction system is negligible compared with other factors such as thermal expansion and gas production. Therefore, in this research, non-condensable gas generation rate can be calculated using Equation 2-37. This equation estimates the non-condensable gas generation rate by removing the thermal expansion effect from the measured overall pressure rate of the reaction system.

$$\left(\frac{dn}{dt}\right)=\left(\frac{V}{RT}\right)\left[\left(\frac{dP}{dt}\right)-\left(\frac{P}{T}\right)\left(\frac{dT}{dt}\right)\right] \qquad 2\text{-}37$$

CHAPTER III

SELECTION OF SAFER REACTIVE CHEMICALS

3.1 Introduction

Selecting the safer chemical is the initial and critical important step in the design of the intensely safer process. This step is used to ensure that the process is inherently safe from the perspective of process chemistry. This strategy is an important lessons learned from Bhopal incident. This incident could be prevented if the alternative manufacturing process was employed, which does not use methyl isocyanate (MIC) as intermediate [5, 51]. The right process chemistry can eliminate the potential hazards in the conceptual design stage.

The selection of safer reactive chemical requires the collecting data about the reactive hazards data and a classification system which can classify reactive chemicals based on reactive hazards. This selection could cause a lot of work especially when the selection needs to be made out of a large number of chemicals. Therefore, an efficient and economic approach is needed to perform the selection of safer reactive chemical, which can assist the application of ISD principles in the process design.

The common practice for the collection of reactive hazards data is through different kinds of experiments. However, as mentioned in the Chapter I, the application of this approach is limited by high investment on test apparatus and lengthy test procedure.

Since the chemical reactivity is significantly affected by the molecular structure, as the alternative approach to estimate reactive hazards, investigation was performed in this research on how to predict hazardous properties of organic peroxides based on the molecular structure. Compared with the experimental approach, this methodology requires much less experiment and therefore is a feasible option for the design of inherently safer process.

A number of early works have already been reported in the field of prediction of hazardous properties. Rules of thumb are the simplest possible methods for reactivity screening, which can identify hazardous materials for further analysis. In this method, chemicals containing functional groups such as nitro group and peroxide functional group can be considered potentially reactive [52]. Also, some programs have been developed for hazard prediction and screening. CHETAH is a program available from American Society for Testing and Materials (ASTM). This program employs "Benson group contribution method" to estimate important hazardous properties such as heat of formation and heat of combustion [53]. CART is a another tool used to estimate adiabatic temperature rise and to classify chemicals based on this parameter [54]. In another work done by Saraf *et al*, computational chemistry techniques were combined with Transition State Theory (TST) for predicting calorimetry data of aromatic nitro compounds [55].

One promising method for estimating reactive hazards is Quantitative Structure-Property Relationship (QSPR). This method employs statistic methodology to screen molecular

properties contributing to desired properties and further derive the correlations between molecular properties and desired properties. Compared with other methods, QSPR can be customized to integrate any molecular property into the prediction model development and therefore is more advantageous in predicting complicated properties such as chemical reactivity. In this research, QSPR was used to reveal the relationships between molecular structure and runaway reaction at the quantum chemistry level and develop prediction models for the desired hazardous properties. The models derived in this research can be used to collect the data of reactive hazards in an efficient way.

Theoretical work has been done to study the molecular structure of organic peroxides and their effects on desired properties. Such previous work serves as the technical basis for the QSPR study on organic peroxides. Lobunez *et al*. studied electric moment of diacyl peroxides and correlated it with conformational properties [56]. Similar work was done by Verderame *et al.* on peroxyesters [57]. Theoretical calculation was conducted by Litinskii to study the quantum properties of some organic peroxide including diacyl peroxides. In his research, some properties such as atomic charge of oxygen in peroxide functional group were identified to correlate with the stability of organic peroxides [58]. Kikuchi studied electronic structure and conformational structure of benzoyl peroxide through quantum calculation [59].

In this study, based on the experimental data collected from DSC tests and previous research on molecular structure of organic peroxides, QSPR study was performed to

develop prediction models for the hazardous properties of organic peroxides. Different regression methods were employed in order to achieve the good accuracy of the prediction results.

After the collection of hazardous properties, a rating system is needed to classify chemicals according to the reactive hazards. The classification of reactive chemicals can help industry to select safer chemical from the class with low hazard rating. One popular rating system for reactive chemical is NFPA 704 [60], which rates reactive hazards of chemicals in the range from 0 to 4. However, this rating system is not suitable for some chemical families such as organic peroxides. According to the data presented in Table 3.1, even though 2-butanone peroxide and cumene hydroperoxide present great difference in thermal stability and heat of reaction, they are rated as the same class by NFPA 704 rating system. This example indicates that NFPA 704 is not sensitive enough for organic peroxides and a more suitable rating system needs to be developed.

Table 3.1 NFPA rating for selected organic peroxides

Chemical	T_0 (^{o}C)	ΔH_r (kJ/mol)	NFPA
2-butanone peroxide	87	483	3
Cumene hydroperoxide	170	253	3

In this research, several types of hazard indices proposed by other researchers were applied on organic peroxides. The rating results were verified in order to determine the one most suitable for organic peroxides. By combing this rating system with the prediction models proposed in this research, this research provides industry an efficient and economic approach to select safer chemical for the process and offers more quantitative information for the decision-making during the design of inherently safer process.

Part of the data in the chapter has been published in *Industrial & Engineering Chemistry Research* (volume 50, issue 3).

3.2 Results

3.2.1 Correlation analysis

Before conducting QSPR study on organic peroxides, a correlation analysis was performed to study the inter-correlation between descriptors. This analysis was used to identify descriptors highly correlated with others, which were excluded from further model regression in order to reduce the inter-correlation between explanatory variables.

According to the correlation coefficient (r) calculated, ε_{LUMO} and η were excluded from QSPR study because of their high correlations with other descriptors ($|r| > 0.9$).

3.2.2 Development of prediction models

a. Onset temperature

All the descriptors listed in Table 2.1 were calculated for 16 organic peroxides using Gaussian 03 software package and the calculation results were presented in Appendix A. After excluding those highly correlated descriptors, all the remaining descriptors selected for the QSPR study of onset temperature were applied to the regression analysis using MLR and PLS methods.

i). MLR method

Through the MLR analysis, a linear model was obtained for the prediction of the onset temperature with four descriptors (Equation 3-1). This regression model is a function of dissociation energy, bond length of the oxygen-oxygen bond, number of peroxide function group and molecular hardness.

$$T_0 = 1777.92 * E_a + 657.65 * d_{OO} - 8.70 * N_P - 202.41 * \eta - 819.65 \qquad 3\text{-}1$$

The calculated values of onset temperature using the prediction model are presented in Table 3.2. The predicted onset temperature was plotted versus experimental data in Figure 3.1 as the overall depiction of MLR analysis results. The validation test results for this prediction model are presented in Table 3.3.

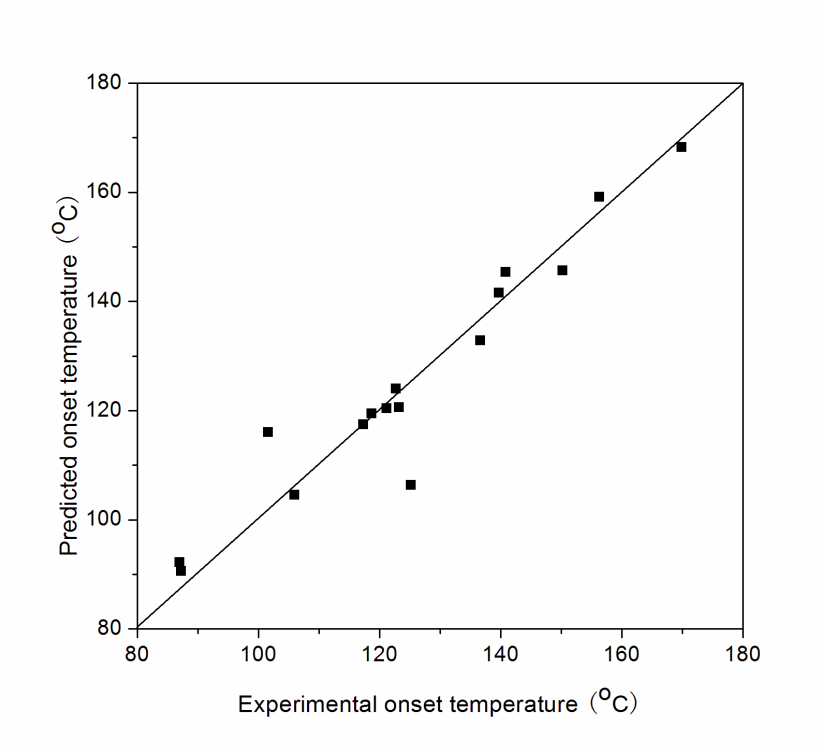

Figure 3.1 Scattering diagram for experimental and calculated onset temperature using MRL model

According to the data presented in Figure 3.1 and Table 3.3, the prediction model derived using MLR method presents a pretty good linear fitting with the experimentally detected onset temperature with R^2 value of 0.916. This model is also proven to be statistically significant according to the *F* value. However, the cross validation test result (R_{CV}^2=0.108) indicates that this model is quite weak in prediction power. This low prediction power implies the existence of over-fitting phenomena in MLR analysis. Over-fitting normally occurs when the model is very complex, such as employing too many parameters relative to the number of observations. In the case of over-fitting, the regression model describes random error rather than the underlying relationship. In this

research, the over-fitting phenomena should be caused by the relatively large number of descriptors (13 descriptors) compared to the limited training set size (16 data). Therefore, the model obtained using MLR method cannot be used in predicting the onset temperature of organic peroxides due to the poor prediction power.

Table 3.2 Experimental and calculated onset temperature of organic peroxides

No.	Substance	T_0 (experimental) (ºC)	T_0 (predicted) (ºC)	
			MLR	PLS
1	Tert-butyl cumyl peroxide	150.3	145.7	145.0
2	Dicumyl peroxide	140.8	145.3	143.0
3	Di-tert-butyl peroxide	139.7	141.6	145.9
4	Benzoyl peroxide	105.9	104.5	106.4
5	Lauroy peroxide	87.0	92.2	90.0
6	Tert-butylperoxy benzoate	122.7	124.0	125.0
7	Tert-butyl peroxyacetate	101.6	116.0	106.6
8	11-bis(t-butylperoxy)-335-timethylclohexane	118.7	119.4	125.4
9	2,2-Bis(t-butylperoxy)butane	123.2	120.6	119.0
10	2,5-Bis(t-butylperoxy)-2,5-dimethylhexane	136.7	132.8	132.5
11	2,4-Pentanedione peroxide	117.3	117.4	114.7
12	Cumene hydroperoxide	169.9	168.2	171.4
13	Tert-butyl(peroxy 2-ethyl-hexyl) carbonate	125.2	106.3	113.7
14	1,1-Di(tert-butylperoxy)cyclohexane	121.2	120.4	118.0
15	2-butanone peroxide	87.2	90.6	90.6
16	Tert-butyl hydroperoxide	156.3	159.1	156.6

Table 3.3 Validation of the prediction model for onset temperature

	R	R^2	R_{CV}^2	F
MLR	0.957	0.916	0.108	29.932
PLS	0.978	0.957	0.859	-

ii). PLS method

As presented in the Section 2.2.3b, PLS method is pretty useful in handling the case with the large number of *x* variables and relative small training set size. Therefore, a mathematic regression was performed again using PLS method to derive the prediction model for onset temperature. Following the procedure presented in Figure 2.2, the final prediction model was obtained after several iterations when R_{CV}^2 cannot be further improved (Equation 3-2). This prediction model is composed of all 13 descriptors employed in the regression analysis. The calculated onset temperature is listed in Table 3.2 and plotted against experimental data in Figure 3.2. The results of the validation test are presented in Table 3.3.

$$\begin{aligned} T_0 &= 55.99 * Q_O + 730.18 * E_a - 29.72 * d_{OO} - 5.35 * N_P - 0.08 * OB \\ &- 0.04 * MW + 3.30 * DM + 0.11 * \angle_{ROOR'} - 3.82 * \angle_{ROO} + 202.75 \\ &* \varepsilon_{HOMO} - 118.01 * \eta - 2.73 * \omega + 23.58 * C + 626.61 \end{aligned} \qquad 3\text{-}2$$

The prediction model derived using PLS method shows a good agreement with the experimental data (R^2=0.957). Also, this model presents adequate prediction power according to cross validation test results (R_{CV}^2=0.859). Compared with MLR method,

PLS analysis shows great capability in handling the over-fitting risk and great improvement on the prediction power of the regression model. According to the validation test results, the prediction model obtained through PLS analysis was adopted for predicting the onset temperature of organic peroxides.

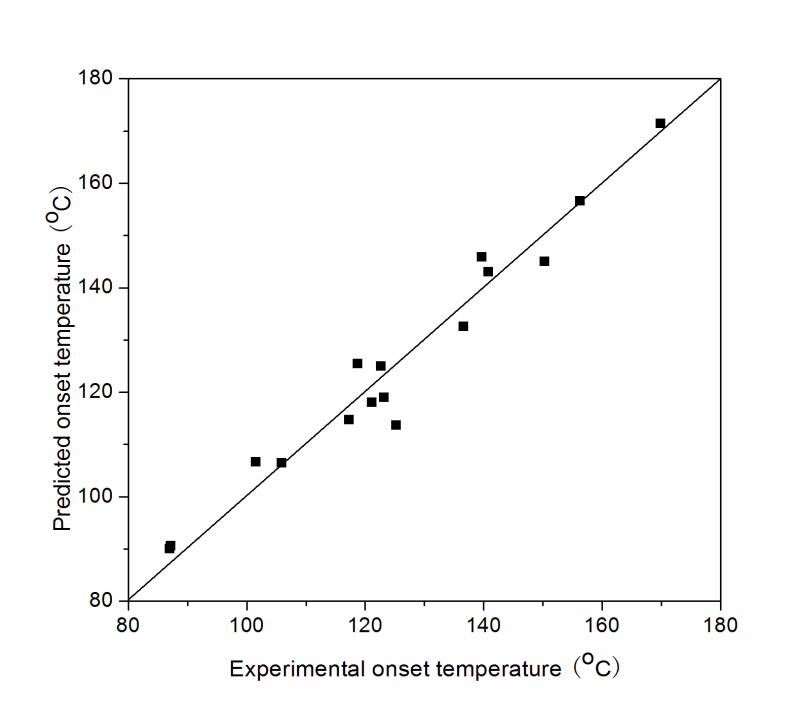

Figure 3.2 Scattering diagram for experimental and calculated onset temperature using PLS model

Based on the prediction model obtained, sensitivity analysis was performed to investigation the contribution of each descriptor to the onset temperature of organic peroxides. In the sensitivity analysis, standardized coefficient can be calculated using Equation 3-3, which gives an immediate indication of the relative significance of each descriptor in the final prediction model. The significance of the descriptor to the onset

temperature is proportional to the absolute vale of standardized coefficient. According to the calculated standardized coefficients listed in Table 3.4, out of the 13 descriptors, bond angle in the peroxide functional group and dissociation energy of oxygen-oxygen bond are two most significant factors contributing to onset temperature.

$$Y = A_0 + A_1 X_1 + A_2 X_2 + \cdots\cdots + A_n X_n$$

$$B_i = \frac{\delta_{x_i}}{\delta_y} A_i \qquad 3\text{-}3$$

Table 3.4 Sensitivity analysis of the onset temperature prediction model obtained through PLS analysis

Descriptor	Coefficient	Standardized coefficient
Q_O	55.987	0.158
E_a	730.178	0.358
d_{OO}	-29.723	-0.019
N_P	-5.349	-0.142
OB	-0.086	-0.145
MW	-0.035	-0.113
DM	3.301	0.108
$\angle_{ROOR'}$	0.107	0.121
$\angle_{ROO}$	-3.824	-0.315
ε_{HOMO}	202.752	0.173
η	-118.013	-0.144
ω	-2.735	-0.002
C	23.580	0.233

b. Heat of reaction

Similarly, QSPR study was performed on heat of reaction of organic peroxides by using both MLR and PLS methods. Besides the highly correlated descriptors, concentration of organic peroxides, the descriptor specifically designed for onset temperature, was excluded in the QSPR study on heat of reaction.

i). MLR

Through mathematic regression using MLR method, the prediction model for heat of reaction was obtained and shown as follows:

$$\Delta H_r = -1952.53 * Q_o + 11153.66 * E_a - 74.42 * N_P - 0.62 * MW - 1178.1 \qquad 3\text{-}4$$

This model is a linear combination of four descriptors: dissociation energy of oxygen-oxygen bonds, number of peroxide functional groups, atomic charge of oxygen and molecular weight. These descriptors were identified as significant factors contributing to the heat of reaction by MLR analysis. Table 3.5 lists all the calculated heat of reaction for organic peroxide, which were plotted against the experimental data in Figure 3.3. The results of validation tests for this model are shown in Table 3.6.

Table 3.5 Experimental and predicted heat of reaction of organic peroxides

No.	Substance	ΔH_d (Experimental) (kJ/mol)	ΔH_d (Predicted) (kJ/mol)	
			MLR	PLS
1	Tert-butyl cumyl peroxide	-177.6	-202.1	-219.2
2	Dicumyl peroxide	-223.9	-244.0	-283.4
3	Di-tert-butyl peroxide	-158.3	-149.6	-155.1
4	Benzoyl peroxide	-90.0	-87.8	-136.2
5	Lauroy peroxide	-305.4	-353.0	-316.2
6	Tert-butylperoxy benzoate	-239.1	-190.5	-178.9
7	Tert-butyl peroxyacetate	-200.8	-180.5	-158.5
8	11-bis(t-butylperoxy)-335-timethylclohexane	-426.9	-412.2	-407.4
9	2,2-Bis(t-butylperoxy)butane	-308.4	-321.4	-317.8
10	2,5-Bis(t-butylperoxy)-2,5-dimethylhexane	-296.5	-264.4	-291.2
11	2,4-Pentanedione peroxide	-664.4	-637.7	-698.3
12	Cumene hydroperoxide	-253.2	-195.7	-199.9
13	Tert-butyl(peroxy 2-ethyl-hexyl) carbonate	-236.1	-276.7	-242.6
14	1,1-Di(tert-butylperoxy)cyclohexane	-427.2	-356.1	-342.6
15	2-butanone peroxide	-483.3	-535.7	-466.8
16	Tert-butyl hydroperoxide	-64.7	-148.4	-142.0

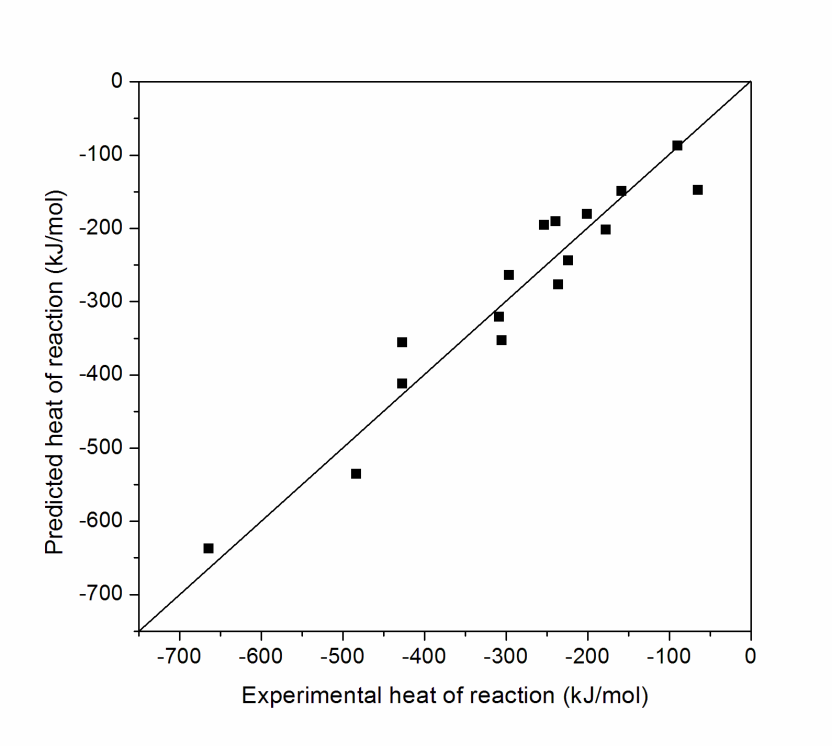

Figure 3.3 Scattering diagram for experimental and calculated heat of reaction using MLR model

According to the data shown in Figure 3.3 and Table 3.6, the model derived through MLR shows a good agreement between the calculated heat of reaction and the experimental data (R^2=0.921). This model was also demonstrated to be statically significant according to *F* test result. However, this regression model has no prediction power at all because of negative R_{CV}^2 (R_{CV}^2= -0.811), which indicates the presence of over-fitting. Similar with the over-fitting scenario identified in the MLR analysis for onset temperature, the relatively large number of descriptors (12 descriptors) and the limited size of training set (16 data) shall lead to the over-fitting in the mathematic regression and therefore result in poor prediction power of the regression model.

Table 3.6 Validation of the regression model for heat of reaction

	R	R^2	R_{CV}^2	F
MLR	0.916	0.921	-0.811	20.815
PLS	0.956	0.913	0.828	-

ii). PLS method

Following the proposed procedure for PLS shown in Figure 2.2, a model with optimized R_{CV}^2 was derived for predicting heat of reaction of organic peroxides using PLS method. This prediction model is a linear combination (Equation 3-5) of five descriptors, including dissociation energy of oxygen-oxygen bond, molecular weight, oxygen balance, energy of the highest occupied molecular orbital, and atomic charge of oxygen. The predicted heat of reaction was presented in Table 3.5 and plotted versus experimental data in Figure 3.4. The validation test results are presented in Table 3.6.

$$\Delta H_r = -1713.721 * Q_O + 8722.592 * E_a - 1.450 * OB - 1.210 * MW - 2400.034 * \varepsilon_{HOMO} - 1893.625 \quad 3\text{-}5$$

As depicted by Table 3.6 and Figure 3.4, the heat of reaction predicted using PLS method satisfactorily fits the experimental data with R^2 of 0.913. This prediction model presents a reasonable predictive power with R_{CV}^2 of 0.828, which is much better than that of the model derived through MLR analysis. Based on the consideration of model

fitting and prediction performance, the model obtained through PLS analysis is recommended in predicting the heat of reaction of organic peroxides.

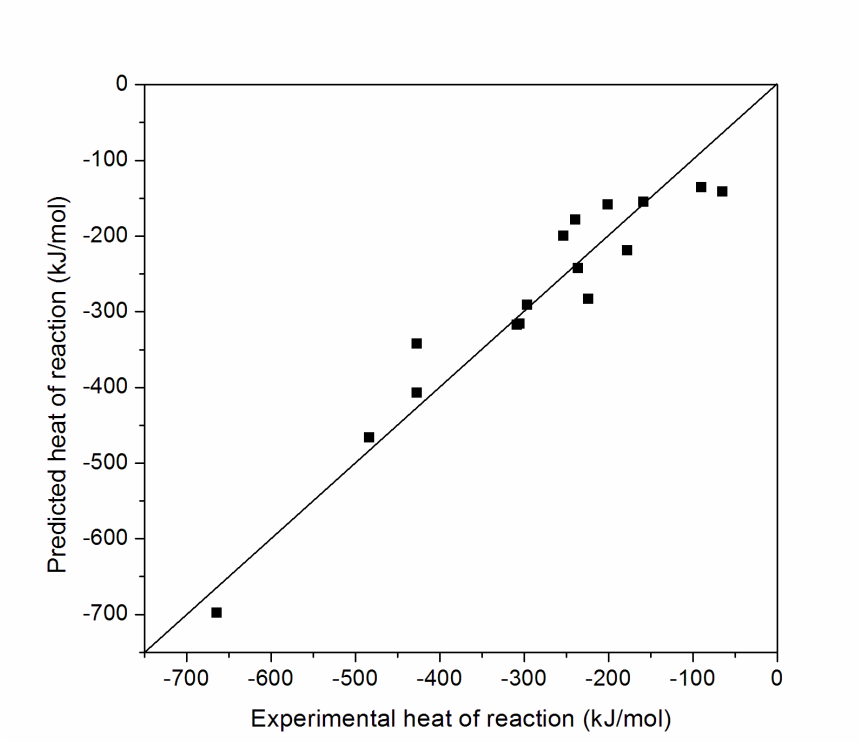

Figure 3.4 Scattering diagram for experimental and calculated heat of reaction using PLS model

Sensitivity analysis was subsequently performed to study the significance of descriptors in the prediction model. The standardized coefficient of all descriptors were calculated and listed in Table 3.7. According to the data of standardized coefficient, atomic charge of oxygen in the peroxide functional group and activation energy are most significant

descriptors contributing to heat of reaction. The atomic charge of oxygen presents negative impact to the heat of reaction due to the negative standardized coefficient.

Table 3.7 Sensitivity analysis of the heat of reaction prediction model obtained through PLS analysis

Descriptor	Coefficient	Standardized coefficient
Q_O	-1713.721	-0.732
E_a	8722.592	0.646
OB	-1.450	-0.372
MW	-1.210	-0.590
ε_{HOMO}	-2400.034	-0.309

3.2.3 Discussion

By comparing the prediction models obtained through QSPR approach, onset temperature was found to be a hazardous property more related to the molecular structure of organic peroxides. The involvement of all 13 descriptors in the prediction model for onset temperature implies that all these molecular properties affect the onset temperature of organic peroxides. Compared with onset temperature, heat of reaction is less influenced by the molecular structure since only 5 descriptors get involved in the prediction model. This phenomenon can be explained by the fact that heat of reaction depends more on the reaction route rather than the molecular structure of the initial sate.

Some descriptors are recognized as significant properties contributing to the reactive hazards of organic peroxides. Dissociation energy of oxygen-oxygen bond is one of the most significant descriptors for onset temperature as well as heat of reaction prediction models. This parameter indicates the easiness of undertaking the initial step of the runaway reaction and is expect to greatly affect the thermal stability of organic peroxides. Also, this result is in agreement with previous study on energetic materials, which reported that heat of reaction is affected by the C-NO_2 bond dissociation energy [24]. The bond angle in peroxide functional group was identified by sensitivity analysis as the second most important descriptor for onset temperature. The importance of bond angle for onset temperature indicates the impact of molecular geometry on the thermal stability of organic peroxides. Another important descriptor for onset temperature is concentration, which is a non-intrinsic descriptor specifically designed for onset temperature of organic peroxide. Sensitivity analysis determines that this descriptor presents positive impact on onset temperature according to its standardized coefficient (0.233). However, this conclusion is not consistent with the previous research results, which found that a concentration increase can lead to a decrease of the onset temperature [28, 29]. The possible explanation for this conflict is that the effect of concentration identified in previous research was neglected in this QSPR study due to its limited influence on onset temperature. It is possible that the concentration effect on onset temperature identified in the this research indicates the intramolecular association between peroxide molecules, which is positive for the thermal stability of organic peroxides [61].

In most cases, validation of the regression model using external data is recommended in order to ensure the prediction power of the model. However, given the fact that the data of reactive hazards are only available for 16 organic peroxides, it is really difficult to divide the data into the test set and training set. In fact, the main difficulty for performing QSPR study on reactive chemicals is the availability of experimental data. As the alternative approach, cross-validation can handle this challenge by using internal data and has been widely used in the field of QSPR research [24, 62]. In this research, the cross-validation test was employed and the R_{CV}^2 was used to quantitatively estimate the prediction power of the prediction models derived.

3.2.4 Hazard classification system

As mentioned in the introduction part of Chapter III, the selection of the safer reactive chemicals not only requires the collection of reactive hazards data but also needs a classification system based on reactive hazards. This classification system enables the more quantitative ranking of chemicals according to their reactive hazards, especially when multiple safety parameters need to be taken under consideration. Based on the classification results, industry can decide which chemicals to employ in the processes, which makes the process chemistry inherently safe.

In this research, three different hazard indices were employed to classify organic peroxides based on the reactive hazards data. The description of these hazard indices are presented in Section 2.4. These hazard indices were developed based on different concept and through different approaches. The classification results were then verified in this research in order to determine the one which is most suitable for the family of organic peroxides.

Using kinetic equations listed in Section 2.4, parameters used in the hazard indices were calculated and presented in Table 3.8. The application of these kinetic equations can avoid the requirement of additional experiments.

By applying calculated parameters to the hazard indices, the rating results for 16 organic peroxides using these three hazard indices were calculated and presented in Table 3.9

Table 3.8 Estimated parameters used in the hazard indices

No.	Substance	T_m (K)	E_a (kcal/mol)	TMR_{ad} (min)
1	Tert-butyl cumyl peroxide	792.09	28.65	97.34
2	Dicumyl peroxide	926.13	34.10	114.31
3	Di-tert-butyl peroxide	560.79	30.14	104.57
4	Benzoyl peroxide	760.27	29.93	101.86
5	Lauroy peroxide	537.93	31.99	111.30
6	Tert-butylperoxy benzoate	682.48	30.14	103.24
7	Tert-butyl peroxyacetate	517.19	31.23	108.97
8	11-Bis(t-butylperoxy)-335-timethylclohexane	435.29	27.01	95.34
9	2,2-Bis(t-butylperoxy)butane	631.83	31.37	107.93
10	2,5-Bis(t-butylperoxy)-2,5-dimethylhexane	866.92	30.24	102.09
11	2,4-Pentanedione peroxide	600.79	31.08	107.31
12	Cumene hydroperoxide	1132.27	27.82	92.70
13	Tert-butyl(peroxy 2-ethyl-hexyl) carbonate	274.77	27.93	102.17
14	1,1-Di(tert-butylperoxy)cyclohexane	482.69	32.31	113.36
15	2-butanone peroxide	1429.26	30.38	99.65
16	Tert-butyl hydroperoxide	721.58	30.23	103.18

Table 3.9 Rating results of organic peroxides

No.	Substance	RHI	TRI	THI	EP
1	Tert-butyl cumyl peroxide	5.53	1.41	128.25	0.17
2	Dicumyl peroxide	5.40	1.51	51.39	0.11
3	Di-tert-butyl peroxide	4.80	1.54	77.35	-0.07
4	Benzoyl peroxide	5.35	2.86	103.25	0.11
5	Lauroy peroxide	4.58	1.09	42.87	-0.16
6	Tert-butylperoxy benzoate	5.14	1.58	91.25	0.04
7	Tert-butyl peroxyacetate	4.58	1.40	53.31	-0.16
8	11-Bis(t-butylperoxy)-335-timethylclohexane	4.66	2.19	115.96	-0.09
9	2,2-Bis(t-butylperoxy)butane	4.90	1.00	64.74	-0.04
10	2,5-Bis(t-butylperoxy)-2,5-dimethylhexane	5.57	2.86	109.39	0.17
11	2,4-Pentanedione peroxide	4.84	1.89	66.02	-0.06
12	Cumene hydroperoxide	6.27	3.56	176.65	0.39
13	Tert-butyl(peroxy 2-ethyl-hexyl) carbonate	3.95	0.60	77.37	-0.45
14	1,1-Di(tert-butylperoxy)cyclohexane	4.38	0.39	30.17	-0.24
15	2-butanone peroxide	6.51	4.55	163.60	0.42
16	Tert-butyl hydroperoxide	5.23	2.04	94.07	0.07

In order to validate the classification results of the three hazard indices employed, the Explosion Potential (EP) was employ in this research [63] and served as the validation

criteria. This is an empirically derived parameter used to separate compounds that can undergo detonation or deflagration. The definition of EP is shown by Equation 3-6.

$$EP = \log(Q_{DSC}) - 0.38\log(T_{DSC} - 25) - 1.67 \qquad 3\text{-}6$$

where Q_{DSC} and T_{DSC} are heat of reaction and onset temperature of the exothermic reaction.

Materials with EP > 0 are considered to have potential to explode, either by detonation or deflagration. Therefore, if the hazard index can effectively classify reactive chemicals, organic peroxides with positive EP should have higher rating than organic peroxides with negative EP. In this study, EP is used to validate the effectiveness of different hazard indices and finally determine which one is most effective in rating organic peroxides according to reactive hazards.

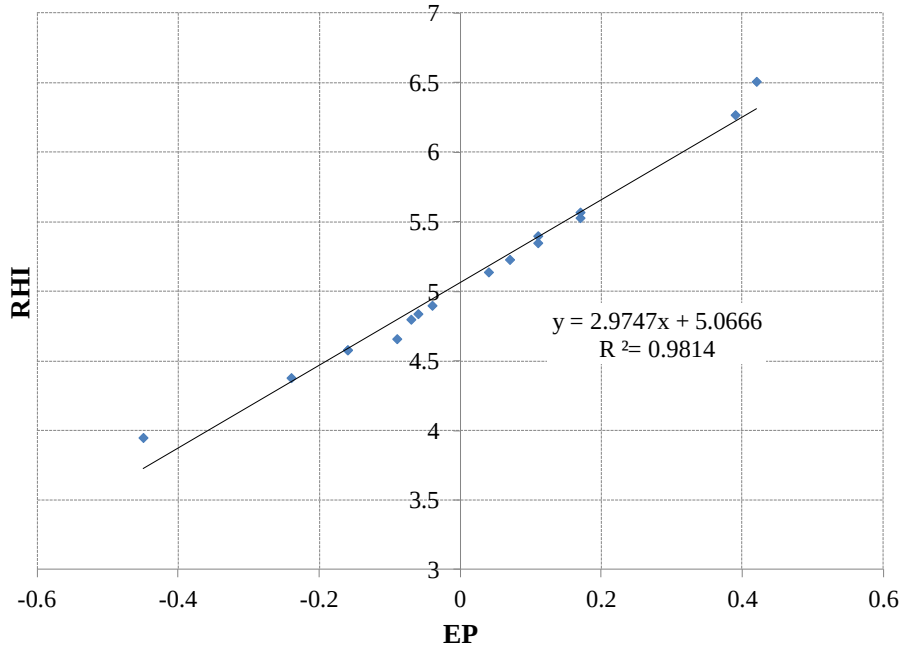

a. RHI

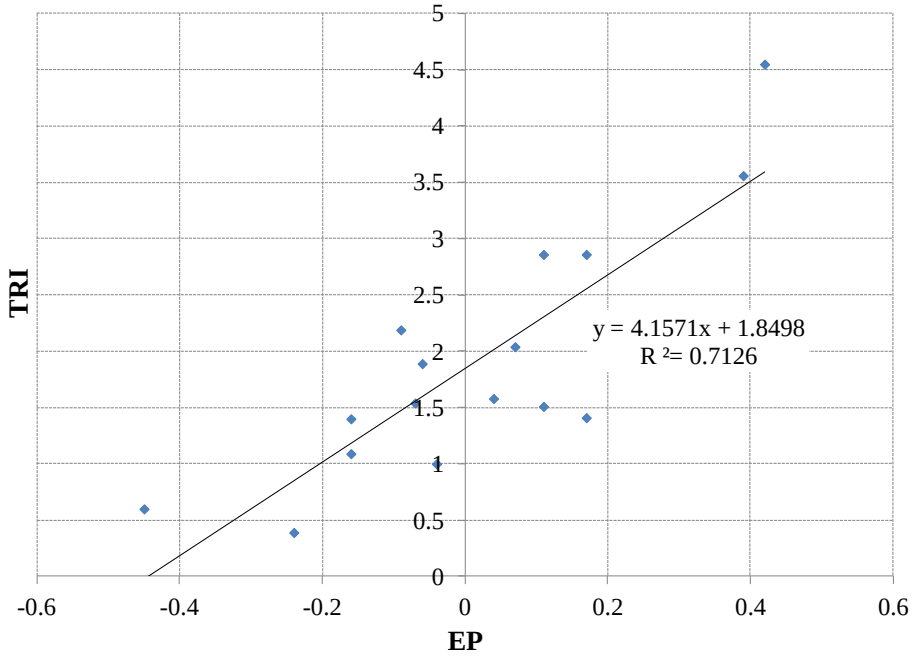

b. TRI

Figure 3.5 Validation of hazard index for organic peroxides

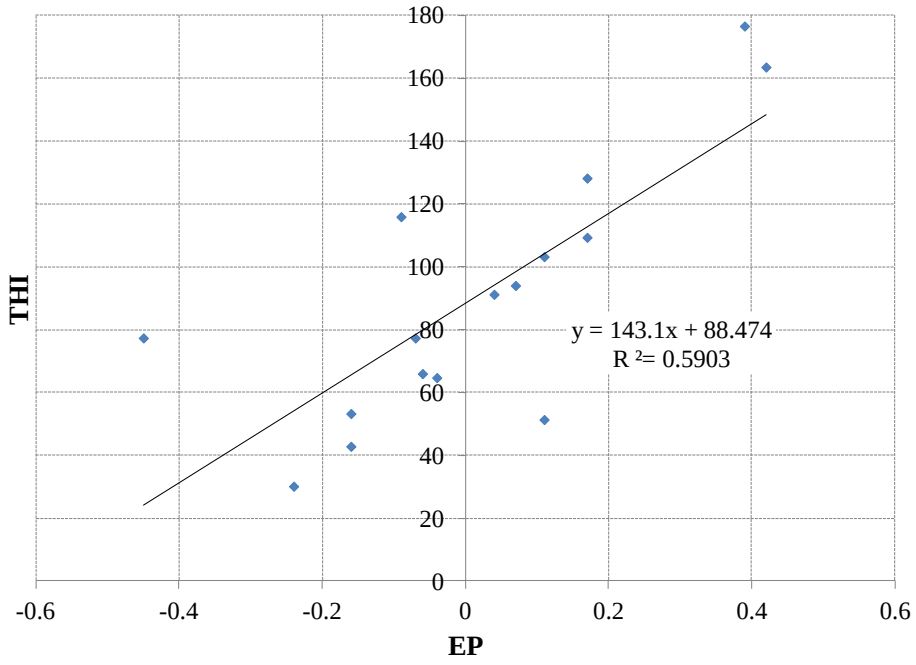

c. THI

Figure 3.5 Continued

Three hazard indices were plotted against EP respectively to evaluate the effectiveness of the classification of organic peroxides based on the reactive hazards (Figure 3.5). The plot of hazard index against EP indicates that only RHI has the good linear relationship with EP and can effectively classify organic peroxides based on reactive hazards. As shown in Figure 3.5a, organic peroxides with potential of explosion (EP>0) have higher rating than peroxide with no potential of explosion (EP<0). But for other two hazard indices (Figure 3.5b and 3.5c), they cannot well distinguish peroxides with the potential of explosion from other chemicals: some organic peroxides with negative EP have even higher rating than chemicals with positive EP. According to the validation results, RHI is determined to be the hazard index most suitable for organic peroxides.

3.3 Conclusions

Through the investigation on organic peroxides using QSPR approach, two prediction models were developed for predicting onset temperature and heat of reaction, two important parameters characterizing the reactive hazards. These two predictions models are shown as follows.

$$T_0 = 55.99 * Q_O + 730.18 * E_a - 29.72 * d_{OO} - 5.35 * N_P - 0.08 * OB - 0.04 * MW + 3.30 * DM + 0.11 * \angle_{ROOR'} - 3.82 * \angle_{ROO} + 202.75 * \varepsilon_{HOMO} - 118.01 * \eta - 2.73 * \omega + 23.58 * C + 626.61$$

$$\Delta H_r = -1713.721 * Q_O + 8722.592 * E_a - 1.450 * OB - 1.210 * MW - 2400.034 * \varepsilon_{HOMO} - 1893.625$$

When using these models to predict reactive hazards of other organic peroxide, the users will only need to spend relative short time on calculating descriptors through molecular simulation and then apply them to the prediction models. The prediction output provides essential information to industry regarding reactive hazards for the initial screening of reactive chemicals.

The selectivity analysis on prediction models identified important molecular properties contributing to the reactive hazards of organic peroxide. These results imply the influence of molecular structure on chemical reactivity throughout the whole family of organic peroxides, and can serve as the technical basis for the future research in this area. Also, the identification of significant molecular properties may help chemists to

find a direction in the design of safer chemicals. It is possible that chemists may manipulate these molecular properties to minimize the reactive hazards associated.

In this research RHI was determined to be the most suitable hazard index for organic peroxides. This hazard index can be applied in conjunction with the predictions models derived: RHI can utilize the reactive hazards data generated by prediction models to rate reactive chemicals according to reactive hazards associated. The output of this rating system provides a quantitative technical basis to support the decision-making on chemical selection during the design of inherently safer process.

CHAPTER IV

DETERMINATION OF SAFER PROCESS CONDITIONS

4.1 Introduction

"Moderate" is another major principle in the design of inherently safer process. After selecting the safer chemicals for the process, it is also important to adopt the safer process conditions to further mitigate the risk associated with the process. The process may still face high risk if it is operated under improper process conditions, even if the safer chemicals are employed in the process. In this part of research, process contaminant, a very important process condition, was investigated. Contaminants in the process may significantly affect the reactive hazards associated with processes by trace amount. Therefore, when designing inherently safer process, it is critical important to identify the incompatibility of possible contaminants with reactive chemicals employed in the process and estimate the effects of contaminants on the reactive hazards. Based on the research results, proper measures can be applied to control the risk imposed by the incompatibility of contaminants with reactive chemicals.

In this research, the incompatibility of iron oxide with Methyl Ethyl Ketone Peroxide (MEKPO) was investigated. MEKPO is a type of organic peroxide widely used as initiator for polymerization reaction and hardener in glass-reinforced plastic manufacture [64]. The chemical structure of MEKPO is shown by Figure 4.1. MEKPO is highly hazardous and has caused several tragic accidents throughout the world. One incident

happened in Tokyo, Japan in 1964, which caused 19 fatalities and 114 injuries. Another more severe incident happened in Taiwan in 1979, leading to 33 fatalities and 44 injuries [65].

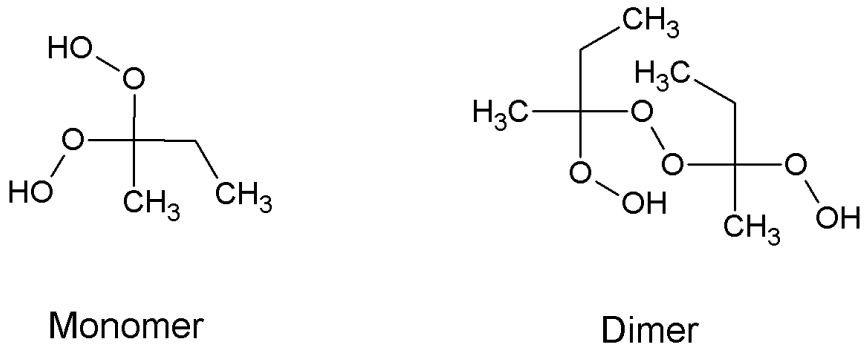

Figure 4.1 Chemical structure of MEKPO

Iron oxide is one of the most common contaminants in process industries. This contaminant has been proven to be incompatible with a variety of reactive chemicals [66-68]. Even though industry has realized that all materials organic peroxides come in contact with in the process should be compatible [69], little work has been done to study the incompatibility of MEKPO with iron oxide, a very common process contaminant.

Tseng studied the incompatibility of MEKPO with iron oxide through calorimetry test and found iron oxide can weaken the thermal stability of MEKPO [70]. However, there is still a gap between the existing understanding on this incompatibility and the need to apply the principle “moderate” in the process design. First, Tseng only performed

calorimetry test under single contaminant concentration. Therefore, it is still beyond our understanding how this contaminant affects reactive hazards of MEKPO within a wide range of contaminant concentration. Second, in previous research, reactive hazards of MEKPO were investigated through DSC test under constant heating rate, whose purpose is to conduct initial screening of reactive chemicals. The information obtained from DSC tests is not enough for guiding the design of inherently safer process. Third, the impact of this incompatibility on operational safety was not investigated in previous research.

In order to address this gap and provide better guidance on the design of inherently safer process, the incompatibility of MEKPO with iron oxide was studied through a systematic approach in this research. This approach is composed of calorimetry test, kinetic modeling and analysis of key safety parameters. Through this research, it was expected to reach the comprehensive understanding on the incompatibility of MEKPO with iron oxide, including the effects on observable exothermic behavior, change on kinetics and change on reaction mechanism. Then, based on this understanding, the impact of the contaminant on operational safety was investigated by estimating and analyzing key safety parameters.

Based on the conclusions drawn in this research, proper measures can be implemented in the process design to minimize the hazards associated with processes. For example, if iron oxide has little or no impact on the reactive hazards and operational safety, then process equipment handling MEKPO can be fabricated by carbon steel. In this case,

mechanical integrity program will be sufficient to monitor and control the contaminant level in the process. Also, safer operating conditions can be determined based on the key safety parameters estimated in this research. However, if iron oxide is proven to significantly affect the reactive hazards and operational safety, carbon steel needs to be replaced by other materials to prevent the potential incompatibility. One example is in pharmaceutical industry, some process equipment handling organic peroxides uses glass as the inner material to avoid the incompatibility of organic peroxides with process contaminants.

Part of the data in this chapter has been published in *Journal of Loss Prevention in the Process Industries* (in press).

4.2 Results and discussions

4.2.1 Uncertainty analysis

In order to estimate the uncertainties associated with the experimental results, two experiments, pure MEKPO and MEKPO with 5 wt% iron oxide, were repeated to calculate the uncertainty for all calorimetric parameters studied in this research. The results of these experiments and calculated uncertainty data are presented in Table 4.1 and 4.2 respectively.

Table 4.1 Uncertainty analysis for APTAC tests performed on pure MEKPO

Test No.	T_0 (°C)	T_{max} (°C)	P_{max} (Psi)	$(dT/dt)_{max}$ (°C/min)	$(dP/dt)_{max}$ (Psi/min)
1	86	212	318	1065	2058
2	90	217	408	1386	3021
S.D.	3	4	64	227	681

Table 4.2 Uncertainty analysis for APTAC tests performed on MEKPO with 5 wt% iron oxide

Test No.	T_0 (°C)	T_{max} (°C)	P_{max} (Psi)	$(dT/dt)_{max}$ (°C/min)	$(dP/dt)_{max}$ (Psi/min)
1	69	226	196	653	952
2	64	237	254	904	862
S.D.	4	8	41	177	64

According to the uncertainty data shown in Table 4.1 and 4.2, all the temperature measurements, including onset temperature and maximum temperature, show quite small uncertainties. However, the uncertainties associated with pressure data are greater than that for temperature. It was found that the uncertainty associated with pressure data for the pure MEKPO test is higher than the test on MEKPO with 5 wt% iron oxide. The great difference in uncertainty is also observed for the maximum self-heating rate and maximum pressure rate. These two parameters present much higher uncertainties for pure MEKPO test than test on MEKPO with 5 wt% iron.

Through the analysis on the working mechanism of APTAC, it is believed that the uncertainties associated with the experimental data obtained from APTAC tests are mainly caused by the failure of capturing the peak value of the temperature/pressure. Since APTAC samples the process parameters (temperature, pressure) at a predefined frequency, it is possible that APTAC may fail to capture the peak value of temperature/pressure when self-heating rate/pressure rate is very high. The difference between the measured peak value and the true peak value can be amplified by the increase of the temperature/pressure rate. Therefore, the great differences of uncertainties for calorimetric parameters (Table 4.1 and 4.2) should be caused by the big differences of self-heating rate and pressure rate between these two tests.

According to the self-heating rate and pressure rate data presented in the table on page 86, experiments performed in this research can be classified into two categories: tests performed under 0 – 0.075 wt% contaminant, and tests performed under 0.3 - 20 wt%. The data of maximum self-heating rate and maximum pressure rate keeps in the similar level within each category but presents big gap between these two categories. According to the analysis presented in the last paragraph, calorimetric parameters should also show similar uncertainties within the each category but show big difference in uncertainties between the two categories. Therefore, the uncertainty data presented in Table 4.1 and Table 4.2 can represents the uncertainty associated with the experimental results in these two categories respectively and were applied in the analysis of experimental results in this research.

4.2.2 Calorimetry study

A series of calorimetry tests were performed using APTAC to quantitatively study the effects of iron oxide on runaway reactions and reactive hazards associated. APTAC tests were performed on pure MEKPO and MEKPO with different levels of iron oxide. According to the contaminant concentration, these tests can be classified into three categories:

- Low contaminant concentration: 0.03 wt%, 0.075 wt, 0.3 wt%,
- Medium contaminant concentration: 1 wt% and 5 wt%
- High contaminant concentration: 10 wt% and 20 wt%.

The details of these tests are listed in Table 4.3.

Table 4.3 Experimental details of APTAC tests

No.	Contaminant (wt%)	MEKPO mass (g)	Bomb mass (g)	Start temperature (^{o}C)	Vapor space (ml)	Φ
1	0	8.15	54.06	30	83.7	3.2
2	0.03	8.18	57.61	35	83.5	3.3
3	0.075	7.99	53.67	35	84.5	3.2
4	0.3	7.99	53.17	35	84.0	3.2
5	1	7.85	53.08	35	87.6	3.2
6	5	7.92	54.65	35	87.5	3.2
7	10	7.78	52.99	35	84.7	3.2
8	20	7.95	52.99	35	84.5	3.2

a. low contaminant concentration range

Temperature and pressure profiles of runaway reactions obtained from APTAC tests within different contaminant concentration ranges are presented in Figure 4.2 – 4.4 respectively. Important parameters such as onset temperature and maximum temperature can be directly obtained or derived from the experimental profiles and are shown in Table 4.4. Based on the experimental results, other parameters such as self-heating rate and pressure rate were calculated and are presented in Figure 4.2 – 4.4 respectively. Important parameters for runaway reaction rate such as maximum self-heating rate and maximum pressure rate are summarized in Table 4.5. Heat of reaction, an important indicator for severity of runaway reaction, was calculated based on the adiabatic temperature increase (Equation 4-1) and are also presented in Table 4.4.

$$\Delta H_r = \phi C_P (T_{\max} - T_0) \qquad 4\text{-}1$$

According to the data presented in Figure 4.2 and Table 4.4, iron oxide has no significant impact on the thermal stability of MEKPO in the low concentration range. With the increase of iron oxide concentration from 0 to 0.3 wt%, the onset temperature of MEKPO kept around 86 ^{o}C. The only exception in this range is the test No.2 performed under 0.03 wt% contaminant. In this test, the onset temperature of MEKPO surprisingly increased by 11 ^{o}C compared with pure MEKPO. This observation is an outlier which does not follow the overall trend of onset tem[erature within this concentration range. Also, this observation does not agree with the expectation that iron

oxide is a contaminant which may weaken the thermal stability of MEKPO. The further analysis on this abnormal phenomenon is presented in Section 4.2.4.

The maximum temperature reached by the runaway reaction within the low contaminant concentration range was between 210 and 220 ^{o}C, indicating no significant influence imposed by iron oxide. Because of the little variation on onset temperature and maximum temperature, within the low contaminant concentration range, runaway reactions have the similar heat of reaction (around 1000 kJ/g). Again, the test No. 2 is an outlier for heat of reaction data, whose heat of reaction is about 10% less than other tests within this range. Similar with maximum temperature trend, the maximum pressure data does not show definite change after applying the uncertainty data.

Self-heating rate and pressure rate are important parameters indicating the runaway reaction rate. The maximum values of these two parameters reached during runaway reaction imply the severity of runaway reaction and are widely used in the design of pressure relief system [71]. By taking account of the uncertainty data, both maximum self-heating rate and maximum pressure rate keep in the same level within the low contaminant concentration range (Table 4.5). The trends of these two parameters indicate the insignificant impact of iron oxide on maximum reaction rate when contaminant falls into this range. But decreasing trends were observed for these two parameters when contaminant level reached 0.3 wt%.

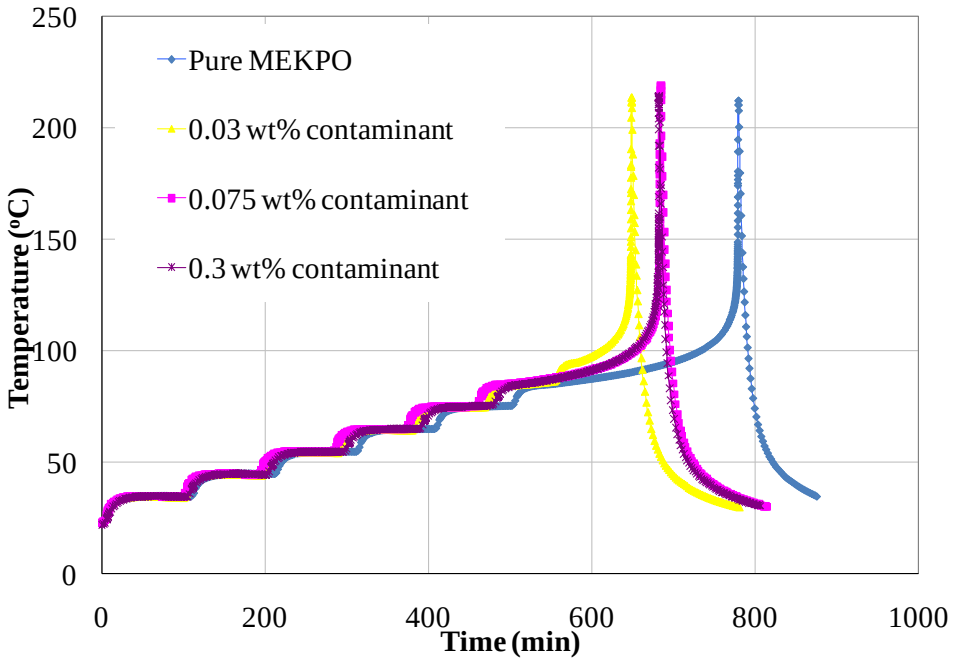

a. Temperature

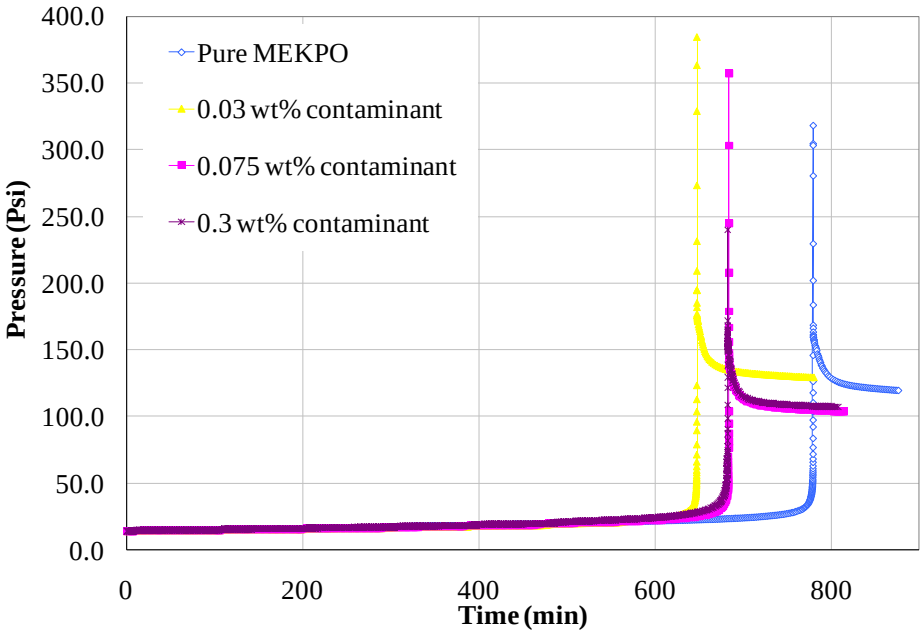

b. Pressure

Figure 4.2 Experimental calorimetric data profiles of MEKPO with contaminant within low concentration range

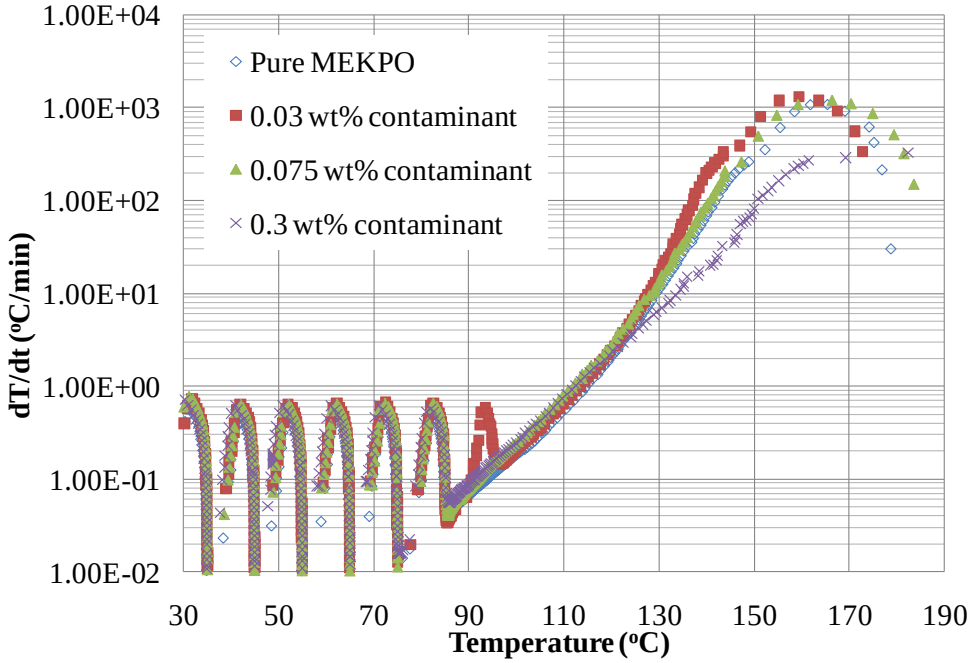

c. Self-heating rate

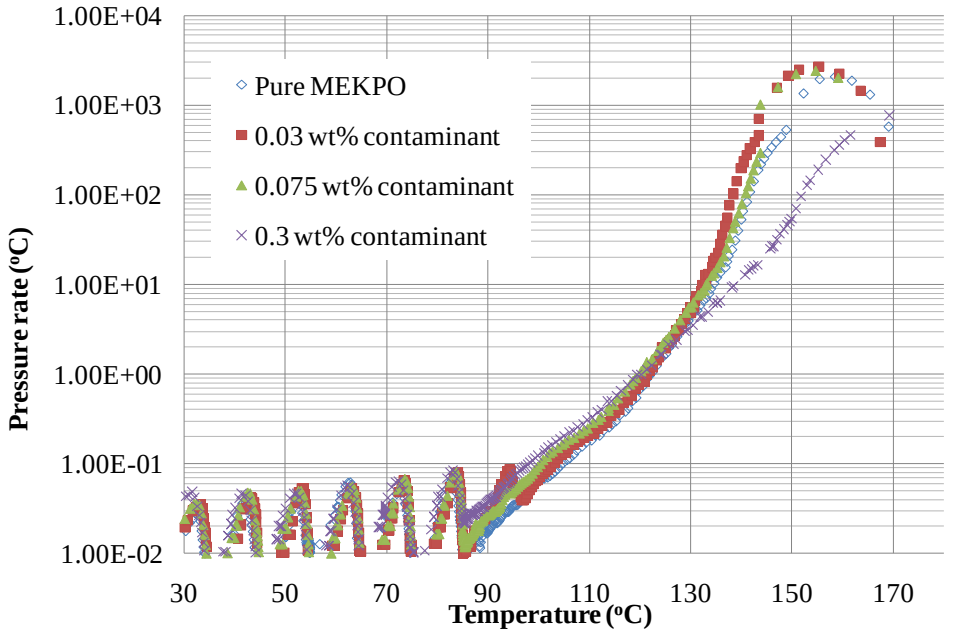

d. Pressure rate

Figure 4.2 Continued

b. Medium contaminant concentration range

In the medium contaminant concentration range, negative impact of iron oxide on the thermal stability of MEKPO was observed. According to data presented in Table 4.4, with the presence of 1 wt% iron oxide, the onset temperature decreased to 76 ^{o}C, which is 10 ^{o}C lower than pure MEKPO. The onset temperature further decreased to 69 ^{o}C when iron oxide increased to 5 wt%.

With the presence of medium level contaminant, runaway reaction can reach higher maximum temperature compared with tests performed under low level of contaminant. As seen in Table 4.4, the maximum temperature data increased by 10 to 20 ^{o}C when contaminant reached medium concentration range. Because of the higher maximum temperature and lower onset temperature, heat of reaction of MEKPO runaway reaction increased by 10 to 20 %. Within this concentration range, maximum pressure of runaway reaction is slightly lower than that in the low contaminant concentration range.

Both maximum self-heating rate and maximum pressure rate show significant reduction compared with those in the low contaminant concentration range (Table 4.5). The dramatic change of these two parameters indicates that the presence of iron oxide can effective depress the maximum reaction rate within the medium concentration range. When iron oxide increased from low level to medium level, even though the thermal stability of MEKPO decreases, the consequence of the runaway reaction becomes less severe.

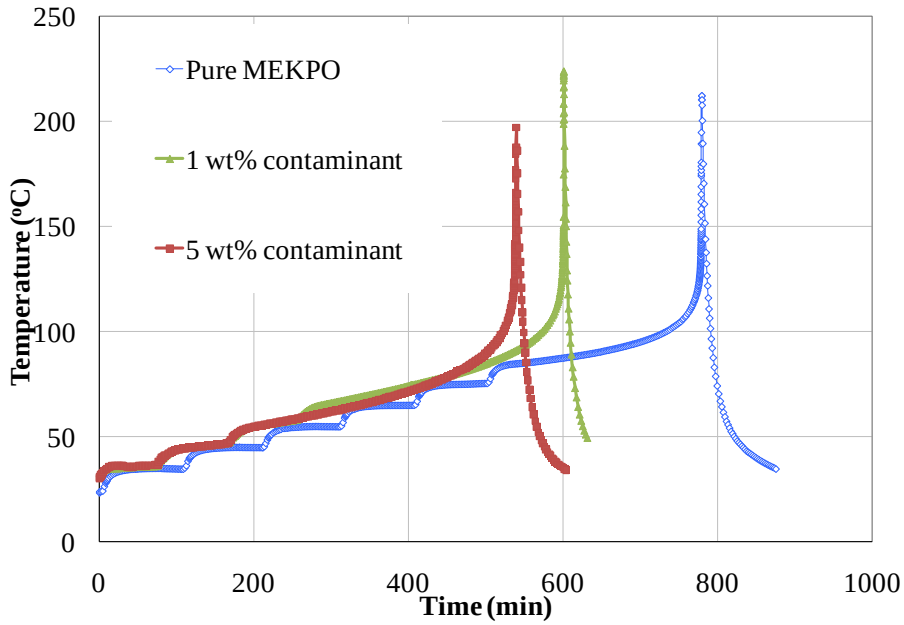

a. Temperature

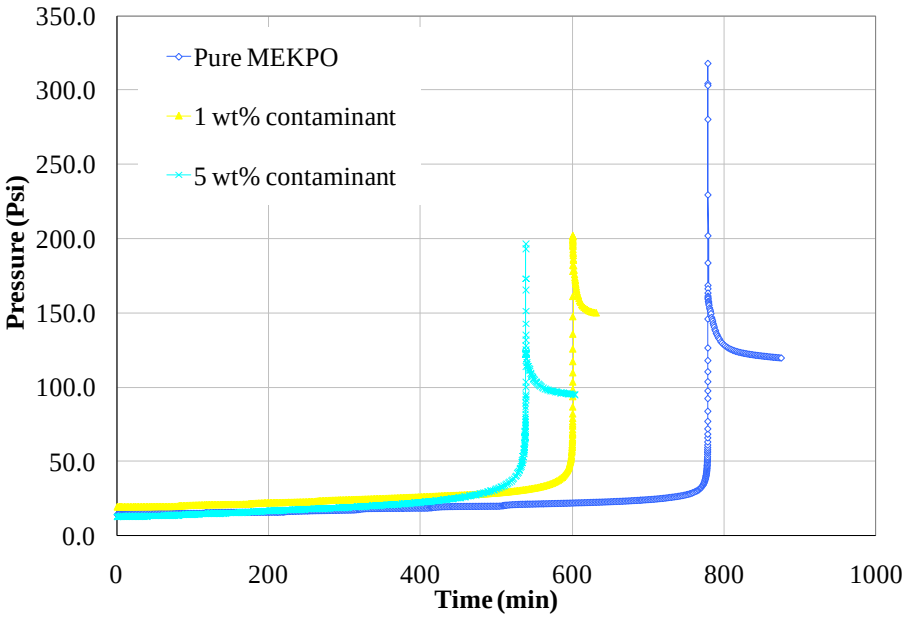

b. Pressure

Figure 4.3 Experimental profiles for APTAC tests performed on MEKPO with contaminant within medium concentration range

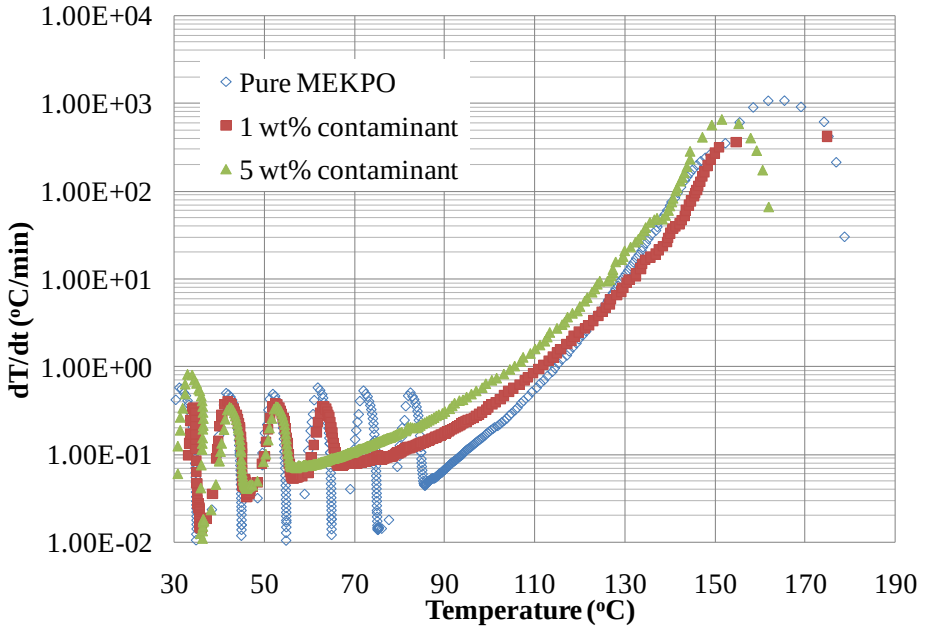

c. Self-heating rate

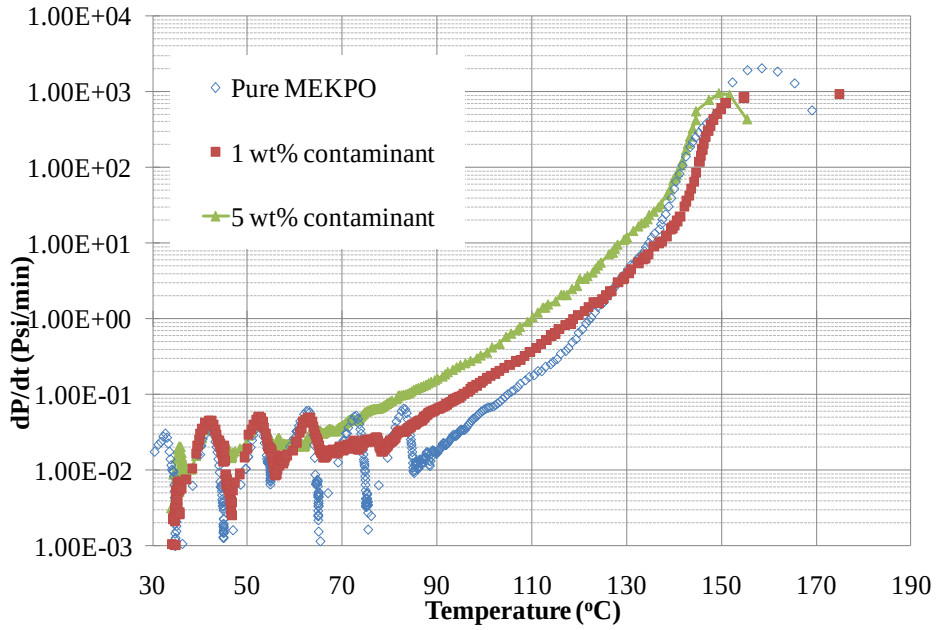

d. Pressure rate

Figure 4.3 Continued

c. High contaminant concentration range

With the further increase of iron oxide concentration, the temperature of MEKPO decreased to 66 ^{o}C and 58 ^{o}C under 10 wt% and 20 wt% contaminant respectively (Table 4.4). The variation of onset temperature implies that the negative impact of iron oxide on MEKPO is further enhanced by the increase of contaminant concentration.

Heat of reaction within this range is significantly higher than other tests. The heat of reaction for MKEPO with 20 wt% iron oxide is almost twice as much as pure MEKPO (Table 4.4). As the result, the maximum temperature of runaway reaction kept on increasing over the high contaminant concentration range.

Within high contaminant concentration range, maximum pressure of runaway reaction becomes much more significant and shows dramatic increase with the increase of contaminant concentration. The maximum pressure for MEKPO with 20 wt% iron oxide is almost three time as that for pure MEKPO (Table 4.4). The dramatic increase of the pressure hazard should be the result of the increase of heat of reaction and non-condensable gas generation. The detailed analysis of non-condensable gas generation is presented in Section 4.2.3.

The maximum self-heating rate and pressure rate show different trends within this range. According to data presented in Table 4.5, the maximum self-heating rate further decreased to 200-300 ^{o}C/min with the increase of contaminant concentration, indicating

the further reduction of maximum reaction rate. However, the maximum pressure rate shows an increase trend within this concentration range. With the increase of contaminant concentration from 10 to 20 wt%,, the maximum pressure rate increased from 600 to 838 psi/min (Table 4.5). It is known that the pressure rise of runaway reaction is mainly caused by the thermal expansion effect and the generation of non-condensable gas. So, since the self-heating rate shows decrease trend within this concentration range, the increase of the maximum pressure rate should be the result of non-condensable gas generation. The significant increase of gas generation can compensate the reduction of self-heating rate, and therefore lead to the increase of maximum pressure rate within this contaminant concentration range.

An interesting phenomenon observed in the high contaminant concentration range is the appearance of the second peak for both self-hating rate and pressure rate profiles. This peak was firstly observed (Figure 4.4c and d) in the test performed under 10 wt% contaminant. The peak value of the second peak reached 12 ^{o}C/min and 263 psi/min respectively for self-heating rate and pressure rate profile (Table 4.5). This peak becomes more significant with the increase of contaminant concentration, whose peak value reached 135 ^{o}C/min and 838 psi/min under 20 wt% contaminant. According to the self-heating rate and pressure rate profiles presented in Figure 4.4c and d, in both tests, the second peak started around 235 ^{o}C, which is higher than the maximum temperature of other tests. The presence of the second peak in the both self-heating rate and pressure rate profiles implies that another exothermic reaction was initiated by the first runaway

reaction. Compared with the main reaction represented by the first peak, the secondary reaction presents minor thermal hazard because of lower maximum self-heating rate than the main reaction. However, this reaction is associated with great pressure hazard because of the higher maximum pressure rate compared with the main reaction.

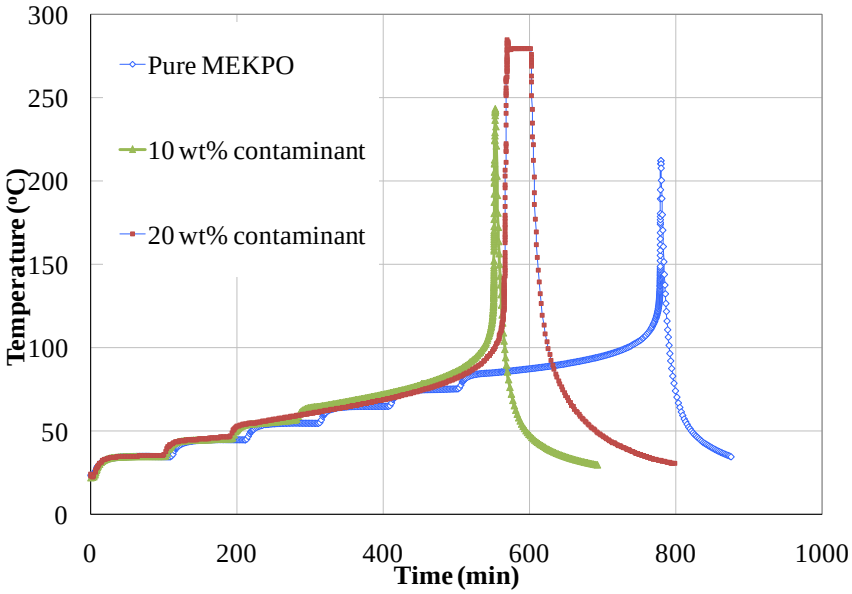

a. Temperature

Figure 4.4 Experimental calorimetric profiles for MEKPO with contaminant within high concentration range

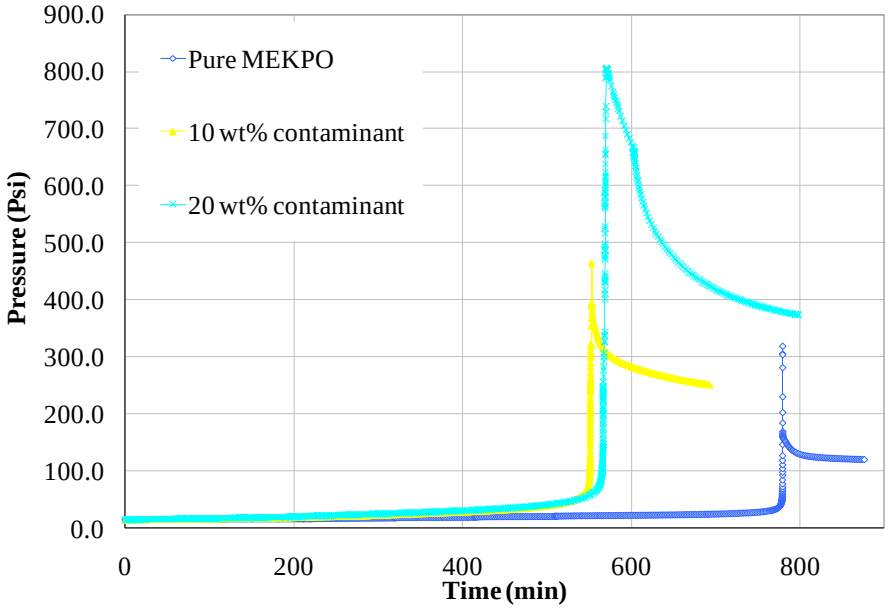

b. Pressure

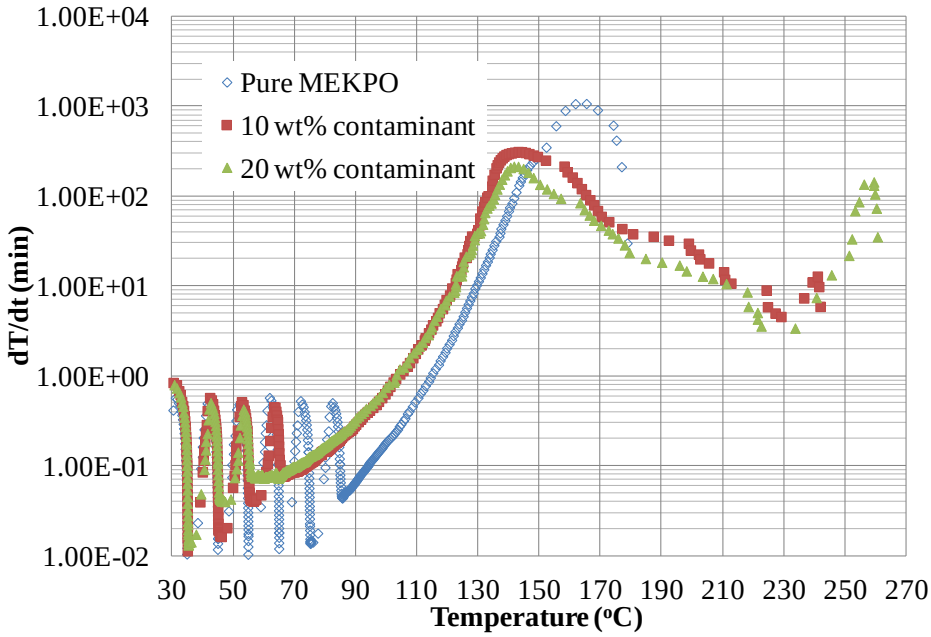

c. Self-heating rate

Figure 4.4 Continued

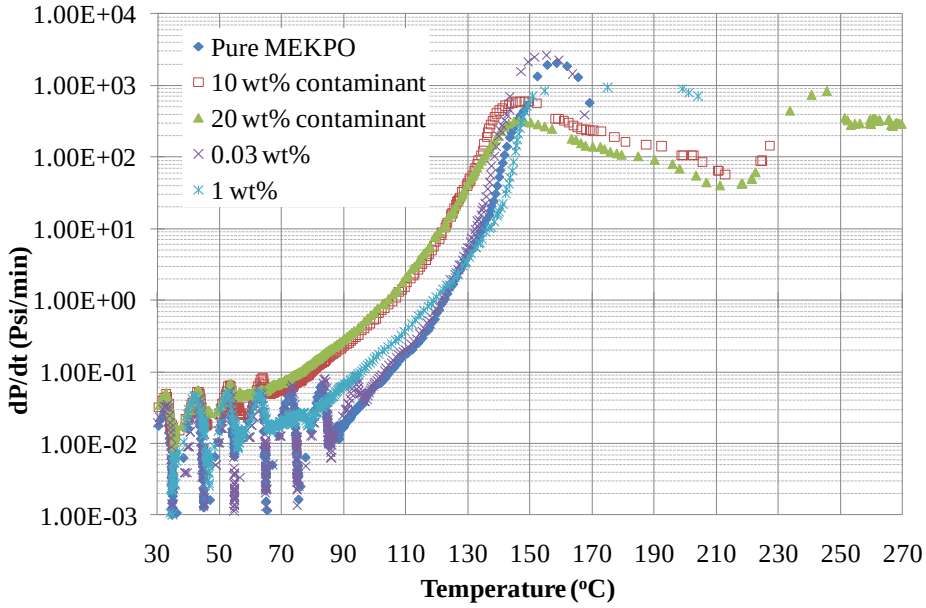

d. Pressure rate

Figure 4.4 Continued

Table 4.4 Calorimetric parameters of MEKPO runaway reaction

Test No.	Contaminant (wt%)	T_0 (°C)	T_{max}(°C)	P_{max} (Psi)	ΔH_r (J/g)
1	0	86	216	318	953
2	0.03	97	214	384	857
3	0.075	86	219	357	975
4	0.3	86	214	240	938
5	1	76	237	202	1180
6	5	69	226	196	1150
7	10	66	243	464	1297
8	20	58	285	806	1663

Table 4.5 Self-heating rate and pressure rate data

Test No.	Contaminant (wt%)	$(dT/dt)_{max}$ (first peak) (^oC/min)	$(dT/dt)_{max}$ (Second peak) (^oC/min)	$(dP/dt)_{max}$ (first peak) (psi/min)	$dP/dt)_{max}$ (Second peak) (psi/min)
1	0	1065	NA	2058	NA
2	0.03	1304	NA	2670	NA
3	0.075	1193	NA	2416	NA
4	0.3	706	NA	849	NA
5	1	529	NA	939	NA
6	5	653	NA	952	NA
7	10	311	12	600	263
8	20	213	135	320	838

d. Summary

Through the analysis of various calorimetric parameters over a wide range of contaminant concentration, it was found that the impact of iron oxide on reactive hazards of MEKPO depends on the contaminant concentration in the reaction system. The trends of the important calorimetric parameters over contaminant concentration are shown in Figure 4.5. The data ranges of these calorimetric parameters for pure MEKPO are indicated by the areas surrounded by dash lines in Figure 4.5.

Iron oxide in low concentration (0 - 0.3 wt%) has almost no effect on the thermal stability of MEKPO as the onset temperature remains in the same level within this range

(Figure 4.5a). MEKPO becomes more unstable when contaminant concentration exceeds 0.3 wt%, where onset temperature decreases with the increase of contaminant level.

The presence of contaminant above a certain level (0.03 wt%) significantly affects the maximum rate of MEKPO runaway reaction (Figure 4.5d and 4.5e). With the contaminant reaches 0.03 wt%, both maximum self-heating rate and maximum pressure rate decrease dramatically. But maximum pressure rate shows increase trend in the high contaminant concentration range (> 10 wt%) due to the generation of non-condensable gas.

As seen in Figure 4.5b and 4.5c, in the low and medium contaminant concentration ranges, both maximum temperature and maximum pressure are considered in the same level given the uncertainty data, though some small variations were observed. However, these two parameters show an obvious increasing trend in the high contaminant concentration range. The increase of the maximum temperature is caused by the increase of heat of reaction. The dramatic increase of maximum pressure is the result of combination of thermal expansion and non-condensable gas generation. The changes of these two parameters indicate the change of reaction mechanism in the high contaminant concentration range.

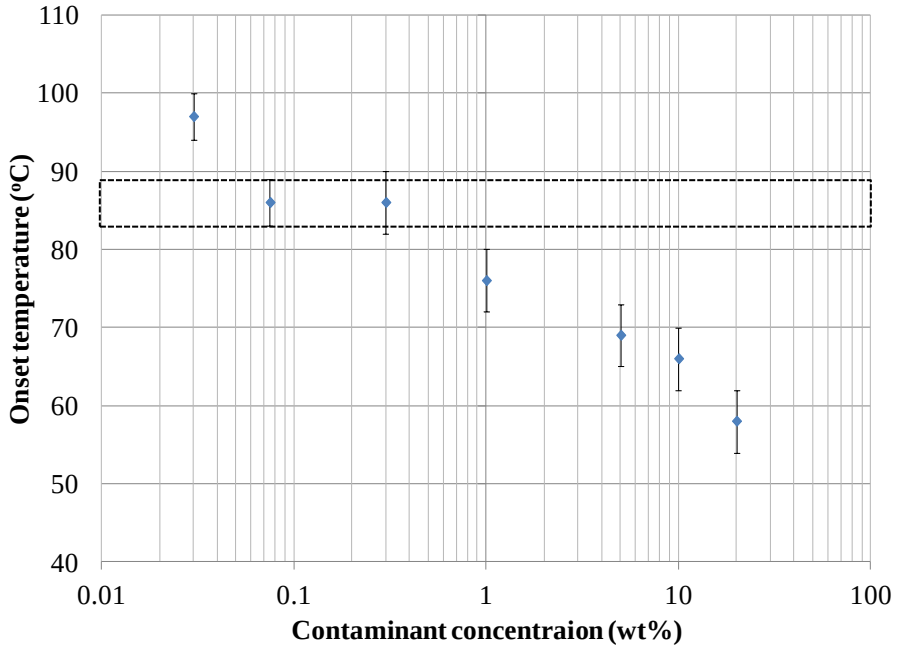

a. Onset temperature

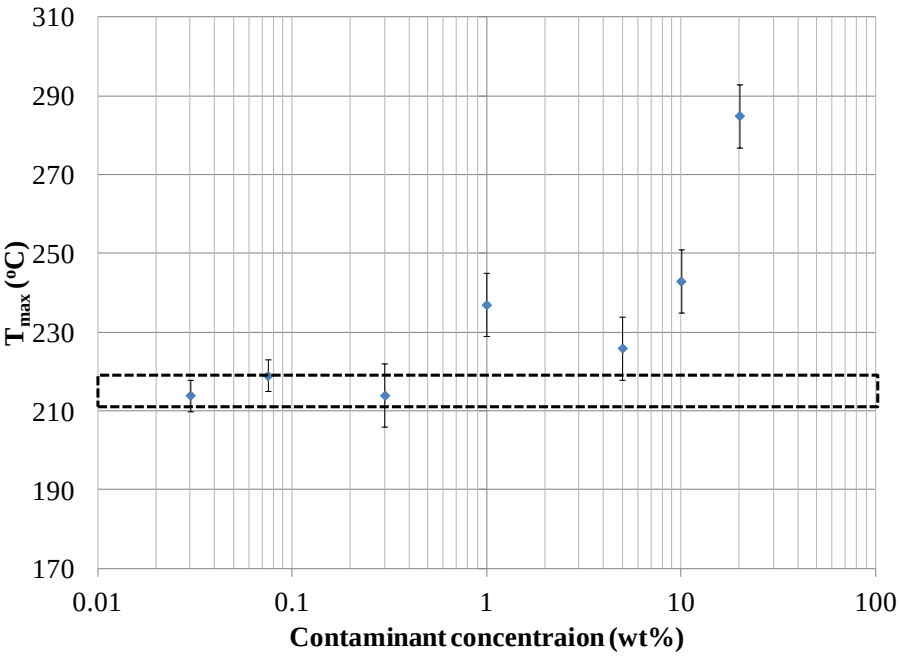

b. Maximum temperature

Figure 4.5 Trends of calorimetric parameters over iron oxide concentration

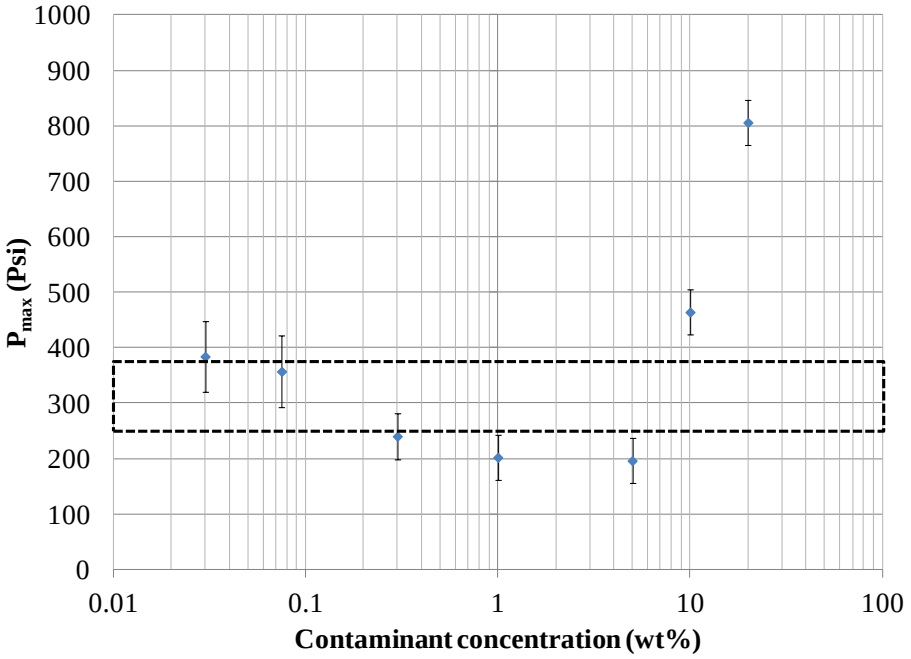

c. Maximum pressure

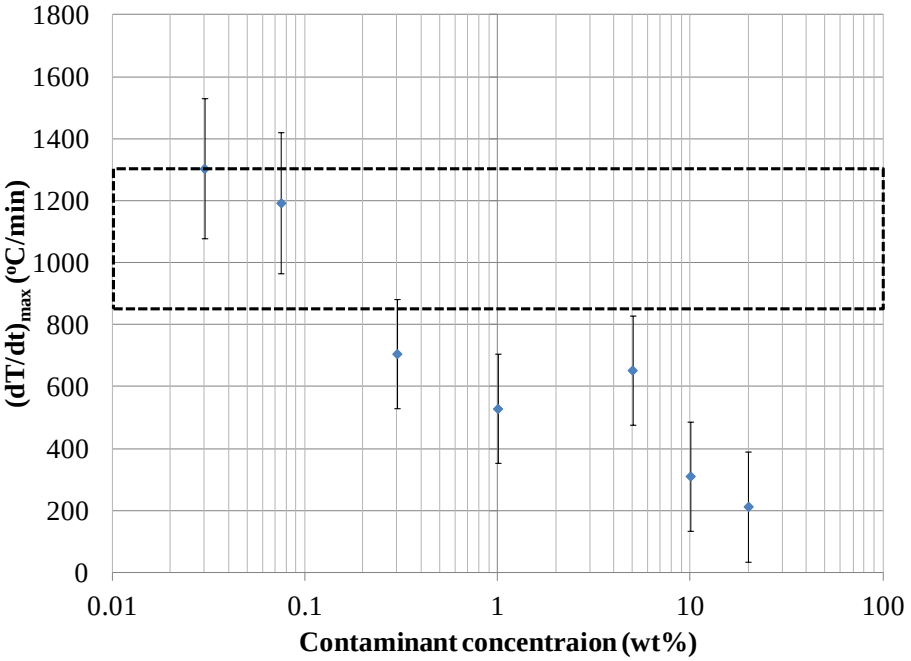

d. Maximum self-heating rate

Figure 4.5 Continued

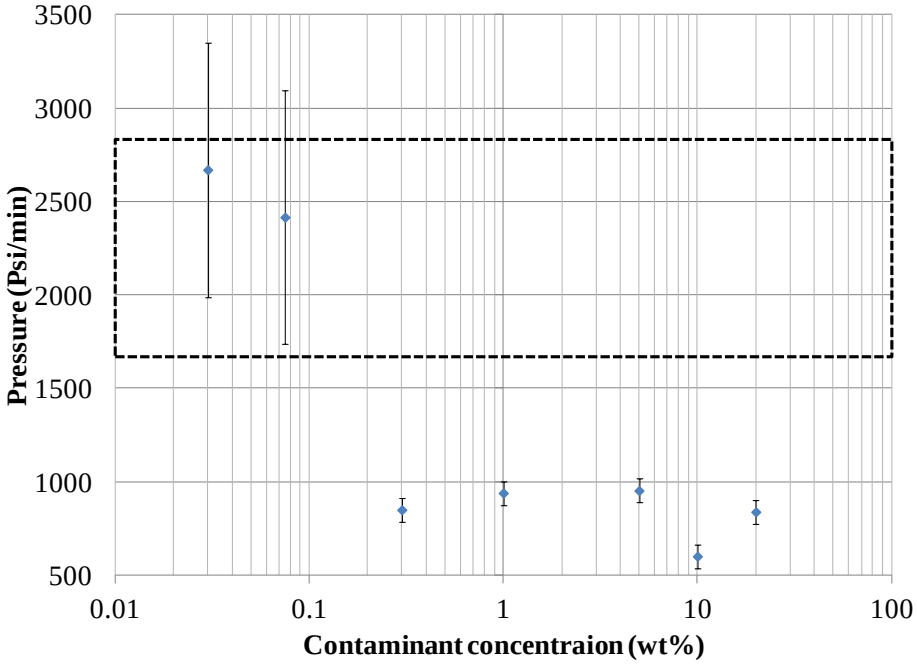

e. Maximum pressure rate

Figure 4.5 Continued

4.2.3 Non-condensable gas generation analysis

Non-condensable gas pressure is defined as the difference between the pressure after the experiment is completed and cooled to a certain temperature and the pressure when the sample is first heated to the same temperature (Figure 4.6). Non-condensable gas generated is the primary hazard during a runaway reaction, since the pressure increase caused by gaseous products formed cannot be tempered by the consumption of latent heat. In this research, the pressure caused by non-condensable gas was used as an

important parameter for measuring pressure hazards and used to estimate the amount of gaseous products produced.

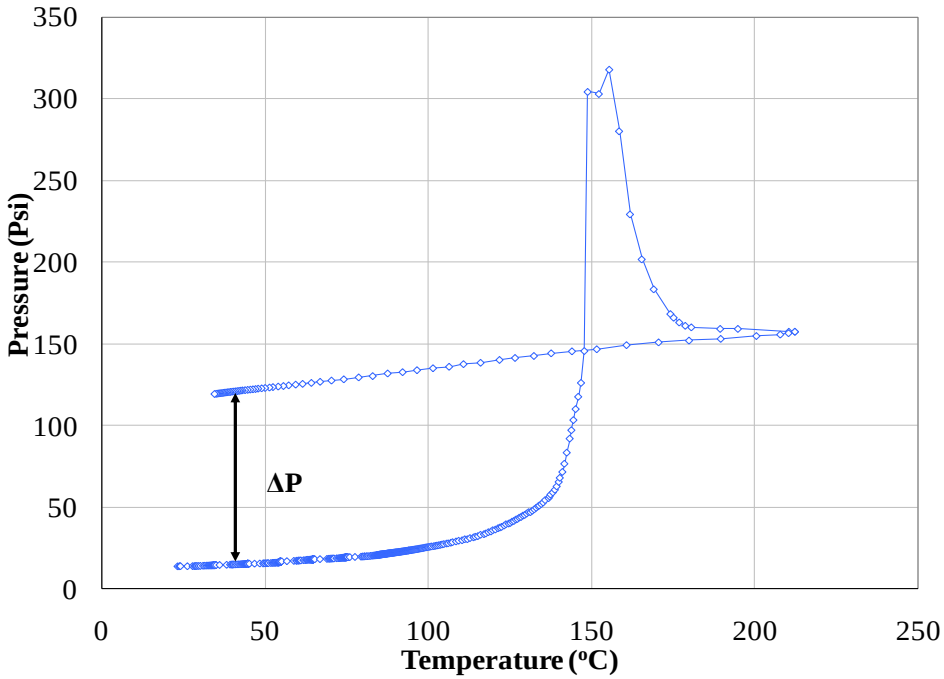

Figure 4.6 Non-condensable gas pressure

The generation of non-condensable gas can be calculated using Equation 4-2. Estimation of parameters such as non-condensable gas pressure, moles of gaseous products and gas produced per liter MEKPO are presented in Table 4.6.

$$\Delta n = \frac{\Delta P V}{RT} \qquad \text{Equation 4-2}$$

where ΔP is non-condensable gas pressure, V is the vapor space in the test cell, T is the temperature under which pressure is measured.

According to the data presented in Table 4.6, it is obvious that pressure hazards caused by non-condensable gas are much more significant in the high contaminant concentration range than other ranges. Within the low and medium contaminant concentration ranges, each liter reactant produces 3.4 – 5.1 mol gaseous products. However, this parameter reached 7.8 mol/l under 10 wt% contaminant and further increased to 11.8 mol/L under 20 wt% contaminant, which is an almost three-fold increase. The dramatic increase of the non-condensable gas production implies the change of reaction mechanism.

Table 4.6 Estimation of non-condensable gas generation

Contaminant (wt%)	ΔP (Psi)	Gaseous product (mol)	Gaseous product per liter reactant (mol/L)
0	117.7	0.039	4.8
0.03	115.2	0.038	4.6
0.075	89.3	0.029	3.7
0.3	92.4	0.030	3.8
1	123.7	0.040	5.1
5	82.3	0.027	3.4
10	236.2	0.078	10
20	358.3	0.118	14.8

The gas generation rate can be calculated by excluding the influence of thermal expansion from the detected pressure rate using Equation 2-37. The calculated gas generation rate was plotted against sample temperature in Figure 4.7. The gas generation rate profiles can help to monitor the dynamic gas production process and further investigate the reaction mechanism. The maximum gas generation rate of different tests was summarized in Table 4.7.

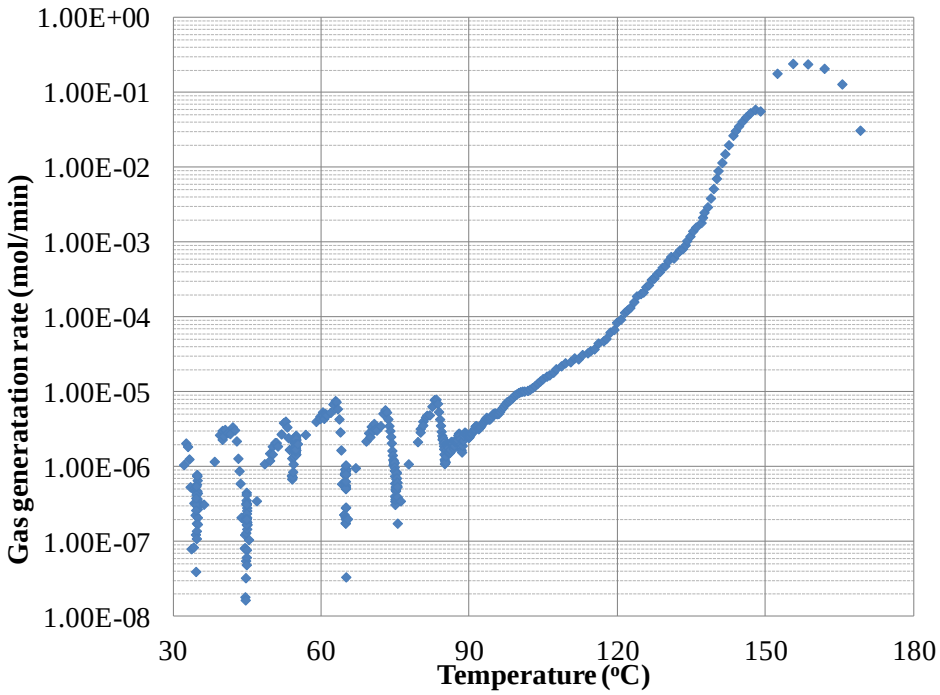

a. Pure MEKPO

Figure 4.7 Gas generation rate profiles for MEKPO runaway reaction

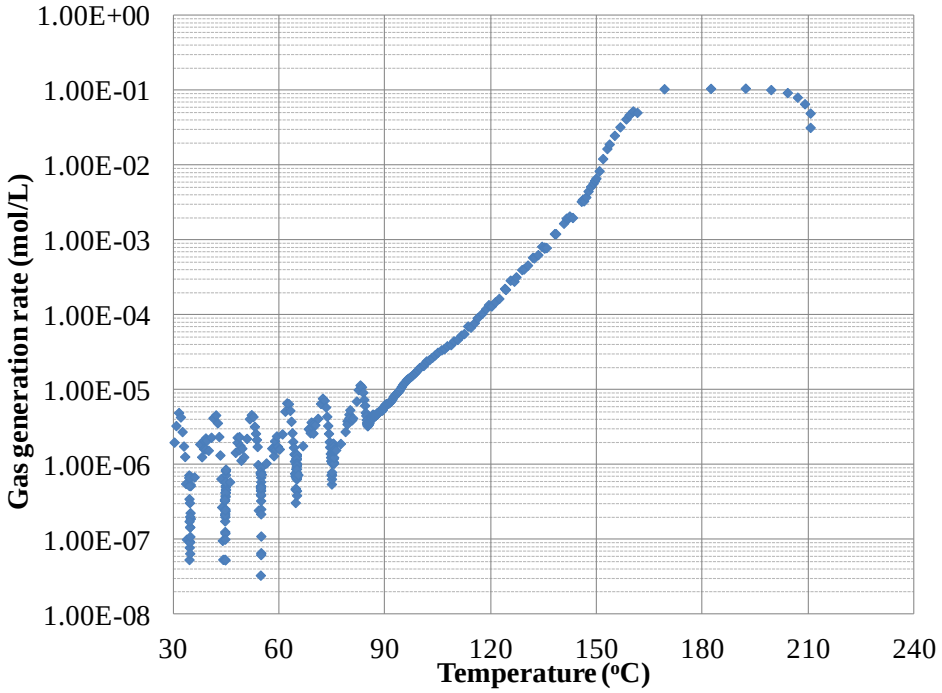

b. 0.3 wt%

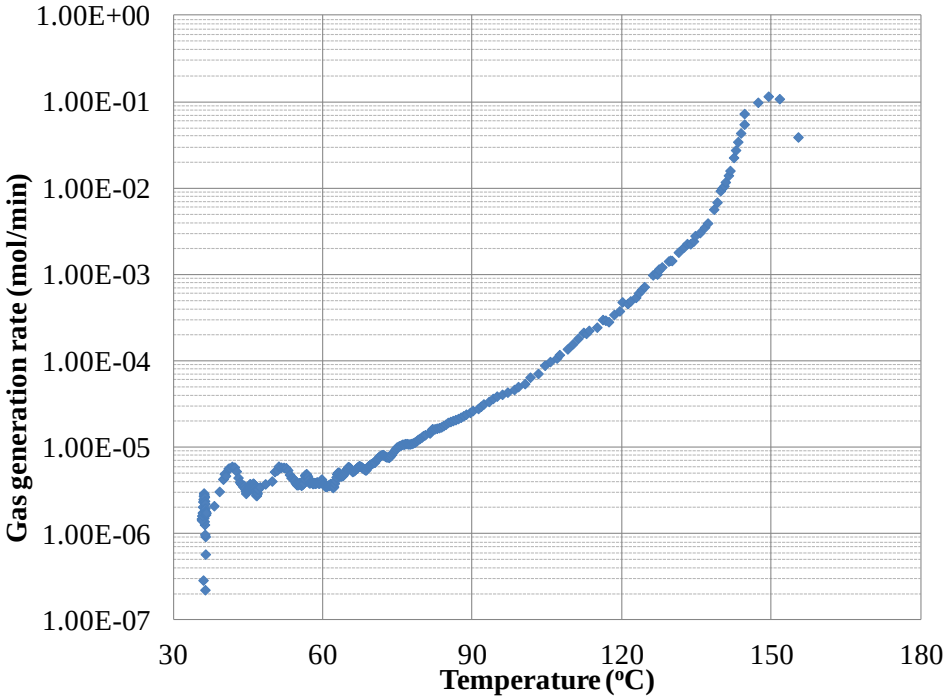

c. 5 wt%

Figure 4.7 Continued

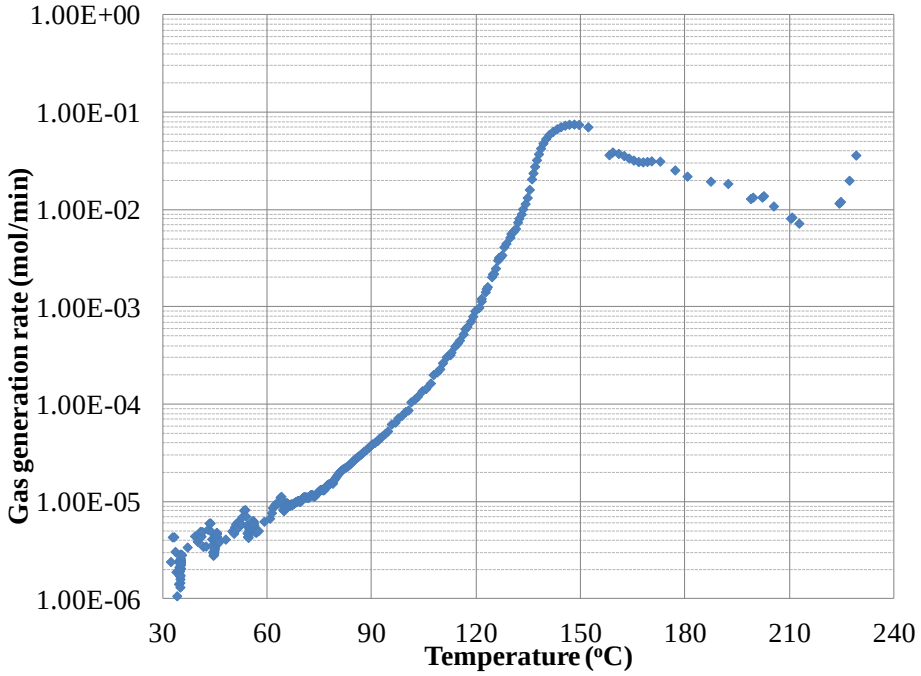

d. 10 wt% contaminant

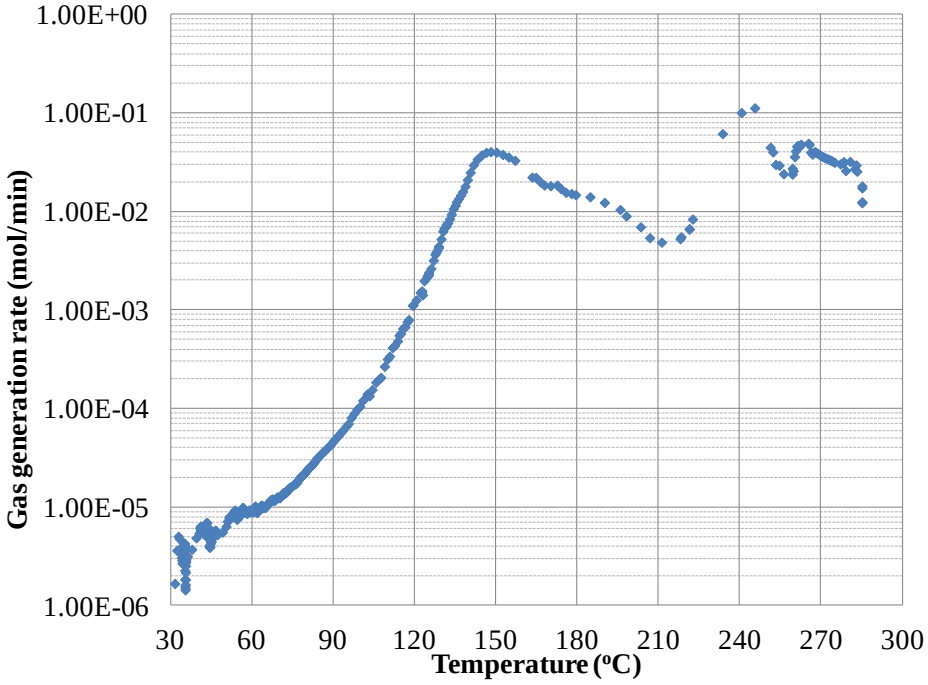

e. 20 wt% contaminant

Figure 4.7 Continued

For pure MEKPO and MEKPO with low and medium levels of contaminant, as presented in Figure 4.7, all the gas generation curves follow the similar trend as self-heating rate (Figure 4.2c and 4.3c) and show only one peak during the runaway reaction. According to the data presented in Table 4.7, the maximum gas generation rate remains in the same range when the contaminant is below 0.3 wt% but shows dramatic reduction when contaminant level reaches and exceeds 0.3 wt%. This trend of maximum gas generation rate is quite similar with the trend for the data of maximum self-heating rate (Table 4.5). The agreement between these two trends indicates the consistent reaction mechanism for runaway reaction with the presence of low and medium levels of contaminant. However, under high level of contaminant, the gas generation rate curve shows two peaks, of which the second peak appears in the high temperature range (Figure 4.7d and 4.7e). Within high contaminant concentration range, the maximum gas generation rate of the second peak increases dramatically over contaminant concentration and is higher than the first peak value under 20 wt% contaminant (Table 4.7). The presence of the second peak of gas generation rate results in the increase of the amount of gas totally produced by the runaway reaction. Also, the gas produced from the reaction corresponding to the second peak can compensate the decrease of reaction rate of the first peak and therefore leads to the increase of the maximum pressure rate within the high contaminant concentration range. The presence of the second gas generation peak implies a possible change of reaction mechanism.

Table 4.7 Parameters of non-condensable gas generation

Contaminant (wt%)	$(dn/dt)_{max}$ (first peak) (mol/min)	$(dn/dt)_{max}$ (second peak) (mol/min)
0	0.24	NA
0.03	0.31	NA
0.075	0.32	NA
0.3	0.10	NA
1	0.12	NA
5	0.12	NA
10	0.08	0.03
20	0.04	0.11

4.2.4 Kinetic investigation

When studying the impact of iron oxide on the reactive hazards of MEKPO, it is important to understand the reaction kinetics behind the observable calorimetric parameters. Investigation on reaction kinetics can help people to get a comprehensive understanding of the runaway reaction and associated hazards from the fundamental point of view and explain the experimental observation obtained from calorimetry test. Also, the solid understanding of the kinetics of runaway reaction can serve as the technical basis for further reaction modeling with different purposes.

In this research, based on the experimental data obtained from APTAC tests, kinetic investigation was performed for MEKPO runaway reaction with the presence of different levels of iron oxide. In previous research, three reaction models were proposed for MEKPO runaway reaction: nth order reaction, autocatalytic reaction and consecutive reaction [72]. The consecutive model is normally used for runaway reaction with multiple peaks. In this research, most of the runaway reactions present only one peak in the self-heating rate profiles. Though under high level of contaminant, runaway reactions presents two self-heating rate peaks, the first peak is still our major concern before of the major thermal hazard associated. Based on the above considerations, consecutive model was excluded from this research. The rest two types of kinetic models, nth order reaction and autocatalytic reaction, were employed in this research. By fitting different type of models to the experimental data, it was expected to identify the right kinetics for the runaway reaction, estimate important kinetic parameters and evaluate the impact of iron oxide on reaction kinetics.

a. n^{th} order reaction

As introduced in Section 2.6.1, nth order reaction model was applied to the experimental data by using the following equation.

$$\log(k^*) = \log\left(\frac{dT}{dt}\frac{(\Delta T_{ad})^{n-1}}{(T_{\max}-T)^n}\right) = \log\left(AC_0{}^{n-1}\right) - \frac{E_a}{RT} \qquad \text{Equation 4-3}$$

By plotting lnk^* versus $-1/T$, a curve can be obtained. Kinetic parameters of the runaway reaction can be estimated by fitting the curve to a linear trend line, whose slop represents $-Ea/R$ and intersect represents $log(AC_0^{n-1})$. During analysis process, the reaction order n was assumed first. The final estimation of reaction order can be determined by looking for the trend line with highest R^2.

In the kinetic analysis, all the experimental data, including temperature and self-heating rate were converted to adiabatic conditions using Equation 2-34, 2-35 and 2-36.

The calculated self-heating rate for all the tests was plotted versus experimental data in Figure 4.8. The estimation of important kinetic parameters using nth order reaction model is presented in Table 4.8. The reaction order of the runaway reaction was determined to be 1 for all the tests.

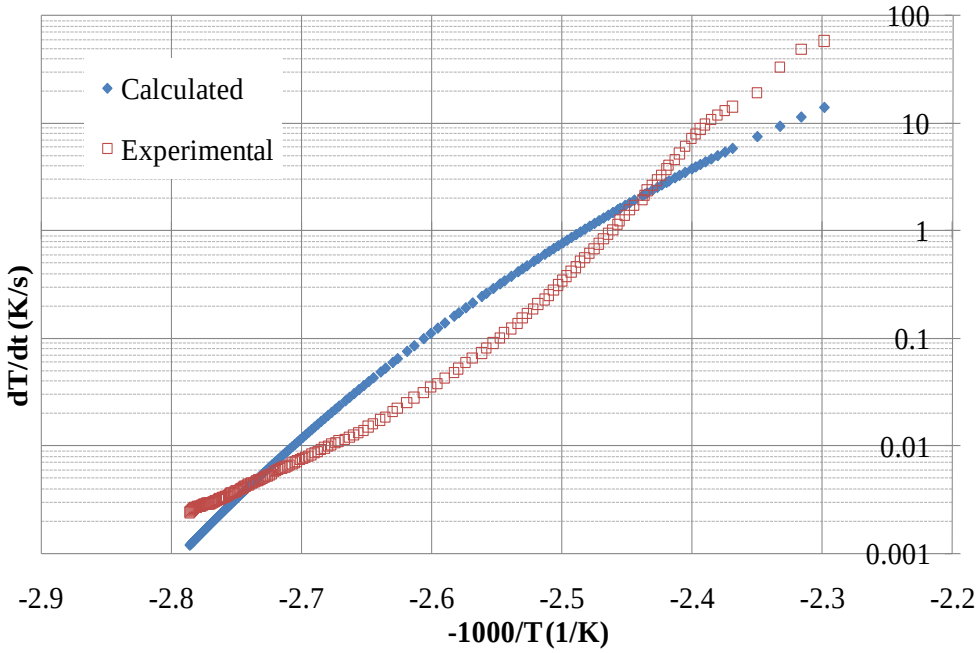

a. Pure MEKPO

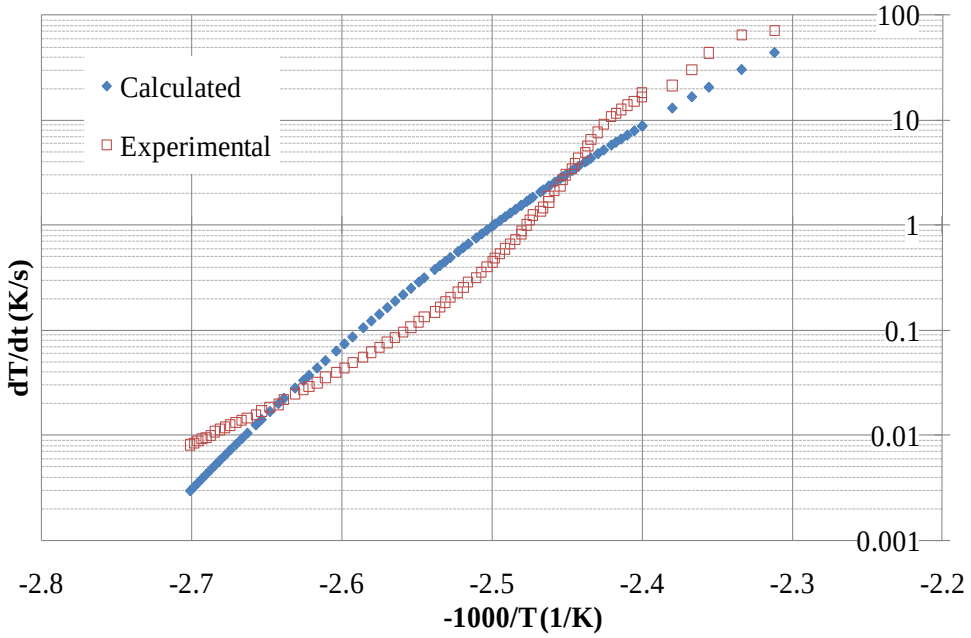

b. 0.03 wt% contaminant

Figure 4.8 Kinetic analyses using nth order reaction model

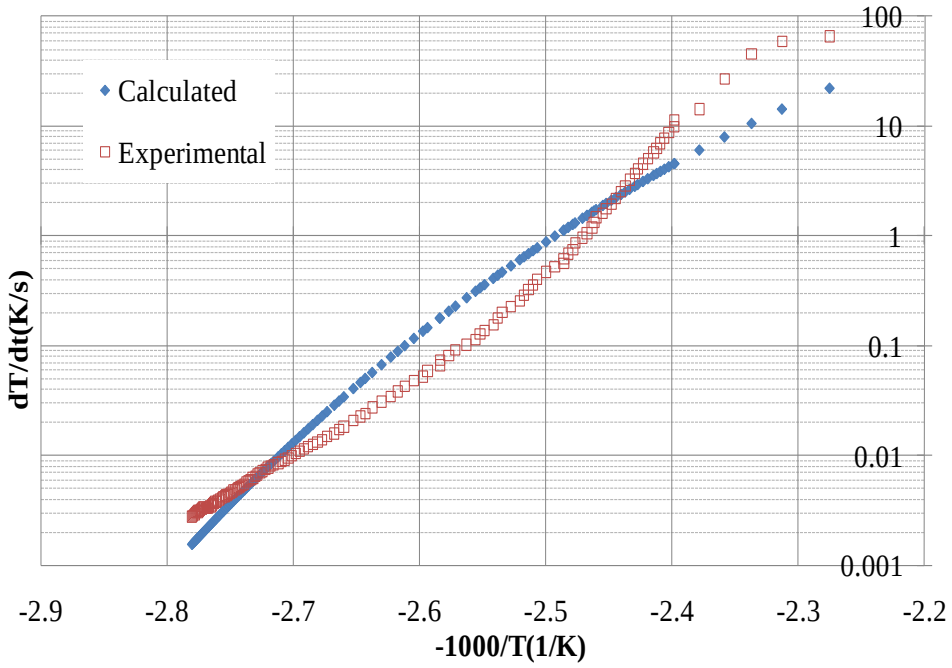

c. 0.075 wt% contaminant

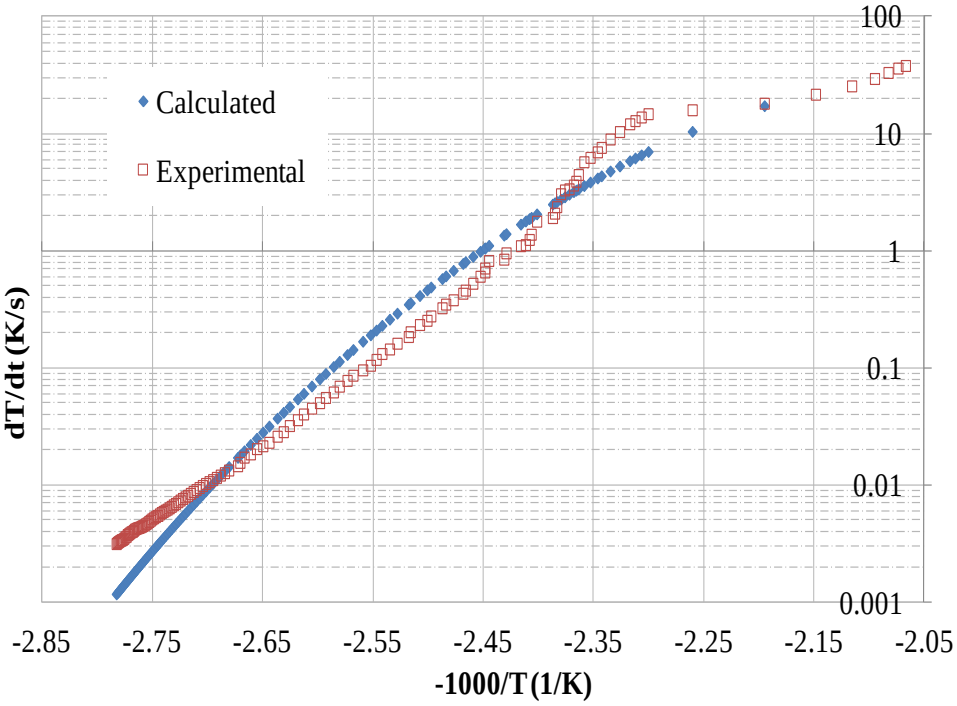

d. 0.3 wt% contaminant

Figure 4.8 Continued

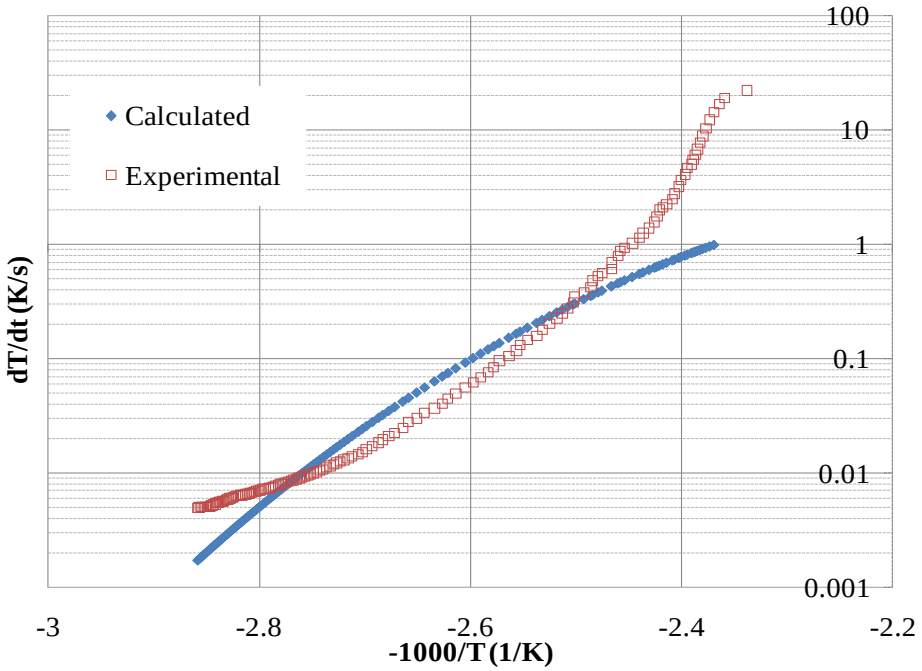

e. 1 wt% contaminant

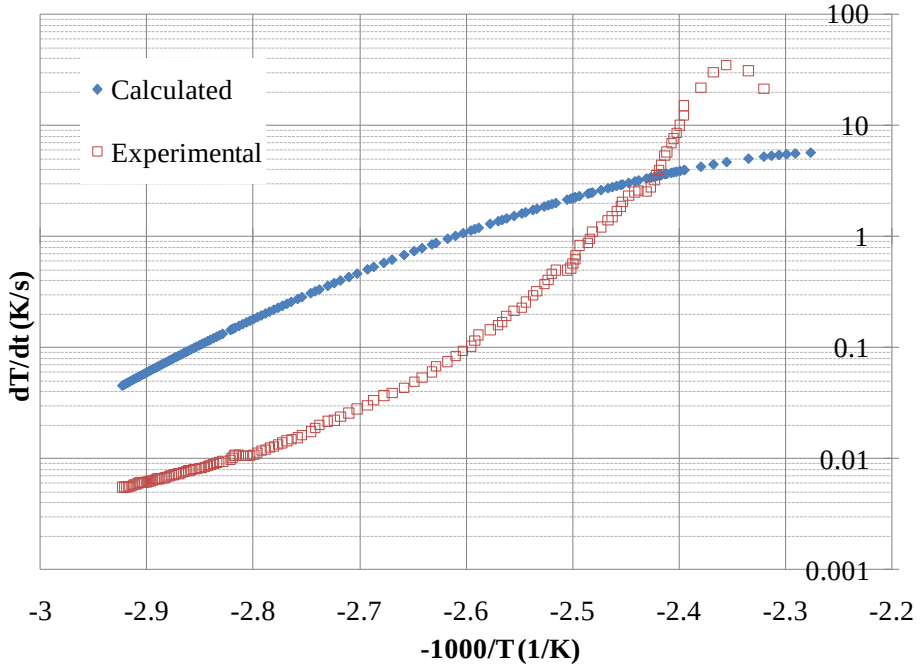

f. 5 wt% contaminant

Figure 4.8 continued

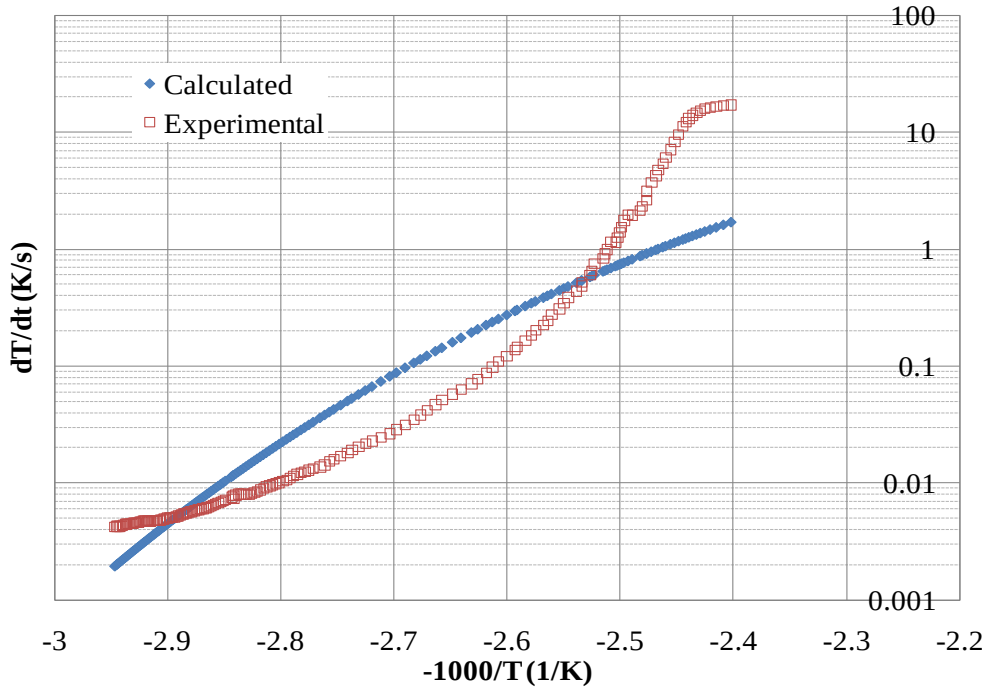

g. 10 wt% contaminant

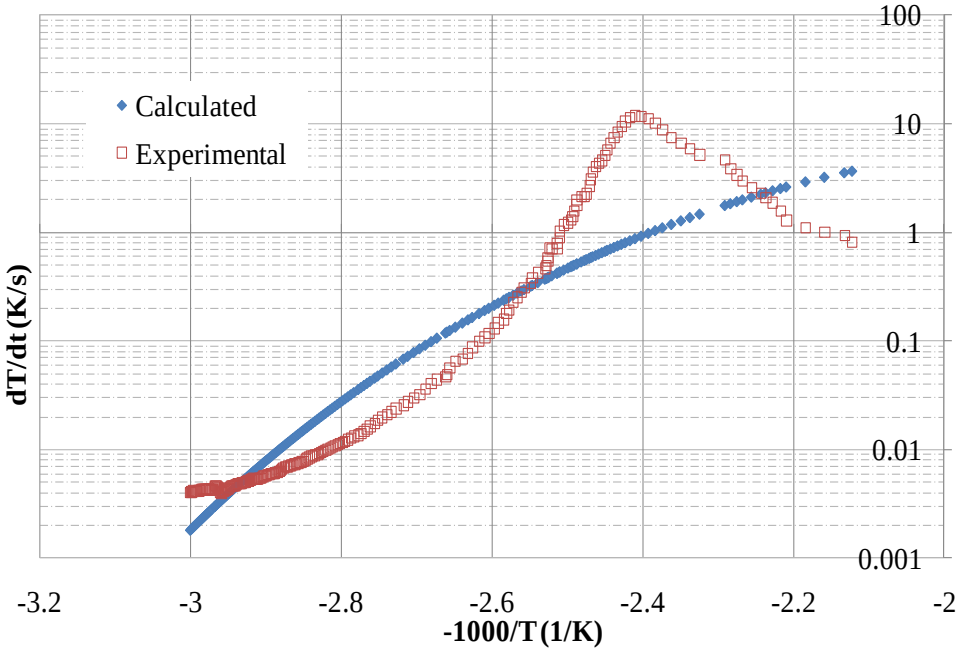

h. 20 wt% contaminant

Figure 4.8 Continued

Table 4.8 Estimation of kinetic parameters using nth order reaction model

Test No.	Iron oxide (wt%)	E_a (kJ/mol)	lnA
1	0	74.5	12.2
2	0.03	89.2	17.2
3	0.075	74.0	12.2
4	0.3	68.9	10.6
5	1	57.8	7.5
6	5	52.6	5.7
7	10	48.3	4.5
8	20	41.1	1.9

The estimated kinetic parameters follow the trend of onset temperature over the contaminant concentration range. According to the data presented in Table 4.8, reaction system with lower onset temperature shows low activation energy and frequency factor. However, by comparing the simulation results against experimental data in Figure 4.8, it was found that the nth order reaction model could not well simulate the runaway reaction process due to the gap between experimental and calculated data. Also, the calculated maximum self-heating rate was found to be much lower than the experimental data for all the tests. This phenomenon implies that the runaway reaction of MEKPO might follow autocatalytic reaction model. The autocatalytic model normally can achieve high self-heating rate because its reaction rate is the function of both reactants and products.

According to the kinetic investigation results, nth order reaction is not the appropriate reaction model representing the runaway reaction of MEKPO with the presence of iron oxide. More advanced kinetic model needs to be developed to study the kinetics of the MEKPO runaway reactions.

b. Autocatalytic reaction model

The basic autocatalytic model employed in this research is shown as follows [73].

$$\frac{d\alpha}{dt} = Ae^{-E_a/RT}(1-\alpha)^{n_1}(z+\alpha^{n_2}) \qquad 4\text{-}4$$

where A is the frequency factor, E_a is the apparent activation energy, α is the conversion, n_1, n_2 and z are parameters used to describe the catalytic effect of MEKPO. Because the experiment was performed in a non-adiabatic environment, the self-heating rate can be calculated using the following equation.

$$C_p m * \frac{dT}{dt} = \Delta H_r m \frac{d\alpha}{dt} * \frac{1}{\phi} \qquad 4\text{-}5$$

where C_P is the heat capacity; m is the sample mass; ΔH_r is heat of reaction; ϕ is thermal inertia factor.

Equations 4-4 and 4-5 can be combined together

$$\frac{dT}{dt} = \frac{\Delta H_r}{C_P \phi} * Ae^{-Ea/RT}(1-\alpha)^{n_1}(\alpha^{n_2} + z) \qquad 4\text{-}6$$

After developing the reaction model, the non-linear optimization method (Equation 4-7) was applied here to validate the model structure and estimate the kinetic parameters. This method uses Least Square Method to achieve the best fit to the experimental data by minimizing the measure of residuals between experimental and simulated responses. The estimated kinetic parameters obtained through non-linear optimization method are listed in Table 4.9. The calculated self-heating rate was plotted against experimental data in Figure 4.9.

$$SS(\overline{P}) = \sum_i w_i \left(Y_{\exp}(t_i) - Y_{sim}(t_i)\right)^2 \rightarrow \min = SS(\overline{P_r}) \qquad \text{Equation 4-7}$$

As seen in Figures 4.9 a-h, the calculated self-heating rate curves show quite good fitting to the experimental data under all contaminant levels, suggesting that an autocatalytic reaction model can represent the runaway reaction of MEKPO and MEKPO contaminated by different levels of iron oxide. A gap between experimental data and kinetic modeling results was observed in the high temperature range. This gap is caused by the fact that activation energy is a function of temperature, which decreases with the increase of temperature. Since the activation energy was assumed to be consistent in the kinetic investigation, in order to reach the same self-heating rate, reaction model needs

to reach higher temperature than the real runaway reaction. From the process safety point of view, the main purpose for developing the kinetic model is to predict when the runaway reaction can occur instead of accurate prediction of the reaction rate when runaway reaction is already quite severe. Therefore, the autocatalytic reaction model develop in this research meets the process safety requirement because the good agreement between simulation results and experimental data over the temperature rage, where runaway reactions are normally initiated.

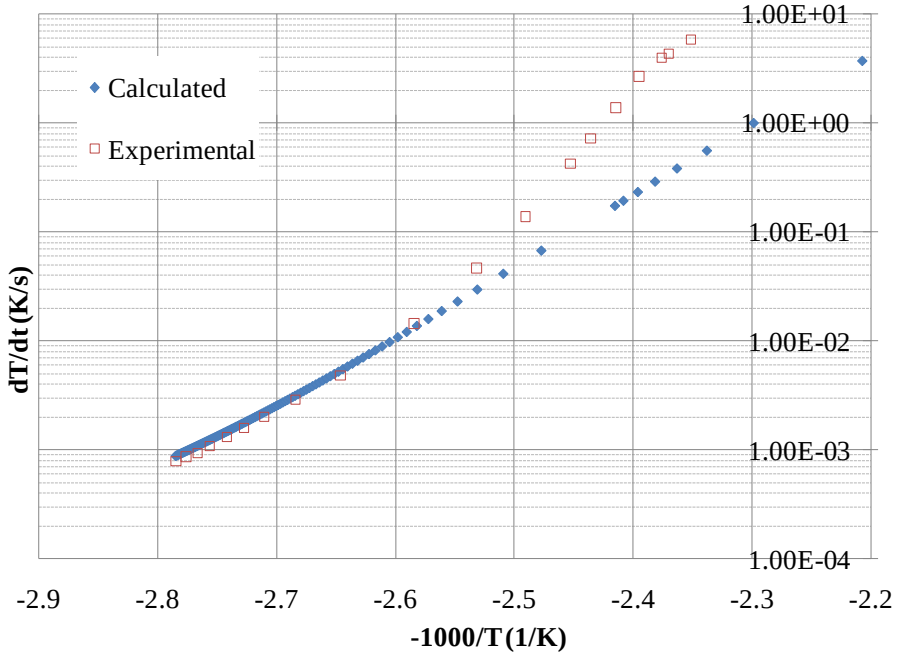

a. Pure MEKPO

Figure 4.9 Kinetic analyses using autocatalytic reaction model

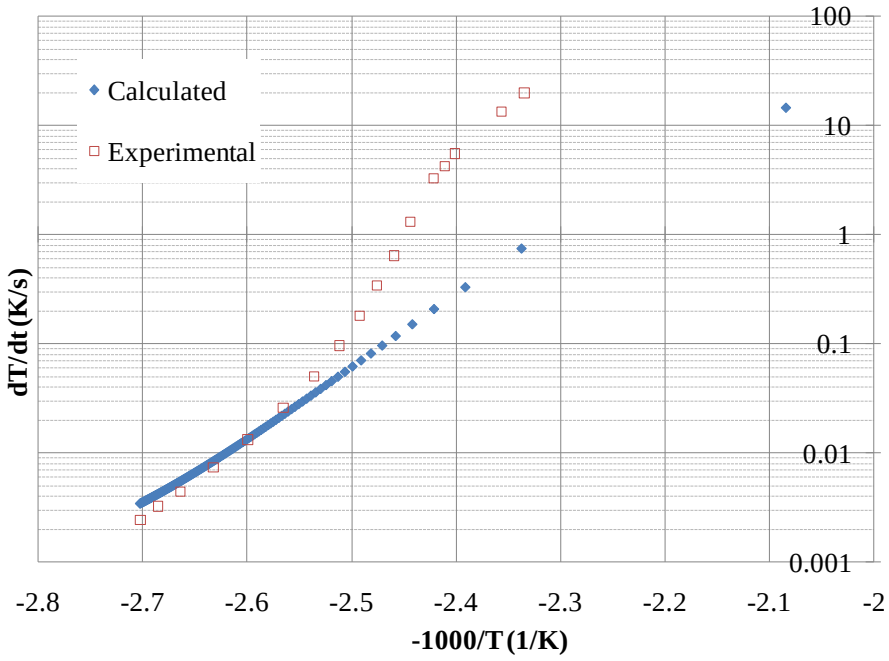

b. 0.03 wt% contaminant

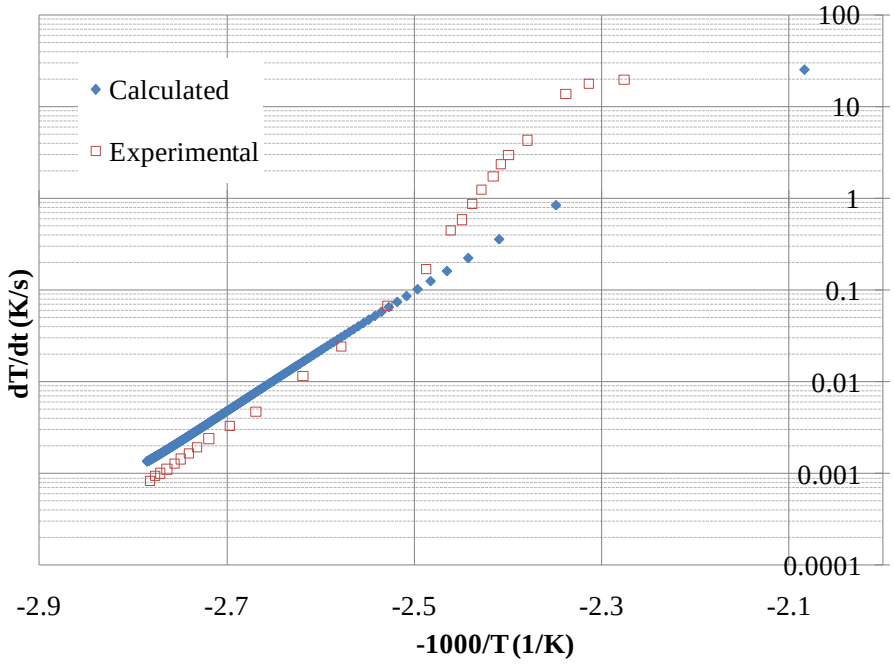

c. 0.075 wt%

Figure 4.9 Continued

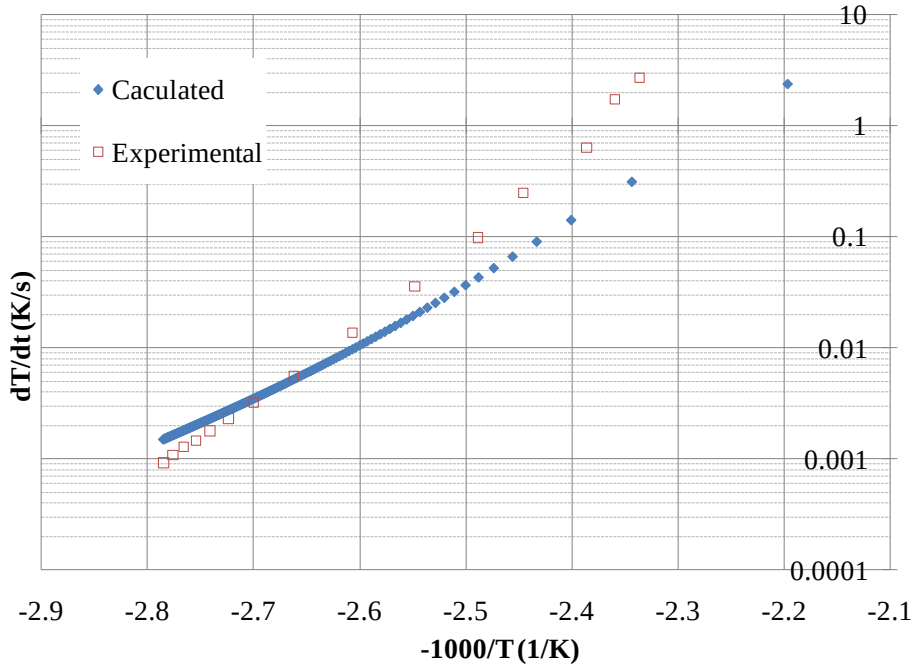

d. 0.3 wt% contaminant

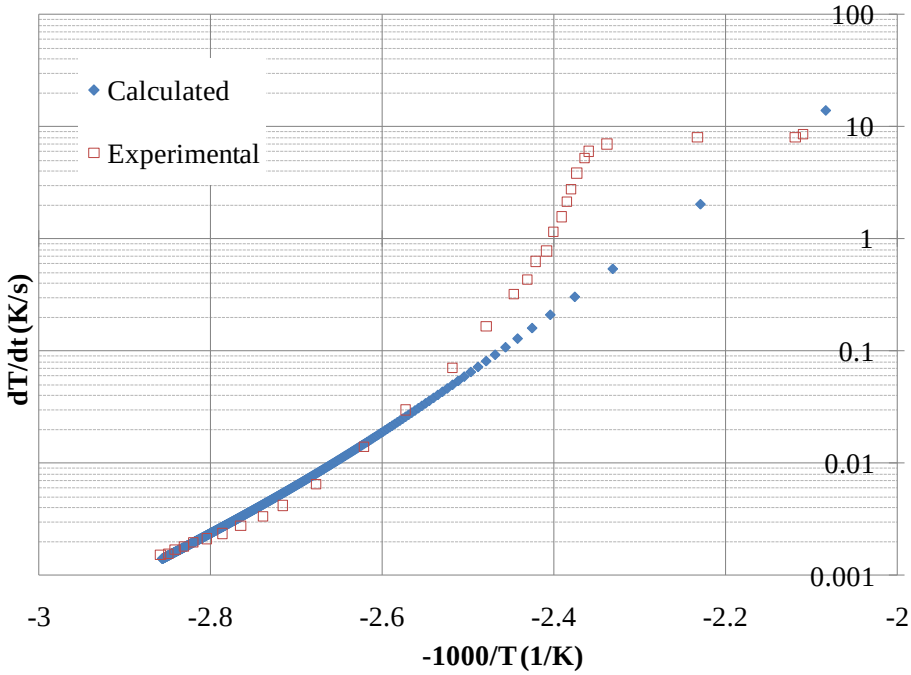

e. 1 wt% contaminant

Figure 4.9 Continued

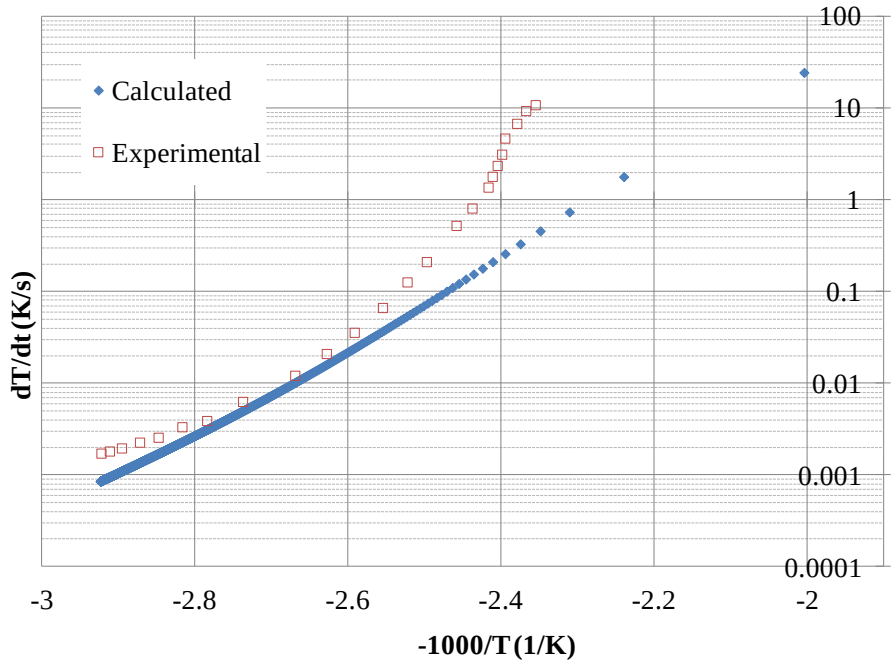

f. 5 wt% contaminant

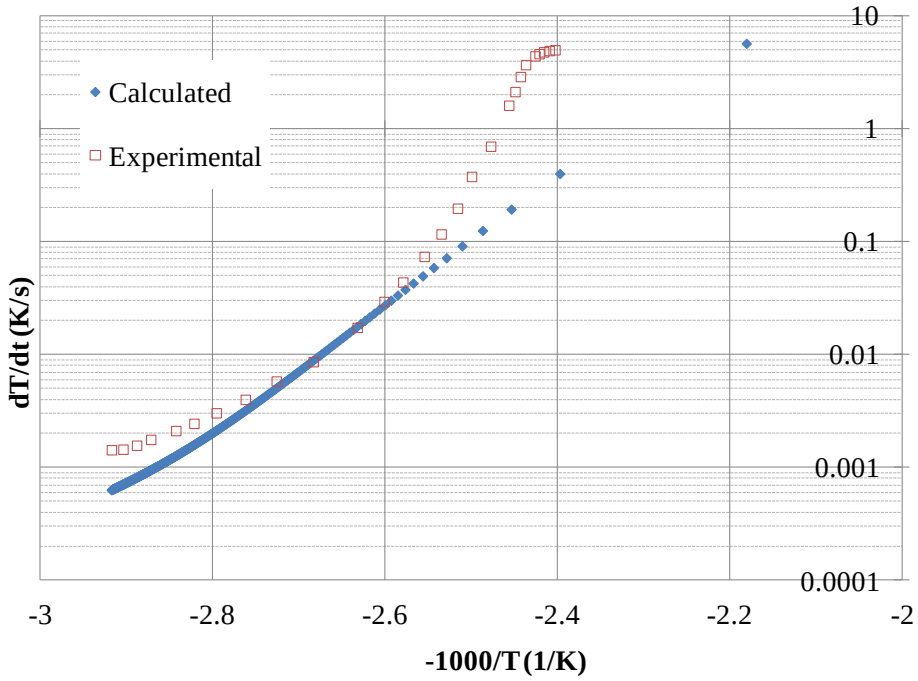

g. 10 wt% contaminant

Figure 4.9 Continued

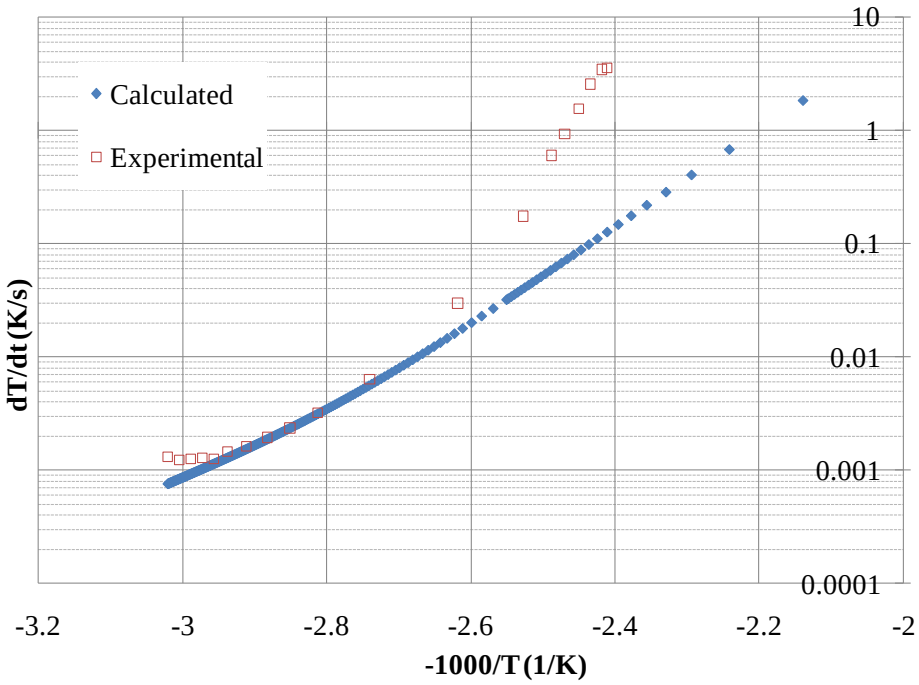

h. 20 wt% contaminant

Figure 4.9 Continued

The kinetic parameters presented in Table 4.9 show the effects of iron oxide on the kinetics of MEKPO runaway reaction. By analyzing the trends of various kinetic parameters, it was found that the trends of major kinetic parameters follow the trend of thermal stability of MEKPO. When the concentration of contaminant is below 0.03 wt%, all major kinetic parameters keep in the same level, indicating no significant change occurred on kinetics. However, starting from 0.3 wt% of iron oxide, the activation energy and frequency factor decrease dramatically with the increase of contaminant concentration: under 20 wt% iron oxide, activation energy is only half of that for pure MEKPO, and *lnA* almost decreases by 2/3 compared with pure MEKPO. The change of

major kinetic parameters leads to the change of reaction rate, and therefore causes the reduction of thermal stability.

Table 4.9 Estimation of kinetic parameters using autocatalytic reaction model

Test No.	Contaminant concentration (wt%)	T_0 (^oC)	n_1	n_2	E_a (kJ/mol)	z	lnA_1
1	0	86	0.22	1.95	97.4	0.1	23.0
3	0.03	97	0.2	1.8	95.8	0.1	23.0
5	0.075	86	0.1	1.3	96.4	0.1	22.9
6	0.3	86	0.1	2.5	81.0	0.1	18.1
7	1	76	0.1	2.5	77.0	0.1	17.2
8	5	69	0.1	2.5	77.6	0.1	16.8
9	10	66	0.1	2.4	64.6	0.02	14.9
10	20	58	0.1	2.5	52.4	0.03	9.9

The phenomena observed earlier that the low level of contaminant (0.03 wt%) makes MEKPO more stable can also be explained based on the kinetic study results. According to the data presented in Table 4.9, in the low contaminant concentration range (0 to 0.3 wt%), all the major kinetic parameters keep in the same level. According to Equation 4-6, if all the kinetic parameters keep in the same level, lower heat of reaction would lead

to lower self-heating rate. So, if we apply the same exotherm detection criteria (e.g. dT/dt=0.05 ^{o}C/min), the exotherm can only be detected at higher temperature for reaction with lower heat of reaction. This means for MEKPO under 0.03 wt% iron oxide, whose heat of reaction is lower, it requires higher temperature to reach the same exotherm detection criteria compared other tests. So, the abnormal increase of onset temperature under 0.03 wt% should be caused by the reduction of heat of reaction.

4.2.5 Evaluation of key safety parameters

When a chemical is decided to be employed in the process, it is important to determine the safe process conditions to ensure the compatibility between chemical and the process environment. So, based on the investigation of the impact of iron oxide on the reactive hazards of MEKPO, some key safety parameters were studied in this research for the purpose of maintaining safety operation in industry. The estimation of these key safety parameters can directly serve industry in determination of the safer process condition. In this research, two safety parameters were investigated: time to maximum rate and self accelerating decomposition temperature.

a. Time to maximum rate

Time to maximum rate (TMR) is defined as the time required for runaway reactions to reach the maximum self-heating rate. This parameter indicates the time available for taking defensive or mitigation measures in the case of process upset [74]. TMR is a critical important parameter used in the safety evaluation of processes where reactive chemicals are used. TMR is normally determined through calorimetry test under an adiabatic

condition [75]. However, determination of TMR through calorimetry test requires expensive testing equipment and lengthy test procedure, and therefore is not the best option for industry. In this research, based on the comprehensive understanding on the kinetics of the runaway reactions and the impact of contaminant on reaction kinetics, we were able to simulate the runaway reaction process under various conditions and estimate TMR in a much more economic and efficient way.

Using autocatalytic model developed in this research, we performed the simulation of runaway reaction process under different levels of contaminant. By applying the following criteria, it is easy to determine the TMR under different conditions.

$$\frac{\partial}{\partial t}\left(\frac{\partial T}{\partial t}\right) = 0 \qquad 4\text{-}8$$

TMR under different initial temperature was calculated for MEKPO with different levels of contaminant and are presented in Table 4.10. The adiabatic condition was assumed for runaway reaction simulation since near-adiabatic conditions are normally achieved by industrial processes. Some of the TMR data were plotted versus initial temperature in Figure 4.10 to shown the TMR trends over initial temperature. According to data presented in Figure 4.10, TMR shows exponential decrease over the temperature range. For example, it takes pure MEKPO 33 hours to reach the maximum self-heating rate under 47 ^{o}C; but this time decreases to about 10 min when the temperature reaches 107

^{o}C. Also, the gap between TMR curves was observed in this research, indicating the great impact posed by iron oxide on TMR.

Table 4.10 Calculated TMR for MEKPO with different levels of iron oxide (unit: hour)

T (^{o}C) / C (wt%)	47	57	67	77	87	97	107
0	33.33	11.94	4.44	1.81	0.75	0.33	0.16
0.03	31.94	11.11	4.17	1.67	0.72	0.32	0.15
0.075	30.56	10.42	3.89	1.56	0.67	0.29	0.14
0.3	18.33	7.64	3.47	1.58	0.78	0.39	0.21
1	8.89	4.00	1.81	0.89	0.46	0.24	0.14
5	13.33	5.83	2.69	1.31	0.67	0.35	0.19
10	5.28	2.50	1.31	0.69	0.39	0.22	0.13
20	3.89	2.36	1.39	0.89	0.58	0.39	0.25

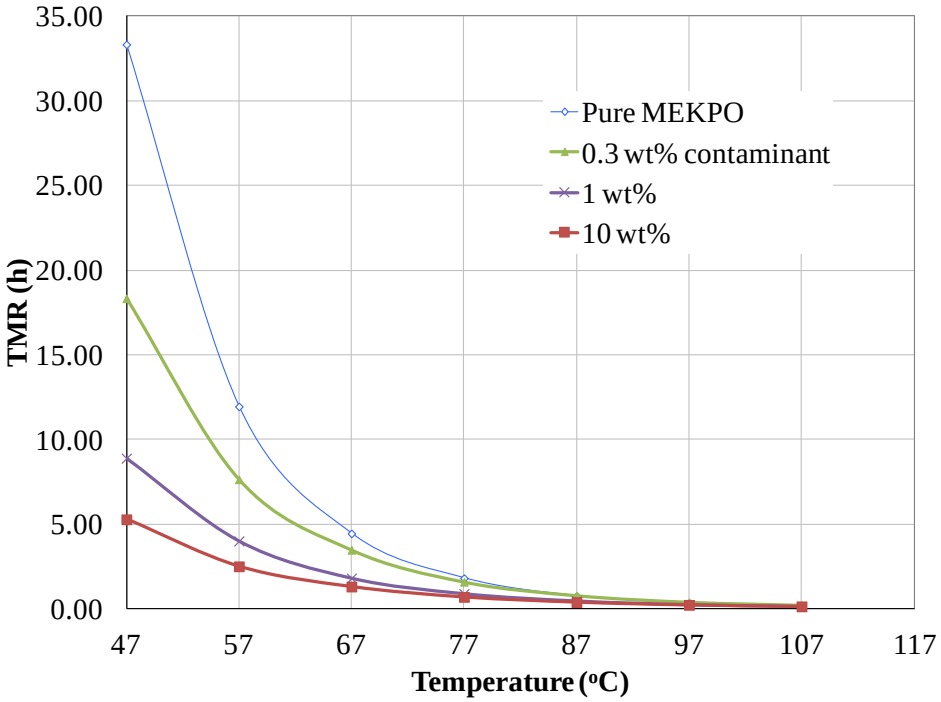

Figure 4.10 Trend of TMR over initial temperature

By plotting TMR of different reaction systems versus initial temperature, a safety diagram was generated in this research (Figure 4.11). By utilizing this safety diagram, it is easy to determine the TMR for a specific reaction system under a certain process temperature. Also, given the criteria for TMR in the process for selected reaction system, we can identify the criteria for process temperature in an efficient way.

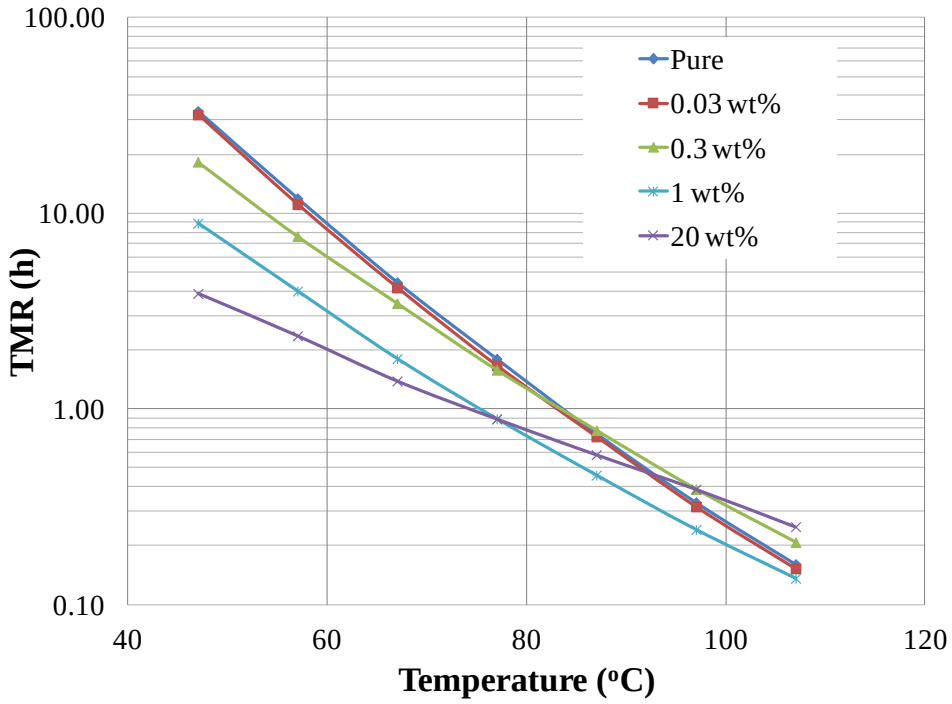

Figure 4.11 TMR safety diagram (Φ=1)

According to the TMR curves presented in Figure 4.11, in the contaminant concentration range of 0 to 0.075 wt%, TMR does not show big difference between MEKPO with different contaminant levels since these curves are quite close to each other. Under 0.3 wt% iron oxide, even though onset temperature of the reaction system is as the same as pure MEKPO, significant reduction of TMR was observed: under the same temperature (320 K), TMR is 18 hours for MEKPO with 0.3 wt% compared with 102 hours TMR for pure MEKPO. This reduction of TMR is caused by the change of kinetic parameters, which lead to the change of reaction rate. When contaminant concentration is beyond 0.3 wt%, TMR decreases dramatically with the increase of the contaminant concentration. However, the gap between TMR curves becomes less and less significant with the

increase of the initial temperature. With the increase of the initial temperature, the different of TMR between different reaction systems starts to decrease, indicating less influence on TMR from iron oxide. This is because when the process temperature is already high especially when it is above onset temperature, all reaction systems quickly join runaway reaction and there is very limited time available to response.

The analysis of TMR of different reaction systems shows that certain level of iron oxide (>0.3 wt%) can significantly decrease the TMR for the process and therefore intensify the hazard associate with the process.

b. Self accelerating decomposition temperature

Self accelerating decomposition temperature (SADT) is a parameter developed by the UN Recommendations for transportation process of organic peroxide or other self-reactive substance packaged [10]. It is defined as the lowest ambient temperature at which the temperature increase of a chemical substance is at least 6 ^{o}C in a specified commercial package during a period of seven days or less. Transportation temperatures can be derived from the SADT according to the recommendations given by the UN committee of Experts on Transport of Dangerous Goods. In common practice, SADT is the maximum temperature allowed for short-term storage to avoid potential runaway reaction.

Several test methods have been recommended by UN committee to determine the SADT, which are shown in Table 4.11. These methods include storage test either at a fixed external temperature or under near adiabatic conditions.

Table 4.11 SADT test methods recommended by UN

Code	Test
H1	The United States SADT test
H2	Adiabatic storage test
H3	Isothermal storage test
H4	Heat accumulation storage test

Each option in Table 4.11 requires the use of specific equipment and lengthy test procedure, and therefore is not the best option for industry especially small companies. As a fact, many manufacturers do not provide SADT data in MSDSs or do not provide data for all package sizes due to the expensive and time-consuming experimental approach.

The autocatalytic reaction model developed earlier can be combined with the heat transfer equation to simulate the SADT test process. The SADT reaction model is depicted by Equation 4-9. In the small size package (25 gallon), the temperature is

assumed to be uniformly distributed because of the relative large ratio of surface area to volume. The value of parameters used in the heat transfer equation are collected from literature [76].

$$C_P M_0 \frac{dT}{dt} = \frac{\Delta H M_0}{\Phi} \frac{d\alpha}{dt} - US(T - T_a) \qquad 4\text{-}9$$

where ϕ is thermal inertia factor, T_a is the ambient temperature; C_P is the heat capacity of the reaction system, U is heat transfer coefficient, T is the temperature in the package, S is wetted surface area, M is the mass of reactant, α is the conversion rate.

An example of determining SADT for pure MEKPO in 25 gallon package is shown in Figure 4.12. In this approach, by utilizing the reaction model, SADT test process can be simulated under different ambient temperature until finding the one which meets the definition of SADT. The simulated SADT for pure MEKPO in 25 gallon is 354 K, and is quite close to the experimental date obtained from the vendor (349 K). The small difference between the calculated and experimental SADT implies that determining SADT through reaction modeling is a reliable approach for some package sizes. The calculated SADT for MEKPO with different levels of iron oxide is presented in Table 4.12.

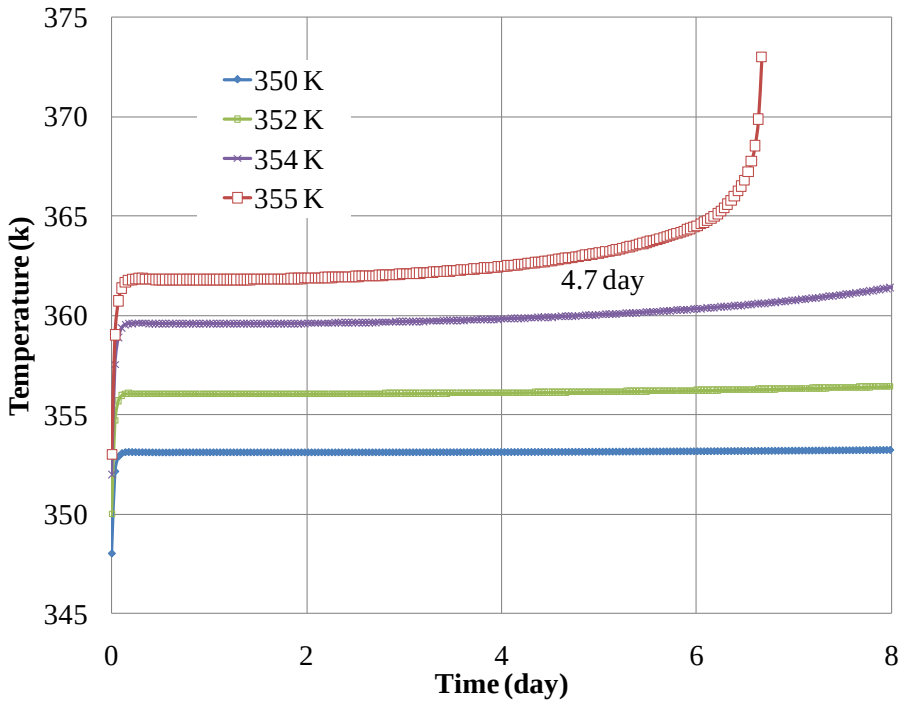

Figure 4.12 Determine SADT through reaction modeling for pure MEKPO in 25 gallon package

According to the data presented in Table 4.12, SADT shows little variation with the increase of contaminant concentration. When contaminant concentration reached 10 wt%, SADT only decreased by 7°C. Compared with trend of onset temperature, SADT shows less decrease over the contaminant concentration range. This phenomenon is caused by the fact that SADT test is conducted in a non-adiabatic environment. Under this condition, heat generated by the exothermic reaction can be transferred to the environment and lead to the less impact on SADT. Only when the heat transfer equilibrium is broken by the increase of reaction rate when contaminant concentration is further increased (20 wt%), SADT started to decease significantly.

Table 4.12 Determination of SADT for MEKPO in 25 gallon package

Contaminant (wt%)	SADT (^oC)	T_0 (^oC)
0	81	86
0.03	80	97
0.075	78	86
0.3	79	86
1	71	76
5	75	69
10	74	66
20	63	58

4.4 Conclusions and discussion

Through the analysis of calorimetric data, kinetic investigation and further estimation of key safety parameters, the role played by iron oxide was studied and the impact imposed by iron oxide on runaway reactions was evaluated. Based on the results of comprehensive analysis, it was found that the role played by iron oxide depends on its concentration and different reaction mechanisms were involved in the runaway reaction of MEKPO.

Iron oxide has almost no effect on runaway reaction when the contaminant concentration is below 0.075 wt%. Within this concentration range, the runaway reaction follows the same reaction mechanism and kinetics as pure MEKPO. As the result, all the important

calorimetric parameters observed keep in the same level, indicating no change occurred on reactive hazards. Also, the estimation of key safety parameters indicates that within this range, iron oxide shows no impact on the safety of process operations where MEKPO is employed.

Iron oxide starts to play a role in runaway reaction when its concentration reaches 0.3 wt%. Within the concentration range of 0.3 – 10 wt%, iron oxide acts as a catalyst for the runaway reaction, leading to the decrease of the activation energy. The runaway reaction still follows the same reaction mechanism as before according to consistent heat of reaction and gas generation. Because of the change in kinetics, MEKPO becomes more unstable but the reaction becomes less severe according to the maximum self-heating rate and pressure rate data. According to the analysis of key safety parameters, within this concentration range, we have less response time when the process upset occurs because of the decrease of TMR. However, the transportation conditions are not greatly affected by the presence of iron oxide within this range due to the small change of SADT.

When iron oxide falls into the high concentration range (>10 wt%), the kinetics of the runaway reaction keeps on changing with activation energy and frequency factor decreasing. Therefore, the stability of MEKPO keeps on decreasing as well as the maximum reaction rate. Within this range, heat of reaction is higher than other tests, indicating the change of reaction mechanism. Because of the higher heat of reaction, the

reaction system can reach higher temperature and initiate another reaction. This reaction is represented by the second peak in self-heating rate and gas generation rate curves shown in Figure 4.13a and 4.13b. This secondary reaction is associated with lower thermal hazard because of its relative low self-heating rate. However, this reaction presents great non-condensable gas pressure hazard. The analysis of key safety parameters indicates that high level iron oxide (>10 wt%) has great impact on TMR and SADT and therefore affects the safety of process operations.

According to the investigation results, iron oxide does not present significant impact on operational safety since it normally remains in a very low level in the process. In this case, carbon steel still can be used to fabricate process equipment handling MEKPO. Also mechanical integrity program should be employed by industry to monitor the level of iron oxide through periodic inspection. The information presented in this chapter such as TMR and SADT can help industry to determine the safer process conditions.

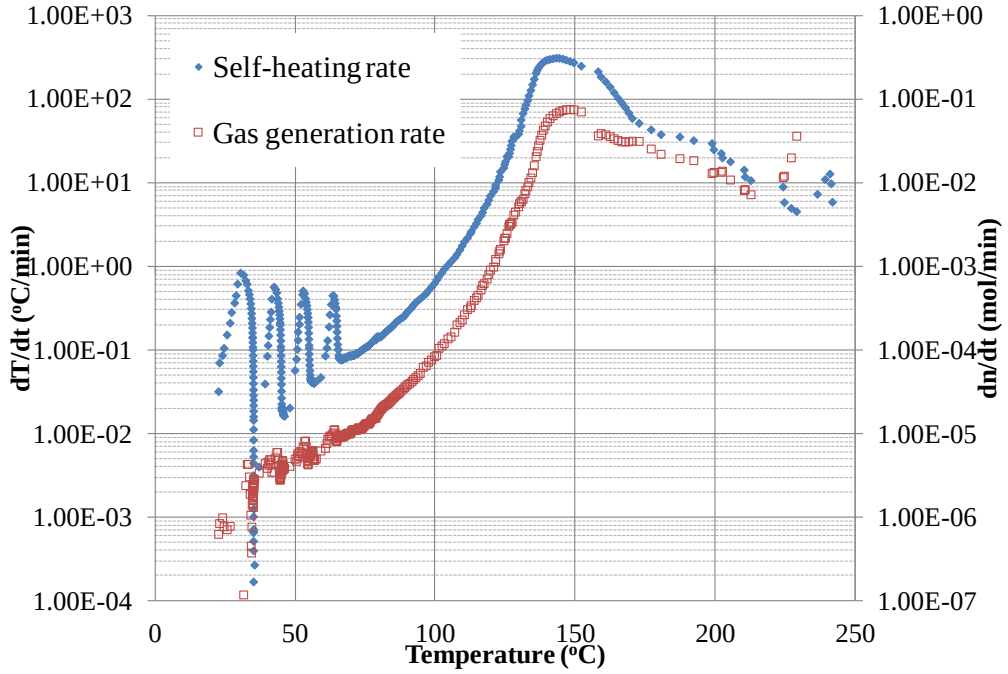

a. 10 wt%

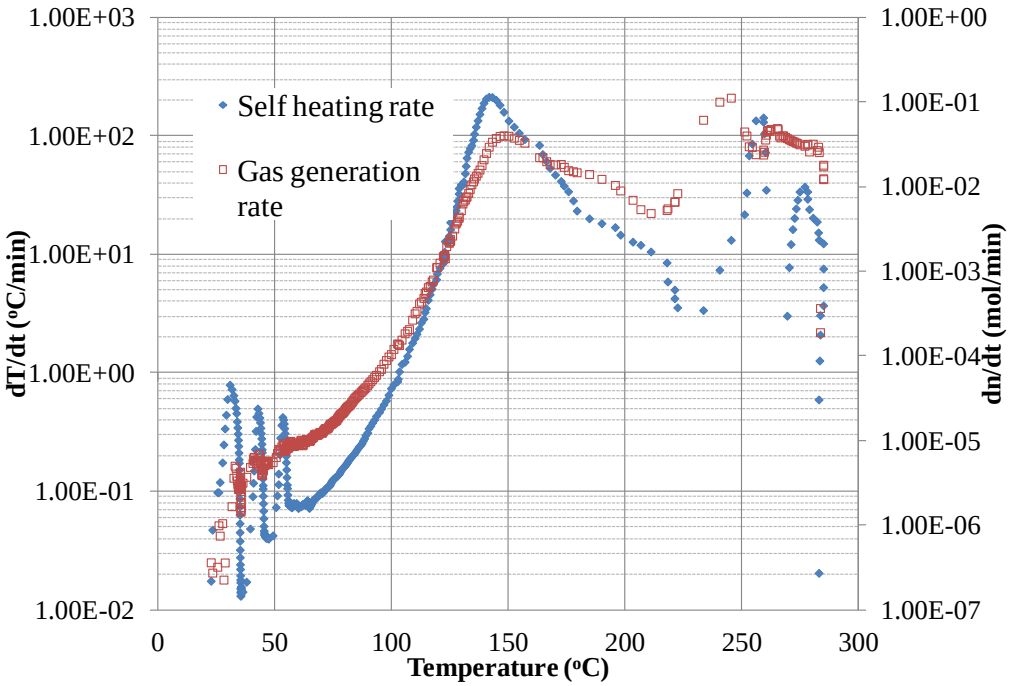

b. 20 wt%

Figure 4.13 Analysis of runaway reaction mechanism

CHAPTER V

CONCLUSIONS AND RECOMMENDATIONS

5.1 Conclusions

A systemic methodology for chemical hazard assessment was developed in this research through the combination of theoretical work and experimental work. This methodology includes the selection of safer reactive chemicals for the process and the determination of safer process conditions.

In the selection of safer chemical part, two prediction models were derived, which can make predictions on onset temperature and heat of reaction of organic peroxides. Through sensitivity analysis of these models, molecular properties such as activation energy and atomic charge of oxygen were found to contribute to the reactive hazards. Also, out of the three hazard indices examined in this research, RHI was determined to be the one most suitable for organic peroxides. By combing prediction models and RHI, we are able to quickly predict hazards properties for a large number of organic peroxides and classify them according the reactive hazards associated.

In the part of determining safer process conditions, as a case study, the incompatibility of MEKPO with iron oxide as the contaminant was investigated. We found that the impact of iron oxide on reactive hazards and operational safety depends on the level of iron oxide in the process. Iron oxide presents almost no impact on reactive hazards as

well as operational safety in low concentration (<0.075 wt%). However, once the concentration of iron oxide exceeds 0.3 wt%, it starts to change kinetics of the runaway reaction and make MEKPO more unstable. The impact of iron oxide also leads to the shorter TMR. With the further increase of contaminant concentration (>10 wt%), runaway reaction follows a different reaction mechanism, which leads to the increase of heat of reaction. Also, within this concentration range, a secondary reaction is initiated when reaction system reaches higher temperature. The secondary reaction presents great non-condensable gas pressure hazard to the process. The presence of high level of iron oxide shows great negative influence on TMR and SADT and therefore presents significant effects on the safety of process operations.

This chemical hazard assessment methodology provides industry a feasible approach to minimize the hazards associated with the process by selecting the right chemical and determining the right process conditions. This methodology can be combined with ISD principles in the process design to make the process inherently safe.

5.2 Recommendations for future work

In the further work, investigation on the reaction mechanism is recommended to study the change of reaction mechanism occurred with the presence of high level of iron oxide. The reaction mechanism of MEKPO runaway reaction can be studied by using equipment such as Gas Chromatography (GC) and High Performance Liquid Chromatography (HPLC). These equipment can analyze the composition of the residual of the reaction system and gaseous products produced during the reaction process, based

on which the reaction pathway can be speculated. Molecular simulation can also be employed in the future research to identify the elementary reactions involved in the runaway reaction of MEKPO, which are difficult to be investigated through experimental approach.

Integrating process optimization into the design of inherently safer process could be another direction for future research in this area. By combing process optimization with the ISD technique, it is expected to reach the balance between process safety and process efficiency in the process design. For example, safety constraints such as onset temperature and TMR obtained from this research can be applied in the process optimization to ensure the process meets the safety criteria. Meanwhile, important considerations in process optimization such as process efficiency and energy cost can be used when selecting safer chemicals for processes.

REFERENCES

1. *Improving Reactive Hazard Management*; CSB: Washington, DC, 2002.

2. Overton, T.; King, G. M. Inherently safer technology: An evolutionary approach. *Process Saf. Prog.* **2006,** *25*, 116.

3. Carrithers, G.; Dowell, A.; Hendershot, D. It's never too late for inherent safety, International Conference and Workshop on Process Safety Management and Inherently Safer Processes, Orlando, FL, October 8-11, 1996; AICHE: New York, 1996.

4. Mannan, M. S. Challenges in implementing inherent safety principles in new and existing chemical processes. Mary Kay O'Connor Process Safety Center, *Texas A&M University, College Station, Texas,* 2002.

5. Bollinger, R. E.; Crowl, D. A. *Inherently Safer Chemical Processes: A Life Cycle Approach*; CCPS/AIChE: New York, 1997.

6. Kletz, T. A. *Plant Design for Safety: A User-Friendly Approach*; Taylor & Francis: London, 1991.

7. Khan, F. I.; Amyotte, P. R. How to make inherent safety practice a reality. *Can. J. Chem. Eng.* **2003,** *81*, 2.

8. Fauske, H. K. The reactive system screening tool (RSST): An easy, inexpensive approach to the DIERS procedure. *Process Saf. Prog.* **1998,** *17*, 190.

9. Freire, E. Differential scanning calorimetry. *Methods Mol. Biol* **1995,** *40*, 191.

10. *UN Recommendations on the Transport of Dangerous Goods. Manual of Tests and Criteria*; United Nations: New York and Geneva, 2002.

11. Noller, D.; Mazurowski, S.; Linden, G.; De Leeuw, F.; Mageli, O. A relative hazard classification of organic peroxides. *J. Ind. Eng. Chem.* **1964,** *56*, 18.

12. Buchwald, P.; Bodor, N. Computer-aided drug design: the role of quantitative structure-property, structure-activity, and structure-metabolism relationships (QSPR, QSAR, QSMR). *Drugs Fut.* **2002,** *27*, 577.

13. Hansch, C. The QSAR paradigm in the design of less toxic molecules. *Drug Metab Rev.* **1984,** *15*, 1279.

14. Gao, H.; Katzenellenbogen, J. A.; Garg, R.; Hansch, C. Comparative QSAR analysis of estrogen receptor ligands. *Chem. Rev* **1999,** *99*, 723.

15. Bradbury, S. P. Quantitative structure-activity relationships and ecological risk assessment: an overview of predictive aquatic toxicology research. *Toxicol. Lett.* **1995,** *79*, 229.

16. Shanley, E. S.; Melhem, G. A. The oxygen balance criterion for thermal hazards assessment. *Process Saf. Prog.* **1995,** *14*, 29.

17. Benassi, R.; Folli, U.; Sbardellati, S.; Taddei, F. Conformational properties and homolytic bond cleavage of organic peroxides. I. An empirical approach based upon molecular mechanics and ab initio calculations. *J. Comput. Chem.* **1993,** *14*, 379.

18. Foresman, J. B.; Frisch, A. E.; Gaussian, I. *Exploring Chemistry with Electronic Structure Methods*; Gaussian, Inc.: Pittsburgh PA, 1996.

19. Swain, C. G.; Stockmayer, W. H.; Clarke, J. T. Effect of structure on the rate of spontaneous thermal decomposition of substituted benzoyl peroxides. *J. Am. Chem. Soc.* **1950,** *72*, 5426.

20. Litinskii, A. O.; Shreibert, A. I.; Balyavichus, L. M. Z.; Bolotin, A. B. Electronic structure, stability, and reactivity of alkyl peroxides. *Theor. Exp. Chem.* **1974,** *7*, 673.

21. Khursan, S. L.; Antonovsky, V. L. Structure, thermochemistry, and conformational analysis of peroxides ROOR and hydroperoxides ROOH (R= Me, But, CF3). *Russ. Chem. Bull.* **2003,** *52*, 1312.

22. Chermette, H. Chemical reactivity indexes in density functional theory. *J. Comput. Chem.* **1999,** *20*, 129.

23. Fayet, G.; Joubert, L.; Rotureau, P.; Adamo, C. On the use of descriptors arising from the conceptual density functional theory for the prediction of chemicals explosibility. *Chem. Phys. Lett.* **2009,** *467*, 407.

24. Fayet, G.; Rotureau, P.; Joubert, L.; Adamo, C. On the prediction of thermal stability of nitroaromatic compounds using quantum chemical calculations. *J. Hazard. Mater.* **2009,** *171*, 845.

25. Parr, R. G.; Szentpaly, L.; Liu, S. Electrophilicity index. *J. Am. Chem. Soc.* **1999,** *121*, 1922.

26. Mulliken, R. S. A new electroaffinity scale; together with data on valence states and on valence ionization potentials and electron affinities. *J. Chem. Phys.* **1934,** *2*, 782.

27. Parr, R. G.; Pearson, R. G. Absolute hardness: companion parameter to absolute electronegativity. *J. Am. Chem. Soc.* **1983,** *105*, 7512.

28. Iwata, Y.; Momota, M.; Koseki, H. Thermal risk evaluation of organic peroxide by automatic pressure tracking adiabatic calorimeter. *J. Therm. Anal. Calorim.* **2006,** *85*, 617.

29. Lu, Y.; Ng, D.; Miao, L.; Mannan, M. S. Key observations of cumene hydroperoxide concentration on runaway reaction parameters. *Thermochimica Acta* **2010,** *501*, 65.

30. *Materials Studio 2.2*; Accelrys Inc.: San Deigo, CA, 2001.

31. Höskuldsson, A. PLS regression methods. *J. Chemom.* **1988,** *2*, 211.

32. Fang, L.; Huang, J.; Yu, G.; Li, X. Quantitative structure-property relationship studies for direct photolysis rate constants and quantum yields of polybrominated diphenyl ethers in hexane and methanol. *Ecotoxicol. Environ. Saf.* **2009,** *72*, 1587.

33. Roy, K.; Ghosh, G. QSTR with extended topochemical atom (ETA) indices. 12. QSAR for the toxicity of diverse aromatic compounds to Tetrahymena pyriformis using chemometric tools. *Chemosphere* **2009,** *77*, 999.

34. Wold, S.; Ruhe, A.; Wold, H.; Dunn III, W. The collinearity problem in linear regression. The partial least squares (PLS) approach to generalized inverses. *SIAM J Sci Stat Comp.* **1984,** *5*, 735.

35. Becke, A. D. Density-functional thermochemistry. III. The role of exact exchange. *J. Chem. Phys.* **1993,** *98*, 5648.

36. Lee, C.; Yang, W.; Parr, R. G. Development of the Colle-Salvetti correlation-energy formula into a functional of the electron density. *Phys. Rev. B: Condens. Matter* **1988,** *37*, 785.

37. Frisch, M. J.; Trucks, G. W.; Schlegel, H. B.; Scuseria, G. E.; Robb, M. A.; Cheeseman, J. R.; Montgomery, J. A.; Vreven, T.; Kudin, K. N.; Burant, J. C.; Millam, J. M.; Iyengar, S. S.; Tomasi, J.; Barone, V.; Mennucci, B.; Cossi, M.; Scalmani, G.; Rega, N.; Petersson, G. A.; Nakatsuji, H.; Hada, M.; Ehara, M.; Toyota, K.; Fukuda, R.; Hasegawa, J.; Ishida, M.; Nakajima, T.; Honda, Y.; Kitao, O.; Nakai, H.; Klene, M.; Li, X.; Knox, J. E.; Hratchian, H. P.; Cross, J. B.; Bakken, V.; Adamo, C.; Jaramillo, J.; Gomperts, R.; Stratmann, R. E.; Yazyev, O.; Austin, A. J.; Cammi, R.; Pomelli, C.; Ochterski, J. W.; Ayala, P. Y.; Morokuma, K.; Voth, G. A.; Salvador, P.; Dannenberg, J. J.; Zakrzewski, V. G.; Dapprich, S.; Daniels, A. D.; Strain, M. C.; Farkas, O.; Malick, D. K.; Rabuck, A. D.; Raghavachari, K.; Foresman, J. B.; Ortiz, J. V.; Cui, Q.; Baboul, A.

G.; Clifford, S.; Cioslowski, J.; Stefanov, B. B.; Liu, G.; Liashenko, A.; Piskorz, P.; Komaromi, I.; Martin, R. L.; Fox, D. J.; Keith, T.; Laham, A.; Peng, C. Y.; Nanayakkara, A.; Challacombe, M.; Gill, P. M. W.; Johnson, B.; Chen, W.; Wong, M. W.; Gonzalez, C.; Pople, J. A. *Gaussian 03, Revision C.02*; Gaussian, Inc.: Wallingford, CT, 2003.

38. Ii, R. D.; Keith, T.; Millam, J.; Eppinnett, K.; Hovell, W. L.; Gilliland, R. *GaussView, Version 3.09*; Semichem Inc.: Shawnee Mission, KS, 2003.

39. Hehre, W. J.; Ditchfield, R.; Pople, J. A. Self-consistent Molecular Orbital Methods. XII. Further Extensions of Gaussian-type Basis Sets for Use in Molecular Orbital Studies of Organic Molecules. *J. Chem. Phys.* **1972,** *56*, 2257.

40. Krishnan, R.; Binkley, J. S.; Seeger, R.; Pople, J. A. Self consistent molecular orbital methods. XX. A basis set for correlated wave functions. *J. Chem. Phys.* **1980,** *72*, 650.

41. Frisch, M. J.; Pople, J. A.; Binkley, J. S. Self consistent molecular orbital methods 25. Supplementary functions for Gaussian basis sets. *J. Chem. Phys.* **1984,** *80*, 3265.

42. Stull, D. R. Linking thermodynamics and kinetics to predict chemical hazards. *J. Chem. Educ.* **1974,** *51*, A21.

43. Wang, Q.; Rogers, W.; Mannan, M. Thermal risk assessment and rankings for reaction hazards in process safety. *J. Therm. Anal. Calorim.* **2009,** *98*, 225.

44. Zhimin, F.; Jinyin, H.; Liang, M.; Weiguo, Y.; Aihong, J. In *Classification for Thermal Stability of 17 Reactive Chemical Substances*, Proceedings of the 2006 International Symposium on Safety Science and Technology, Shanghai, China, October, 24-27, 2006; China Occupational Safety and Health Association: 2006.

45. Höhne, G.; Hemminger, W.; Flammersheim, H. J. *Differential Scanning Calorimetry*; Springer Verlag: New York, 2003.

46. Carreto-Vazquez, V. H.; Hernandez, I.; Ng, D.; Rogers, W. J.; Mannan, M. S. Inclusion of pressure hazards into NFPA 704 instability rating system. *J. Loss Prev. Process Ind.* **2010,** *23*, 30.

47. *APTAC Operation Manual*; Arthur D. Little: Boston, 1999.

48. Incropera, F. P.; De Witt, D. P.; Bergman, T. L.; Lavine, A. S.; DeWitt, B.; Dewitt, D. P.; Van Hove, L.; DeWitt-Morette, C.; Cartier, P. *Fundamentals of Heat and Mass Transfer*; John Wiley and Sons Inc.: New York, 1985.

49. Kossoy, A.; Akhmetshin, Y. Identification of kinetic models for the assessment of reaction hazards. *Process Saf. Prog.* **2007,** *26*, 209.

50. Yaws, C. L. *Chemical Properties Handbook: Physical, Thermodynamic, Environmental, Transport, Safety, and Health Related Properties for Organic and Inorganic Chemicals*; McGraw-Hill: New York, 1999.

51. Kletz, T. A. *Process Plants: A Handbook for Inherently Safer Design*; CRC: Boca Raton, FL, 1998.

52. Urben, P. G.; Pitt, M. J. *Bretherick's Handbook of Reactive Chemical Hazards*; Elsevier: Burlington, MA, 2007.

53. Seaton, W. H.; Freedman, E.; Treweek, D. N. *CHETAH-The ASTM Chemical Thermodynamic and Energy Release Evaluation Program*; American Society for Testing and Materials: Philadelphia, 1974.

54. Melhem, G.; Shanley, E. On the estimation of hazard potential for chemical substances. *Process Saf. Prog.* **1996,** *15*, 168.

55. Saraf, S.; Rogers, W.; Mannan, M. S. Application of transition state theory for thermal stability prediction. *Ind. Eng. Chem. Res.* **2003,** *42*, 1341.

56. Lobunez, W.; Rittenhouse, J. R.; Miller, J. G. The electric mometns of organic peroxides. 1. Dialkyl peroxides, alkyl hydroperoxides and diacyl peroxides. *J. Am. Chem. Soc.* **1958,** *80*, 3505.

57. Verderame, F. D.; Miller, J. G. Electric moments of organic peroxides 3. Peresters. *J. Phys. Chem.* **1962,** *66*, 2185.

58. Litinskii, A. O.; Rakhimov, A. I.; Shatkovskaya, D. B.; Bolotin, A. B. Estimation of the stability of functional organic peroxides from the electronic structure indices and the bond energy parameters within the framework of the modified indo method. *J. Struct. Chem.* **1978,** *19*, 342.

59. Kikuchi, O.; Hiyama, A.; Yoshida, H.; Suzuki, K. Electronic-structure and homolytic dissociation of dibenzoyl peroxide *Bull. Chem. Soc. Jpn.* **1978,** *51*, 11.

60. *NFPA 704: Standard System for the Identification of the Hazards of Materials for Emergency Response*; National Fire Protection Association: Quincy, MA, 2001.

61. Belyaev, V. A.; Yablonskii, O. P.; Vinogradov, A. N.; Bystrov, V. F. Self-association of hydrocarbon hydroperoxides. *Theor. Exp. Chem.* **1972,** *6*, 110.

62. Katritzky, A. R.; Rachwal, P.; Law, K. W.; Karelson, M.; Lobanov, V. S. Prediction of polymer glass transition temperatures using a general quantitative structure- property relationship treatment. *J. Chem. Inf. Comput. Sci.* **1996,** *36*, 879.

63. Yoshida, T.; Yoshizawa, F.; Itoh, M.; Matsunaga, T.; Watanabe, M.; Tamura, M. Prediction of fire and explosion hazards of reactive chemicals. I: Estimation of explosive properties of self-reactive chemicals from SC-DSC data. *Kogyo Kayaku* **1987,** *48*, 311.

64. Fu, Z. M.; Li, X. R.; Koseki, H.; Mok, Y. S. Evaluation on thermal hazard of methyl ethyl ketone peroxide by using adiabatic method. *J. Loss Prev. Process Ind.* **2003,** *16*, 389.

65. Yeh, P.-Y.; Shu, C.-M.; Duh, Y.-S. Thermal Hazard Analysis of Methyl Ethyl Ketone Peroxide. *Ind. Eng. Chem. Res.* **2002,** *42*, 1.

66. Wang, Y.-W.; Shu, C.-M.; Duh, Y.-S.; Kao, C.-S. Thermal Runaway Hazards of Cumene Hydroperoxide with Contaminants. *Ind. Eng. Chem. Res.* **2001,** *40*, 1125.

67. Peng, D.; Chang, C.; Chiu, M. Thermal analysis of RDX with contaminants. *J. Therm. Anal. Calorim.* **2006,** *83*, 657.

68. Cisneros, L. O.; Rogers, W. J.; Mannan, M. S.; Li, X.; Koseki, H. Effect of Iron Ion in the Thermal Decomposition of 50 mass % Hydroxylamine/Water Solutions. *J. Chem. Eng. Data* **2003,** *48*, 1164.

69. McCloskey, C. Safe handling of organic peroxides: An overview. *Plant Oper. Prog.* **2004,** *8*, 185.

70. Tseng, J.; Shu, C.; Yu, Y. Thermal hazard simulations for methyl ethyl ketone peroxide induced by contaminants. *Korean J. Chem. Eng.* **2005,** *22*, 797.

71. Crowl, D. A.; Louvar, J. F. *Chemical Process Safety: Fundamentals with Applications*; Pearson Education Canada: Toronto, Canada, 2011.

72. Tseng, J.-M.; Shu, C.-M.; Gupta, J. P.; Lin, Y.-F. Evaluation and modeling runaway reaction of methyl ethyl ketone peroxide mixed with nitric acid. *Ind. Eng. Chem. Res.* **2007,** *46*, 8738.

73. Liu, L.; Wei, C.; Guo, Y.; Rogers, W. J.; Sam Mannan, M. Hydroxylamine nitrate self-catalytic kinetics study with adiabatic calorimetry. *J. Hazard. Mater.* **2009,** *162*, 1217.

74. Stoessel, F. Experimental study of thermal hazards during the hydrogenation of aromatic nitro compounds. *J. Loss Prev. Process Ind.* **1993,** *6*, 79.

75. Heemskerk, A.; Hordijk, A.; Lanning, A.; Lont, J.; Schell, H.; Schuurman, P. *Guidelines for Chemical Reactivity Evaluation and Application to Process Design*. AIChE, New York, USA 1995.

76. Lin, W.; Wu, S.; Shiu, G.; Shieh, S.; Shu, C. Self-accelerating decomposition temperature (SADT) calculation of methyl ethyl ketone peroxide using an adiabatic calorimeter and model. *J. Therm. Anal. Calorim.* **2009,** *95*, 645.

APPENDIX

Table A1. List of descriptors calculated for 16 organic peroxides used in this study

	Q_O	E_a	d_{OO}	N_P	OB	MW	DM	$\angle_{ROOR'}$	$\angle_{ROO}$	ε_{HOMO}	ε_{LUMO}	H	μ	ω	C
1	-0.444	17.64	1.473	1	-261.16	208.3	0.498	156.21	107.68	-0.226	-0.005	0.220	-0.115	0.030	0.94
2	-0.450	16.84	1.474	1	-266.27	270.4	0.364	157.15	107.59	-0.228	-0.012	0.216	-0.120	0.033	0.98
3	-0.442	18.65	1.473	1	-251.71	146.2	0.438	160.31	107.59	-0.222	0.032	0.254	-0.095	0.018	0.98
4	-0.584	9.88	1.439	1	-191.58	242.2	0.019	177.41	108.80	-0.264	-0.058	0.206	-0.161	0.063	0.7
5	-0.507	8.90	1.445	1	-268.94	398.6	0.882	84.90	111.07	-0.282	-0.010	0.272	-0.146	0.039	0.97
6	-0.473	14.66	1.451	1	-214.21	194.2	2.677	116.24	110.21	-0.261	-0.047	0.213	-0.154	0.055	0.98
7	-0.450	15.54	1.454	1	-181.54	132.2	2.458	117.22	110.26	-0.269	0.007	0.276	-0.131	0.031	0.55
8	-0.447	13.03	1.474	2	-248.60	302.5	1.123	143.22	108.01	-0.227	0.018	0.245	-0.104	0.022	0.92
9	-0.461	14.24	1.471	2	-225.35	234.3	1.078	153.33	107.56	-0.227	0.020	0.248	-0.103	0.022	0.5
10	-0.471	18.29	1.473	2	-247.93	290.4	0.806	162.25	107.70	-0.222	0.030	0.252	-0.096	0.018	0.9
11	-0.362	2.97	1.483	1	-145.96	230.2	0.378	173.32	105.83	-0.251	-0.063	0.187	-0.157	0.066	0.34
12	-0.317	29.99	1.459	1	-231.27	152.2	1.536	114.07	104.31	-0.243	-0.007	0.236	-0.125	0.033	0.88
13	-0.458	13.27	1.450	1	-227.27	246.4	1.890	116.16	109.31	-0.271	0.009	0.280	-0.131	0.031	0.95
14	-0.442	15.32	1.469	2	-233.49	260.4	1.139	137.60	109.32	-0.233	0.023	0.256	-0.105	0.021	0.80
15	-0.440	7.77	1.464	3	-144.62	210.2	1.285	138.71	108.05	-0.254	-0.014	0.240	-0.134	0.037	0.35
16	-0.316	30.59	1.458	1	-195.34	90.1	1.789	110.95	104.48	-0.254	0.031	0.286	-0.112	0.022	0.61

VITA

Name: Yuan Lu

Address: Room 420, Jack E. Brown Building, 3122 TAMU, Texas A&M University, College Station, TX 77843

Email Address: luyuan.ecust@gmail.com

Education: B.S., Biochemical Engineering, East China University of Science and Technology, 2003

M.S., Fermentation Engineering, East China University of Science and Technology, 2006

M.S., Chemical Engineering, Texas A&M University, 2008